Title
SOME NUCLEAR AND ELECTRONIC GROUND-STATE PROPERTIES OF Pa233, Am241 AND 16-hr Am242

Author
Winocur, Joseph.

Publication Date
1960-04-13

UCRL 9174

UNIVERSITY OF CALIFORNIA

Ernest O. Lawrence

Radiation Laboratory

SOME NUCLEAR AND ELECTRONIC GROUND-STATE PROPERTIES OF Pa^{233}, Am^{241}, AND 16-hr Am^{242}

DISCLAIMER

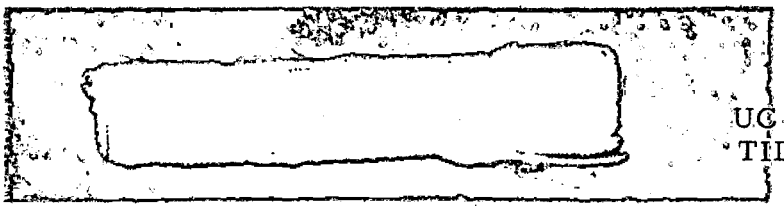

UCRL-9174
UC-34 Physics and Mathematics
TID-4500 (15th Ed.)

UNIVERSITY OF CALIFORNIA

Lawrence Radiation Laboratory
Berkeley, California

Contract No. W-7405-eng-48

SOME NUCLEAR AND ELECTRONIC GROUND-STATE PROPERTIES OF Pa^{233}, Am^{241}, and 16-hr Am^{242}

Joseph Winocur

(Thesis)

April 13, 1960

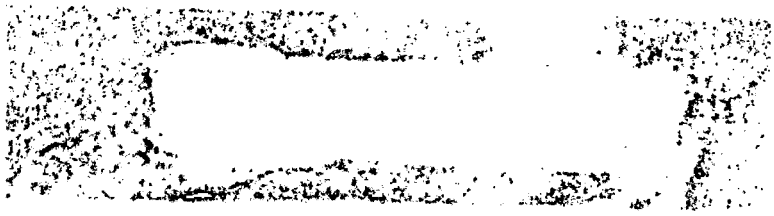

Printed in USA. Price $2.50. Available from the
Office of Technical Services
U. S. Department of Commerce
Washington 25, D.C.

SOME NUCLEAR AND ELECTRONIC GROUND-STATE PROPERTIES OF Pa^{233}, Am^{241}, and 16-hr Am^{242}

Contents

SOME NUCLEAR AND ELECTRONIC GROUND-STATE PROPERTIES OF Pa^{233}, Am^{241} and 16-hr Am^{242}

Joseph Winocur

Lawrence Radiation Laboratory
University of California
Berkeley, California

April 13, 1960

ABSTRACT

The atomic-beam, magnetic-resonance method has been used to study some properties of the nuclear ground-state and the low-lying electronic states of three radioactive actinide isotopes. The following results were obtained:

Isotope	$T_{1/2}$	I	J	g_J	a(Mc)	b(Mc)
Pa^{233}	27.4d	3/2	11/2	0.8141(4)	+595(40)	-2400(300)
			9/2	0.8062(15)		
			7/2	0.7923(15)		
		μ_I(measured) = 3.4(1.2) nm				
Am^{241}	458 yr.	5/2*	7/2*	1.9371(10)	±17.144(8)	∓123.82(10)
Am^{242}	16 hr	1	7/2	1.9371(10)	±10.124(10)	± 69.639(40)

The starred results are confirmations of earlier measurements made by optical spectroscopy.

The observed electronic energy levels of protactinium very probably arise from the configuration $(5f)^2$ (6d) $(7s)^2$. Experimental transition intensities indicate that the ordering of these levels is probably inverted. From the observed hfs constants of Pa^{233} and detailed calculations involving the electronic wave functions, we infer the following values of the nuclear moments:

$\mu_I(Pa^{233}) = +2.1$ nm

$Q\ (Pa^{233}) = -\ 3.0$ barns.

From the ratios of the hfs constants of the two americium isotopes, together with the optically measured nuclear moments of Am^{241}, it follows that

$\mu_I(Am^{242}) = \pm\ 0.33$ nm

and

$Q\ (Am^{242}) = \mp\ 2.76$ barns.

A description of the experimental technique, and an analysis of the results are presented.

I. INTRODUCTION

This paper describes an investigation of the isotopes Pa^{233}, Am^{241}, and 16-hr Am^{242}, performed by the atomic-beam, magnetic-resonance spectroscopy method. Most of the results of these experiments have been published,[1,2] or will be published shortly.[3,4] This research is part of a general program to study the nuclear and electronic ground-state properties of the actinide elements. Previous atomic-beam measurements of actinide elements have been carried out by Hubbs, et al., under the direction of Professor W. A. Nierenberg, on Pu^{239}, Np^{239}, Np^{238}, and Cm^{242}.[5-9] At present, research is expanding rapidly into the rare earth region of the periodic chart, where many radioactive isotopes can easily be produced by means of pile production. Two new atomic-beam apparatuses are being built at the laboratory, which will make possible very precise hyperfine structure (hfs) measurements. They can be used to measure accurately the nuclear dipole moment, from its interaction with an applied magnetic field. Furthermore, the high-current, 88-in. cyclotron under construction at the Lawrence Radiation Laboratory should make possible the study of cyclotron-produced radioactive isotopes with low reaction cross sections. Also, some transcurium isotopes may soon be available in sufficient quantity for atomic-beam studies. These advancements offer exciting possibilities for future research.

II. EXPERIMENTAL METHOD

A. Theoretical Foundations

1. Introduction

The proper values of the Hamiltonian function form the basis for interpretation of the experimental data. Therefore we will begin by discussing the appropriate Hamiltonian for the system under investigation. For all practical purposes, the system in atomic-beam research is a beam of noninteracting atoms moving with thermal velocity and subject to external forces of magnetic origin only. To this degree of approximation, and with the further assumption of a simple atomic system with n electrons moving about a point nucleus with charge Ze, the nonrelativistic Hamiltonian is given by

$$\mathcal{H} = \sum_i \left(p_i^2/2m - Ze^2/r_i\right) + \sum_{i>j} e^2/r_{ij} + \sum a_{n\ell_i} \vec{\ell}_i \cdot \vec{s}_i + \mathcal{H}_{hfs} + \mathcal{H}_{mag.} \quad \text{(II-1)}$$

Here r_i is the distance of the ith electron from the nucleus, r_{ij} is the mutual distance of the ith and jth electrons $\sum_{i>j} e^2/r_{ij}$ is the electrostatic interaction between electrons, and $\sum_i a_{n\ell} \vec{\ell}_i \cdot \vec{s}_i$ is the magnetic interaction of the electronic orbits and spins. The hyperfine-structure Hamiltonian, $\mathcal{H}_{hfs}$, is defined as the noncentral interaction between nucleus and electrons. The magnetic-energy operator, $\mathcal{H}_{mag.}$, arises from the interaction of the atom with an external magnetic field.

The Hamiltonian function as written, is too complex to permit the exact calculation of the eigenvalues. The usual approach is to separate $\mathcal{H}$ into a spherically symmetric part,

$$\mathcal{H}_0 = \sum_i \left[p_i^2/2m + U(r_i)\right], \quad \text{(II-2)}$$

and a nonspherical part, $V = \mathcal{H} - \mathcal{H}_0$, where $U(r_i)$ is the spherically symmetric potential seen by an electron as screened by all of the other electrons. This approach permits a separation of variables so that the eigenfunctions of $\mathcal{H}_0$ may be written as a product of single-electron wave functions (Hartree functions) or as an antisymmetrized product (Hartree-Fock functions). The electrostatic plus fine-structure interactions then remove the degeneracy with respect to how the individual angular momenta are coupled to yield a total electronic angular momentum, J, where $\vec{J} = \Sigma(\vec{\ell}_i + \vec{s}_i)$. In most atoms, the electrostatic interaction is much larger than the spin-orbit interaction, so that the individual ℓ_i and s_i add separately to give a total orbital angular momentum L, and a total spin, S. The fine-structure perturbation then splits the L-S terms to produce the multiplet structure. In the heavier elements, the fine-structure interaction increases until it may become of the same magnitude as the electrostatic energy, so that L and S are no longer good quantum numbers. For $\Sigma a_{n\ell_i} \vec{\ell}_i \cdot \vec{s}_i >> \Sigma e^2/r_{ij}$, the ℓ_i and s_i of each atom are tightly coupled to form j_i, the total angular momentum of the ith electron. The electrostatic energy than acts as a perturbation that splits the J levels.

The next term in the Hamiltonian is the hyperfine-structure interaction. It couples the electronic angular momentum J, with the nuclear spin, I, to form the total angular momentum, F, which may take any of the values $|I-J|$, $|I-J+1|$, .. . $I+J$. This interaction for all atomic systems is much smaller than any of the previously discussed terms in the Hamiltonian. Therefore only matrix elements of $\mathcal{H}_{hfs}$ diagonal in J are important. The off-diagonal elements in J make a second-order contribution to the hfs energy which is proportional to $\Delta W/\Delta E$. Here ΔW is the hfs energy, and ΔE is the separation of the nearest J state that is coupled by the hfs interaction.

The final term in the Hamiltonian, $\mathcal{H}_{mag.}$, splits each hyperfine level into $2F+1$ levels. Here F is no longer a good quantum number, but its projection, m, along the quantization axis, taken as the direction of the magnetic field, is a good quantum number.

2. Hyperfine Structure

Hyperfine structure has been the subject of many treatises,[10-13] the most recent being that of Schwartz.[13] The eigenvalues of the hfs Hamiltonian are usually found in an IJF representation, since these are the quantum numbers most characteristic of the atom in the absence of any external forces. It is useful to derive the diagonal matrix elements in an $Im_I Jm_J$ representation as well, because they will have direct application to the americium investigations. Since the hfs is an invariant quantity, it may be written as the contraction of two spherical tensors,

$$\mathcal{H}_{hfs} = \sum_k \sum_q (-)^q M_{k,q} N_{k,-q} \equiv \sum_k M_k \cdot N_k , \qquad \text{(II-3)}$$

where $N_{k,q}$ is a spherical tensor of rank k which operates in the space of the electronic coordinates only, and $M_{k,q}$ operates on the nucleons in the same manner. We wish to calculate the expectation values of $\mathcal{H}_{hfs}$ in states having the quantum numbers $Im_I Jm_J$:

$$W_{m_I m_J} = (Im_I Jm_J \left| \mathcal{H}_{hfs} \right| Im_I Jm_J) . \qquad \text{(II-4)}$$

By means of the Wigner-Eckart theorem, the dependence of this expression upon the projection quantum numbers may be factored out.

$$W_{m_I m_J} = \sum_k (-)^{J-m_J} \begin{pmatrix} J & 0 & J \\ -m_J & 0 & m_J \end{pmatrix} (J \left\| N_k \right\| J) (-)^{J-m_J} \begin{pmatrix} I & k & I \\ -m_I & 0 & m_I \end{pmatrix} (I \left\| M_k \right\| I) . \qquad \text{(II-5)}$$

The bracket expression is a Wigner 3-j symbol. The double-barred quantities, called reduced matrix elements, are independent of any magnetic quantum numbers. The hfs interaction constants, A_k, are defined by[13]

$$A_k = (JJ \left\| N_k \right\| JJ)\,(II \left\| M_k \right\| II). \tag{II-6}$$

Applying the Wigner-Eckart theorem to the matrix elements on the right side of (II-6), and combining with (II-5) leads to

$$W_{m_I m_J} = \frac{\sum_k A_k (-)^{J-m_J} (-)^{I-m_I} \begin{pmatrix} J & K & J \\ -m_J & 0 & m_J \end{pmatrix} \begin{pmatrix} I & k & I \\ -m_I & 0 & m_I \end{pmatrix}}{\begin{pmatrix} J & k & J \\ -J & 0 & J \end{pmatrix} \begin{pmatrix} I & k & I \\ -I & 0 & I \end{pmatrix}} . \tag{II-7}$$

The expressions for the dipole (k=1), quadrupole (k=2), and octupole (k=3) terms are

$$W_{m_I m_J}(k=1) = A_1\, m_I m_J / IJ , \tag{II-8a}$$

$$W_{m_I m_J}(k=2) = A_2 \left[3m_J^2 - J(J+1)\right] \left[3m_I^2 - I(I+1)\right] / J(2J-1)\, I\,(2I-1), \tag{II-8b}$$

and

$$W_{m_I m_J}(k=3) = \frac{A_3 m_I m_J \left[3J(J+1) - 5m_J^2 - 1\right] \left[3I(I+1) - 5m_I^2 - 1\right]}{I(I-1)(2I-1)J(J-1)(2J-1)} . \tag{II-8c}$$

One can obtain the energy eigenvalues in an IJFm representation by transforming from the $m_I m_J$ representation via

$$\left| IJFm \right) = \sum_m (-)^{I-J-m_J} \sqrt{2F+1} \begin{pmatrix} I & J & F \\ -m_I & m_J & m \end{pmatrix} \left| Im_I Jm_J \right) . \tag{II-9}$$

and applying Eqs. (II-7). It is simpler, however, to employ a theorem due to Racah:

$$(IJFm \left| M_k \cdot N_k \right| IJFm) = (-)^{I+J+F} \begin{Bmatrix} F & J & I \\ k & I & J \end{Bmatrix} (I \left\| M_k \right\| I)(J \left\| N_k \right\| J). \tag{II-10}$$

The curly-bracket expression is the Wigner 6-j symbol, and the last two terms are the same reduced matrix elements that appeared in the previous formulas. The hyperfine-structure energy, which is now labelled by F, is given by

$$W_F = \sum_k (IJFm \left| N_k \cdot M_k \right| IJF_m) . \qquad \text{(II-11)}$$

The first three terms in this expansion are

$$W_F(k=1) = A_1 C/2IJ ,$$

$$W_F(k=2) = 3A_2 \left[C(C+1) - \frac{4}{3} I(I+1) J(J+1)\right] /2I(2I-1) J(2J-1),$$

and

$$W_F(k=3) = \frac{5A_3 \left[C^3+4C^2 + \frac{4}{5} C\{-3I(I+1)J(J+1)+I(I+1)+3\} -4I(I+1)J(J+1)\right]}{4I(I-1)(2I-1)J(J-1)(2J-1)} \qquad \text{(II-12)}$$

where $C = F(F+1) - I(I+1) - J(J+1)$. The A_k's are related to the frequently used hyperfine-structure constants a, b, and c, as follows: $A_1 = IJa$, $A_2 = b/4$, and $A_3 = c$.

An important problem is to evaluate the interaction constants in terms of the nuclear moments. The expressions for a and b for a single relativistic electron bound to a nucleus, as given by Schwartz, are [13]

$$a = \pm \frac{2\mu_I \mu_0 (2J+1)}{\alpha a_0 IJ(J+1)} \int r^{-2} FG \, dr, \quad \text{which is } \pm \text{ as } j = l \mp \tfrac{1}{2}, \qquad \text{(II-13a)}$$

and

$$b = \frac{e^2 Q(2J-1)}{(2J+2)} \int r^{-3} (F^2 + G^2) \, dr. \qquad \text{(II-13b)}$$

Here α is the fine structure constant, a_0 is the Bohr radius, $\mu_0 \equiv |e|\hbar/2mc$ is the Bohr magneton, and F and G are the relativistic radial wave functions. The nuclear magnetic dipole moment, μ_I, and electrical quadrupole moment, Q, are defined by

$$\mu_I = \left[II \left| \sum_i (g_L L_z + g_S S_z)_i \right| II \right] \mu_0 m/M \qquad \text{(II-14a)}$$

and

$$Q = \left[II \left| \sum_i g_L (3z^2 - r^2)_i \right| II \right] , \qquad \text{(II-14b)}$$

where g_L is one for protons and 0 for neutrons, g_S is the nucleon-spin g factor, and m and M are the electronic and nuclear masses. The nuclear moments are related to the nuclear matrix elements by

$$\mu_I = (II \,|M_1|\, II) \qquad \text{(II-15a)}$$

and

$$Q = (2/e)\,(II \,|M_2|\, II) . \qquad \text{(II-15b)}$$

The equations for a and b also apply to the interaction of a single valence electron outside closed subshells of other electrons. If there is more than one valence electron, the electronic wave function must be expressed in terms of the single-electron wave functions in accordance with the electronic coupling scheme. For the special, but useful, case in which non-s electrons are coupling to the Hund's rule ground-state term, $S = \sum_\ell n_\ell/2$, $L = \sum_\ell n_\ell/2\,(2\ell - n_\ell + 1)$, the forms of the interaction constants can be written explicitly as

$$a = \frac{\mu_I \mu_0}{IJ(J+1)} \sum_{\ell} \left\langle \frac{1}{r^3} \right\rangle_{n\ell} \left[\left[J(J+1)+L(L+1) - S(S+1) \right] (2\ell - n_\ell + 1) n_\ell / 2L \right.$$

$$\pm \frac{n_\ell (2\ell - n_\ell + 1)(2\ell - 2n_\ell + 1)}{2LS(2L-1)(2\ell+3)(2\ell-1)} \left\{ L(L+1) \left[J(J+1) + S(S+1) - L(L+1) \right] \right.$$

$$\left. \left. - \frac{3}{2} \left[J(J+1) - L(L+1) - S(S+1) \right] \left[J(J+1)+L(L+1)-S(S+1) \right] \right\} \right] \qquad \text{(II-16a)}$$

and

$$b = e^2 Q \frac{\left[3K(K+1) - 4L(L+1)J(J+1) \right]}{2L(2L-1)(J+1)(2J+3)} \sum_{\ell} (\pm) \left\langle \frac{1}{r^3} \right\rangle_{n\ell} \frac{n_\ell (2\ell - n_\ell + 1)(2\ell - 2n_\ell + 1)}{(2\ell-1)(2\ell+3)} \qquad \text{(II-16b)}$$

with

$$K = S(S+1) - L(L+1) - J(J+1), \qquad \text{(II-16c)}$$

and where n_ℓ is the number of electrons in the ℓ orbital. The sums are taken over all orbitals that contain less than a full shell of electrons. The positive signs apply to shells that are less than half full and the negative signs apply to shells that are more than half full. In the latter case, n_ℓ is taken as the number of electrons missing from a full shell. The derivation of Eq. (II-16a) has been published.[6] Equation (II-16b), which was derived by W. A. Nierenberg, is not yet published.[14] (A derivation is presented in Appendix A.) When $n_\ell = 1$, and $S = \frac{1}{2}$, these formulas reduce, as they must, to the nonrelativistic expressions for the dipole and quadrupole interaction constants of a single electron:

$$a = 2 \mu_I \mu_0 \left\langle \frac{1}{r^3} \right\rangle_{n\ell} L(L+1)/IJ(J+1) \qquad \text{(II-17a)}$$

and

$$b = e^2 Q \left\langle \frac{1}{r^3} \right\rangle_{n\ell} (2J-1)/(2J+2) . \qquad \text{(II-17b)}$$

3. Magnetic Interaction

If I and J are good quantum numbers, the Hamiltonian expressing the interaction of the electrons and the nucleus with an applied magnetic field may be written

$$\mathcal{H}_{mag.} = - \vec{\mu}_J \cdot \vec{H} - \vec{\mu}_I \cdot \vec{H} , \qquad \text{(II-18)}$$

where $\vec{\mu}_J$ and $\vec{\mu}_I$ are the electronic and nuclear magnetic moments, and $\vec{H}$ is the applied field. The electronic and nuclear g factors are defined by

$$\mu_J = g_J \mu_0 J,$$

and

$$\mu_I = g_I \mu_0 I . \qquad \text{(II-19)}$$

Thus, we have

$$\mathcal{H}_{mag.} = - g_J \mu_0 J_z H_z - g_I \mu_0 I_z H_z , \qquad \text{(II-20)}$$

where we have taken the magnetic field to be in the z direction. In an $Im_I Jm_J$ representation, $\mathcal{H}_{mag.}$ is diagonal:

$$(Im_I Jm_J \left| \mathcal{H}_{mag.} \right| Im_I Jm_J) = - g_J \mu_0 m_J H_z - g_I \mu_0 m_I H_z . \qquad \text{(II-21)}$$

In an Fm representation, there will be matrix elements connecting states for which F differs by ±1. However, if $\mathcal{H}_{mag.}$ is much smaller than any other term in the Hamiltonian, then the eigenvalues of $\mathcal{H}_{mag.}$ are given to a good approximation by the diagonal matrix elements:

$$(IJFm \left| \mathcal{H}_{mag.} \right| IJFm) = - g_J \mu_0 H_z m \left[F(F+1) + J(J+1) - I(I+1) \right] / 2F(F+1)$$

$$- g_I \mu_0 H_z m \left[F(F+1) + I(I+1) - J(J+1) \right] / 2F(F+1). \qquad \text{(II-22)}$$

In atomic-beam research, measurements are made on the components of the hfs in a magnetic field. To the approximation that I and J are good quantum numbers, the only part of the total Hamiltonian that needs to be considered for this application is

$$\mathcal{H}' = \mathcal{H}_{hfs} + \mathcal{H}_{mag.} \quad . \tag{II-23}$$

This expression is not diagonal in either the low-field Fm representation, or in the high-field $m_I m_J$ representation. The eigenvalues must therefore be obtained by using one representation as a basis and then performing a transformation that brings the energy matrix into diagonal form.

There are no matrix elements connecting states that differ in m, so that the $(2I+1)(2J+1)$-order secular equation is factored into $2(I+J)+1$ determinants, one for each value of m. The maximum order of any determinant is either $2I+1$ or $2J+1$, whichever is smaller. For the special instance when I or J is equal to $\frac{1}{2}$, the highest-order polynomial expression is at most quadratic, and the eigenvalues of the energy matrix can be written in exact form. The solution for $J = \frac{1}{2}$ is

$$W = -\frac{\Delta W}{2(2I+1)} - g_I \mu_0 m H_z \pm \frac{\Delta W}{2}\left[1+4mx/(2I+1)+x^2\right]^{1/2} \tag{II-24}$$

where

$$\Delta W = ha(2I+1)/2, \quad \text{and} \quad x = (g_I - g_J)\mu_0 H_z/\Delta W \, .$$

The sign of the square root is $\pm$ as $F = I \pm 1/2$. This equation was first derived by Breit and Rabi.[15] Figure 1 is a plot of W/a vs x for K^{39}, which is characterized by $J = 1/2$, $I = 3/2$, and $g_I > 0$

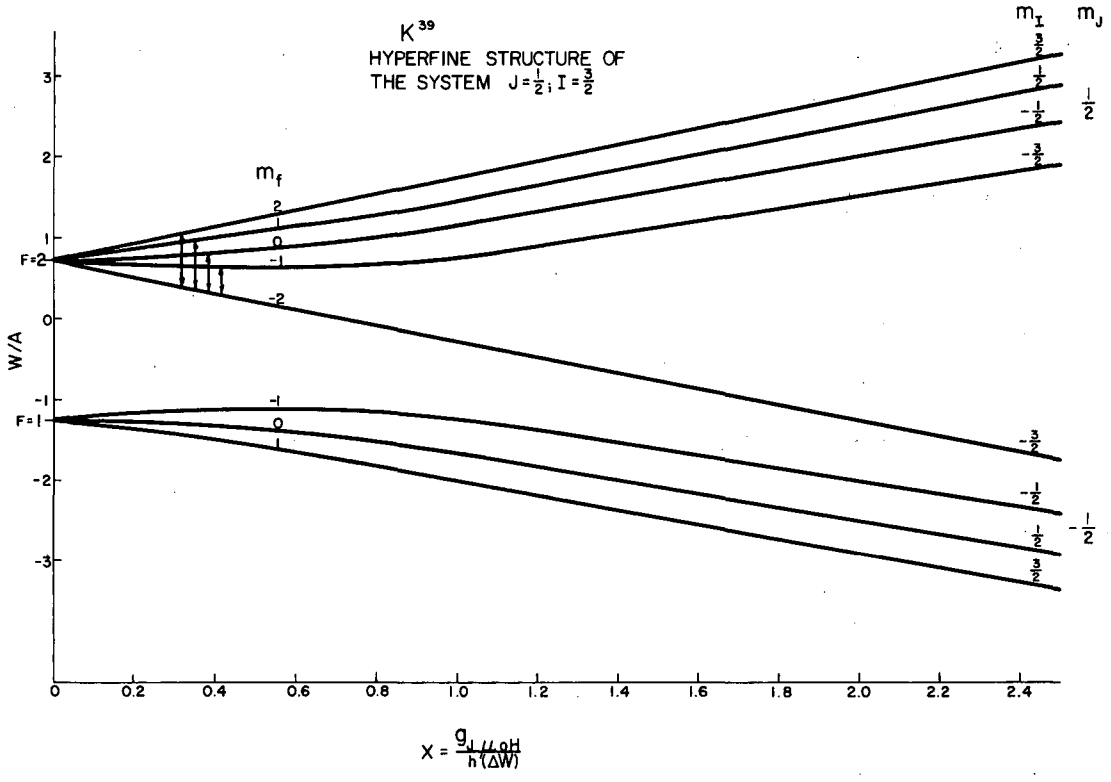

Fig. 1. Energy levels of the system I - 3/2, J=11/2, in a magnetic field.

B. Apparatus

The atomic-beam apparatus employed in these investigations utilizes the atomic-resonance method as originated by Rabi[16] and modified by Zacharias.[17] A schematic diagram of the apparatus is shown in Fig. 2. Details of its construction are well presented in the thesis of G. Brink;[18] therefore, no attempt will be made to discuss any physical details of the apparatus except in those few cases where modifications were necessary. In the protactinium research, special problems arose in connection with attaining a sufficiently high oven temperature. Also, because of the high radiation level of this isotope, rapid loading of the oven into the oven loader was important. For these reasons, the oven loader was modified. Figure 3 is a picture of the oven-loader assembly used in this work. Glass Kovar, which frequently cracked at elevated temperatures, were replaced with ceramic bushings. The oven is held in place by a 0.040-in. tantalum rod which fits into a 3/16-in. sleeve on the high-voltage connecting rod. The oven is heated by electron bombardment. The filament is a 0.010-in. thoriated-tungsten wire which has been coated with a colloid carbon-suspension (Aquadag) to increase the electron emission. The application of 300 watts of power to the oven heats it to about 3000°C. No breakdowns occured in the oven loader, but the neoprene O-ring through which the brass cylinder that holds the oven loader must slide burned out frequently. Each time this occured, the machine had to be let down to air in order to replace the O-ring. Satisfactory service was finally obtained from O-ring made of Uiton. Oven design is different for each of the two elements studied (see Fig. 4) and will be discussed later.

Table I lists the radiofrequency equipment used in the present work. The hairpin that carries the rf current is a section of shorted 50-ohm coaxial line (see Fig. 5). The rf loop can be used to excite either sigma or pi transitions. Sigma transitions ($\Delta m=0$) are

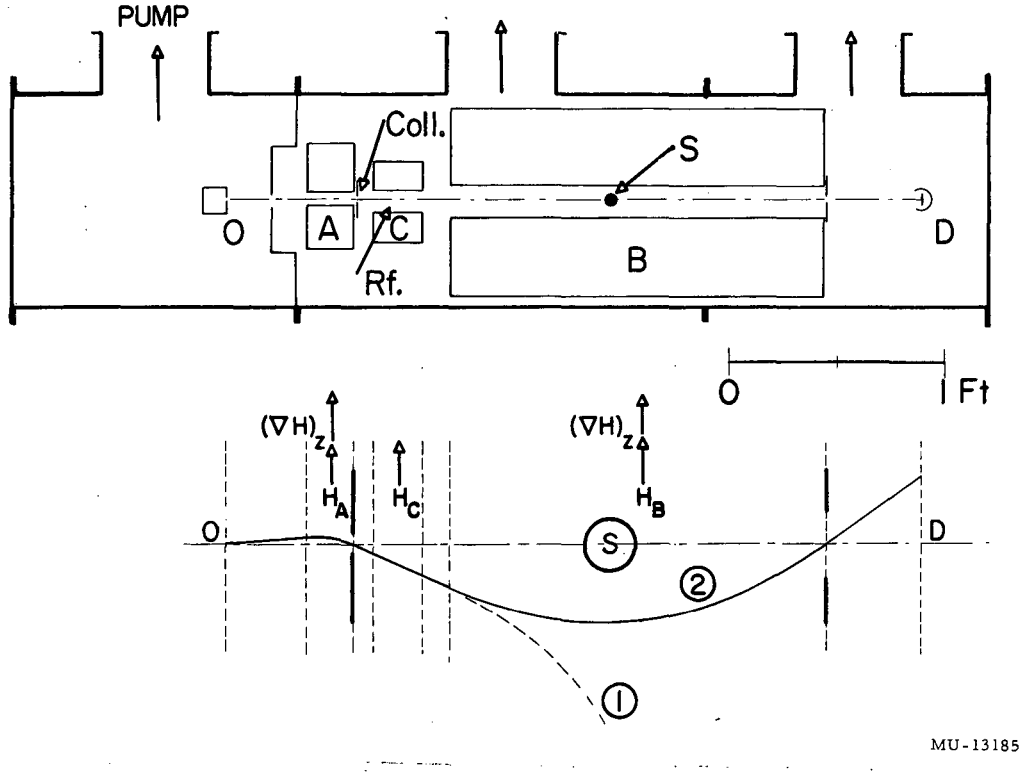

Fig. 2. Schematic arrangement and trajectory in an atomic-beam, flop-in apparatus.

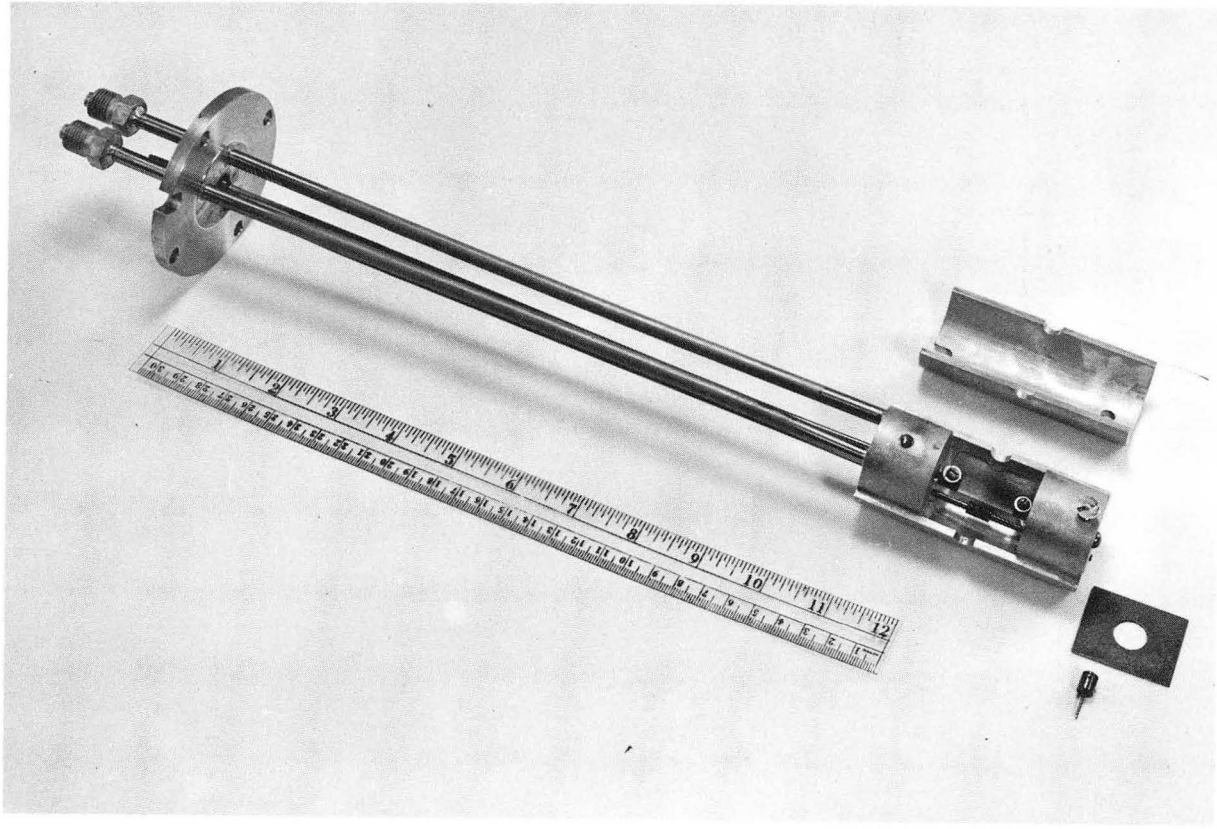

ZN-2453

Fig. 3. Electron-bombardment oven-loader assembly used in protactinium research.

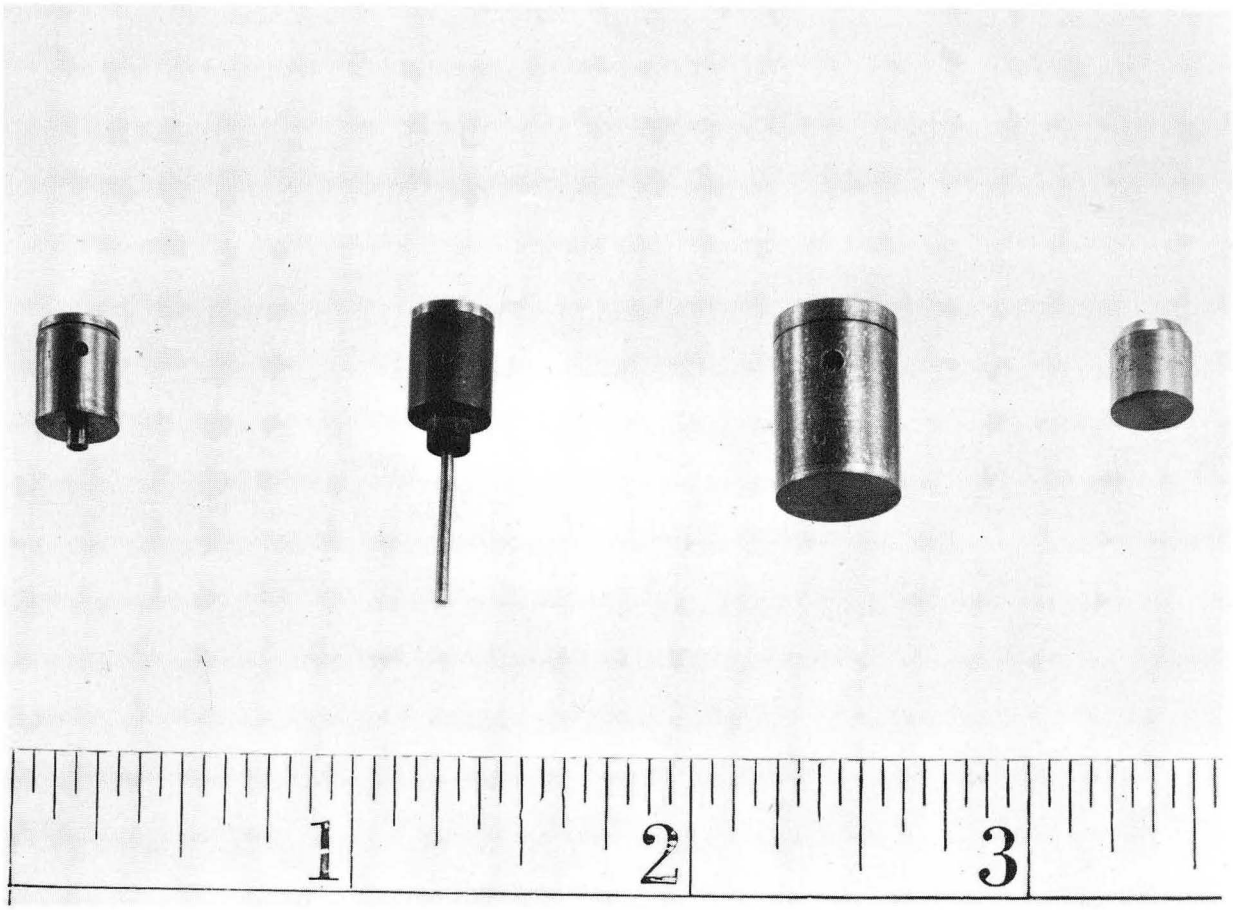

ZN-2451

Fig. 4. Atomic-beam ovens. Left to right: tantalum oven for Pa research, tungsten oven for Pa research, and molybdenum oven and inner liner for Am research.

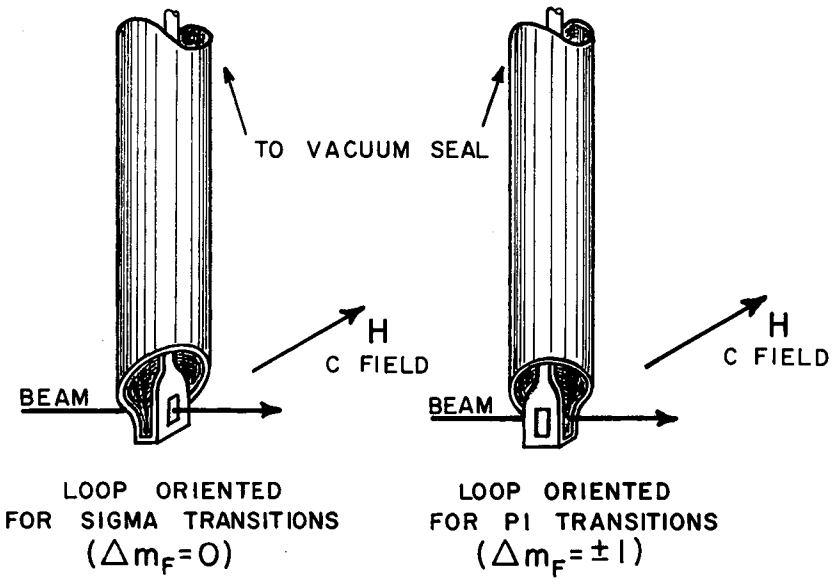

MU-18042

Fig. 5. Dual-purpose radio frequency loop.

Table I

Radiofrequency equipment

Equipment	Frequency range (Mc)
Oscillators	
General Radio 805-C	0.016 to 50
Hewlett Packard 608A	10 to 500
General Radio 1208-B	65 to 500
General Radio 1209-B	250 to 920
Hewlett Packard 612A	450 to 1250
Airborne Instruments Lab. Type 124C	220 to 2500
Hewlett Packard 540A transfer oscillator	100 to 200
Amplifiers	Frequency range (Mc)
ifi 500 wide-band amplifier	0.5 to 240
ifi 510 wide-band amplifier	0.5 to 240
Hewlett Packard 491A traveling-wave tube amplifier	1200 to 4000
Other Equipment	
Hewlett Packard 524B electronic counter	
Hewlett Packard 524A and 524B frequency-converter units	

produced by components of the rf field parallel to the C field, and pi transitions ($\Delta m=1$) are produced by components of the rf field perpendicular to the C field.

Potassium-39 was used exclusively as the calibration isotope in all of the runs. The C field was usually calibrated after each 5-min exposure. If the C field drifted measurably between settings, then the resonance was repeated. Typical full line widths at half maximum were about 50 kc at low field, and about one part per thousand at high fields. The counting rates were normalized by taking a direct beam exposure (with magnets on) after each resonance exposure.

The radioactive beam is collected on freshly flamed platinium discs, 0.495-in. in diameter and 0.001-in. thick. The collection efficiency for protactinium and americium is high, and reproducible. The Pa^{233} and 16-hr Am^{242} isotopes are counted in continuous-flow proportional beta counters. Americium-241 is counted in fission-alpha simple transistorized counters.

More discussion of the atomic-beam magnetic-resonance technique may be found in references 19 to 21. Applications to radioactive elements are discussed by W. A. Nierenberg.[22, 23]

C. IBM Routines

To facilitate the analysis of experimental results, two routines utilizing the IBM-653 computer were constructed.[23] The first routine computes the eigenvalues of the Hamiltonian [Eq. (II-23)] as a function of the magnetic field. Only the dipole and quadrupole terms are included in the hfs part of the Hamiltonian. The input information is the nuclear spin, I, the electronic angular momentum, J, the total angular momenta and magnetic quantum numbers of two levels, F_1, m_1; F_2, m_2, and b/a. The output contains the eigenvalues of the two levels, their difference, and the derivative of the difference with respect to the magnetic field.

The second routine takes a set of data and performs a least-squares fit to yield a, b, the errors in a and b, and χ^2 for the optimum fit. A parameter which measures the closeness of fit between the observed and the theoretical frequencies, χ^2 is defined by

$$\chi^2 = \sum_i (f_{obs.} - f)_i^2 \Big/ \left[(\Delta f_{obs.})_i^2 + \left(\frac{\partial f}{\partial H} \right)_i^2 \Delta H_i^2 \right].$$

Here $f_{obs.}$ and f are the observed and calculated frequencies, $\Delta f_{obs.}$ is the uncertainty of the measurement, H is the magnetic field, and ΔH is the field uncertainty. The sum is taken over all observed resonances.

A disadvantage of the second routine is that the value of g_J must be known, presumably from the stable isotope of the element under study. However, there are many elements for which accurate values of g_J have not been measured. In order to circumvent this difficulty, the routine was modifed for the IBM 704.[24] The new routine computes a and b for a fixed g_J or else varies g_J together with a and b, and calculates the error in g_J, a, and b, for minimum χ^2. Other advantages which the new routine offers are higher speed, greater flexibility, and more easily comprehensible output form.

Another program written for the IBM 704 has been very useful for analyzing electronic structure. Given an arbitrary matrix $W=A+\lambda B$, where A(e.g., the electrostatic energy in L-S coupling) is diagonal, and B(e.g. the spin-orbit energy) is not, the routine will compute the eigenvalues and eigenvectors of W, as a function of λ by using Given's method.[25] Furthermore, it will use the eigenvectors to transform an arbitrary matrix such as that of g_J, a, or b, into the new coordinate system. The diagonal elements of the transformed matrix are the expectation values of the variables g_J, etc. in the new basis.

III. PROTACTINIUM-233

A. Introduction

The long-lived isotope of protactinium, Pa^{231}, was discovered by Hahn and Meitner in 1917 and, independently, by Soddy and Cranston at about the same time.[26] In 1934, Schuler and Gollnow observed the arc spectrum in the range 6500 to 4300 Å, and measured the nuclear spin to be I=3/2.[27] This is the earliest recorded spin measurement of a radioactive nuclide.

The atomic-beam measurements of Np and Cm are pertinent to the investigations of Pa. Neutral atoms of these elements have the ground state configurations $(5f)^4(6d)(7s)^2$, $(5f)^7(6d)(7s)^2$, and $(5f)^2(6d)(7s)^2$, respectively. The most appropriate basis for interpretation of the electronic coupling in these elements is one in which the 5f electrons and the 6d electron couple independently to form two systems with angular momenta J_1 and J_2, respectively. Momenta J_1 and J_2 then couple to form a total angular momentum, J. This is called J-J coupling. Physically, it corresponds to a situation in which the electrostatic interaction between shells is much smaller than any interactions within each shell.

In section IIID1, we shall calculate to first order the electrostatic interaction energy and the electronic g factors of Pa in the J-J coupling scheme. The calculated and experimental results will then be compared, in order to test the validity of the J-J coupling model.

The nuclear data is interpreted in terms of the Bohr-Mottelson-Nilsson model of the nucleus.

B. Beam Production

Protactinium-233 is produced by neutron irradiation of Th^{232}, leading to 23.5-min Th^{233}, which beta decays into 27.4-day Pa^{233}. Two grams of thorium-metal slivers were bombarded for 10 days at a flux of 2×10^{14} neutrons/cm^2-sec to yield about 50 curies of material. The isotope was identified from its decay rate, and from a γ-pulse-height analysis (Fig. 6).

Many difficulties were encountered in the initial effort to form an atomic beam of protactinium. Although we could detect the radioactive Pa^{233} when the target material was evaporated in the tantalum source oven, it was clear from the observed throw-out ratio that the beam contained a large fraction of molecules. The throw-out ratio, defined as the ratio of the direct beam intensity at the detector with the deflecting magnets turned off to the beam intensity with the magnets on (with the stop wire out in both cases), is a measure of the molecular content of the beam. A small ratio indicates that the beam probably contains a large fraction of molecules.

We observed a throw-out ratio of less than 2/1 in protactinium. This indicated that about 50% or less of the beam was atomic. A low-field search was made with the beam of protactinium that has been produced by evaporation of the target material. No resonances were observed. We then decided to look for a chemical procedure that would yield a beam with a higher fraction of atoms. To this end, we attempted the carbon-reduction technique, described in references 7 and 9, on both the thorium metal and on oxidized thorium. Neither effort produced any change in the beam characteristics.

Next we tried to separate the protactinium from the thorium, in the belief that the thorium in some way was interfering with the reduction of the protactinium. A TTA-benzene extraction method was not satisfactory because a large residue was left with the separated protactinium. Another separation method known to work efficiently with actinide elements is that of anion-exchange. We

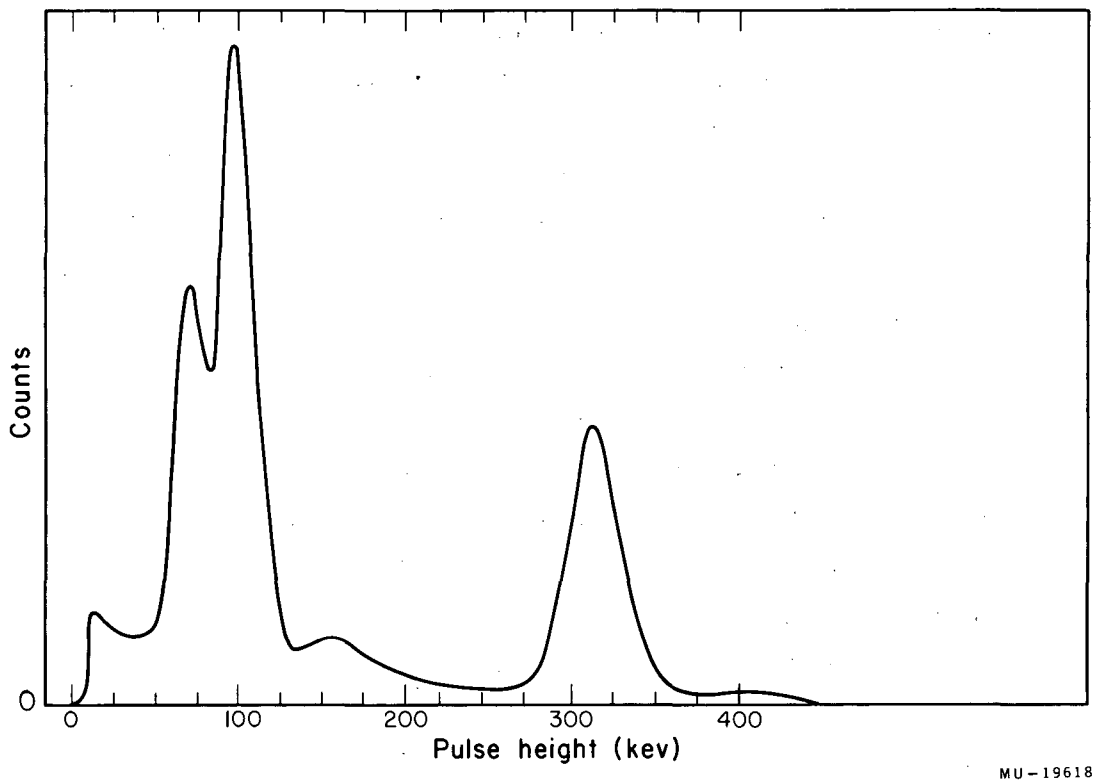

Fig. 6. Gamma pulse-height spectrum of Pa^{233}.

performed the separation, employing this method, and obtained protactinium with no contaminants and virtually no thorium present. The procedure is to dissolve the thorium-protactinium target in concentrated HCl and to run the solution through a column containing Dowex-1 anion resin. The thorium runs through the column, but the protactinium is adsorbed. A small amount of additional HCl is added to wash out any thorium still in the column. The protactinium is then eluted with 3.0M HCl-0.01M HF. The addition of a small fraction of fluoride ion to the eluant causes the protactinium to be more rapidly desorbed from the column.

The protactinium solution was boiled down to a fraction of a milliliter. A large excess of HNO_3 was then added and the solution again was boiled down to just a few drops. About one drop was pipetted from the solution into the tantalum source oven and evaporated to dryness. The HNO_3 is added so that the oxide rather than the chloride would be present. An excess of carbon was also added to the oven with the protactinium before placing the oven into the oven chamber of the apparatus. When heat is applied to the mixture, considerable out-gassing occurs, until a temperature of about $1500^{\circ}C$ is reached. The outgassing presumably is due to CO escaping when the carbide is formed. No appreciable amount of beam is detected until the oven reaches a temperature of about $2500^{\circ}C$. Then, at a critical temperature, the beam becomes very intense and the temperature must be lowered in order to reduce this intensity to the desired level. This effect is probably due to the sudden dissociation of the carbide. The measured throw-out ratio in this instance was 4/1, indicating that the beam was at least 75% atomic and probably higher. Resonances were subsequently observed with this beam. At least for the present, the procedure just described was considered satisfactory.

For purposes of investigating the hyperfine structure of the atom, the beam possessed a particularly undesirable characteristic. The background, which was normally about 0.1% of the full beam would begin to increase slowly after approximately an hour of running time. For low-field observations, this effect was unimportant, since typical resonance intensities were several tenths of a percent. However, high-field resonances on the order of 0.15% became difficult, if not impossible to observe. Of necessity, we experimented with various techniques to eliminate the high background. Believing that the increase in background was due to creep, we tried a differently designed oven, one which contained an inner liner with a sharp lip. This particular oven design was effective for the investigations of Pu^{239}, [6] the americium isotopes discussed in this paper, and many of the rare earths. It did not, however work for protactinium. We also experimented with various oven materials in order to eliminate the high background. Among those tried were tantalum with a carbon inner liner, carbon, tantalum with a tungsten inner liner, tungsten, and tungsten with a tungsten inner liner. In addition, a lanthanum reduction technique similar to that used on americium oxide (section IVB4) was attempted. None of the above-mentioned endeavors yielded any noticeable improvements in the background behavior.

Thinking that perhaps interaction of the protactinium with the tantalum slits might affect the background, we now tried a tungsten oven without any slits, the atoms escaping through a 0.040-in.-diam hole drilled in the wall of the oven. The slits on the tungsten oven had been made from tantalum foil, because tungsten cannot be spot welded onto tungsten. In spite of the large oven aperture, the background decreased to only 0.05% of the full beam and remained this low for over 10 hr. of running time. Believing that at last a satisfactory oven design had been discovered, we repeated this technique with a similar tungsten oven only to find that the background had risen again.

A tantalum shield containing a 0.060-in.-diam circular hole colinear with the oven slit was attached to the ground plate in front of

the oven. If the high background were due to the formation of a layer of material on the front face of the oven, then the aperture should have decreased the background. It did not.

Next we redesigned the oven so that the exit slit was small enough to form a well-collimated beam without the necessity of attaching tantalum slits. Ovens were made from tungsten, by using a 0.020-in.-diam circular exit aperture, and from a 90% tantalum-10% tungsten alloy into which were drilled two 0.010-in.-diameter holes, one above the other. The background observed from the tungsten oven was as low as 0.01% of the full beam, but the resonance intensities also decreased, so that the signal-to-noise ratio of the intermediate field resonances remained at about 2/1. The alloy oven was also fairly successful in that the background remained at approximately 0.05%, and resonant intensities were double the background. However, a smaller fraction of the protactinium could be evaporated from the alloy oven than from the tungsten oven.

The high background was apparently caused by the interaction of protactinium with tantalum. This mechanism would also explain the decrease of recovered beam from the alloy oven.

C. Experimental Observations

1. Low-Field Data

The initial procedure of the investigation is to make a search at some low value of the magnetic field for all observable flop-in transitions. In order to improve the precision of the measurement and to resolve any resonances that may overlap, the transitions are then followed to successively higher values of the field. To the extent that F remains a good quantum number, the resonant frequency is given by the low-field formula (II-22). The nuclear term, for our present purposes is neglected. Thus we have

$$\nu = \frac{F(F+1) + J(J+1) - I(I+1)}{2F(F+1)} \; g_J \mu_0 H_z/h \,, \qquad \text{(III-1)}$$

where I, J, and g_J must be determined from the observed data. When more than one electronic level is present in the beam, the resonances associated with each J state are fitted to this formula for a different value of J and g_J. Eight individual transitions belonging to three separate electronic states and a nucleus with spin 3/2 were observed at values of the magnetic field from 2.8 to 20.8 gauss. The experimental data is summarized in Table II. The weighted mean values of g_J, as determined from this data, are:

$J = 11/2$: $g_J = -0.8145\ (10)$
$J = 9/2$: $g_J = -0.8062\ (15)$
$J = 7/2$: $g_J = -0.7923\ (15)$.

To within the experimental accuracy, no deviations from the low-field formula were observed. Resonances in the states of maximum F for each of the three J states observed at 20.8 gauss are shown in Fig. 7. Observed ratios of resonance intensities indicate that the ordering of the low-lying electronic levels is probably inverted. A schematic drawing of the splitting of the hfs levels in a magnetic field, for the system I=3/2, J=11/2, is shown in Fig. 8.

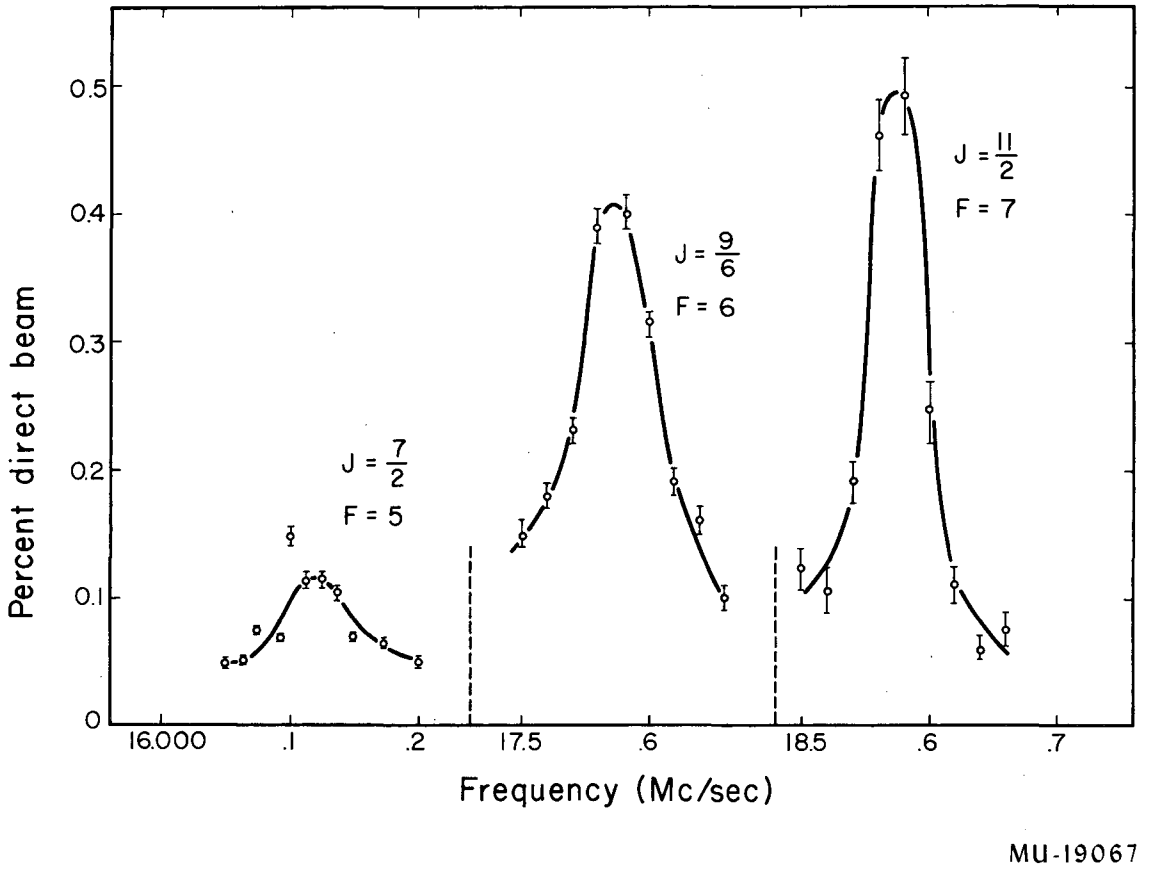

Fig. 7. Observed Pa^{233} resonances at 20.75 gauss.

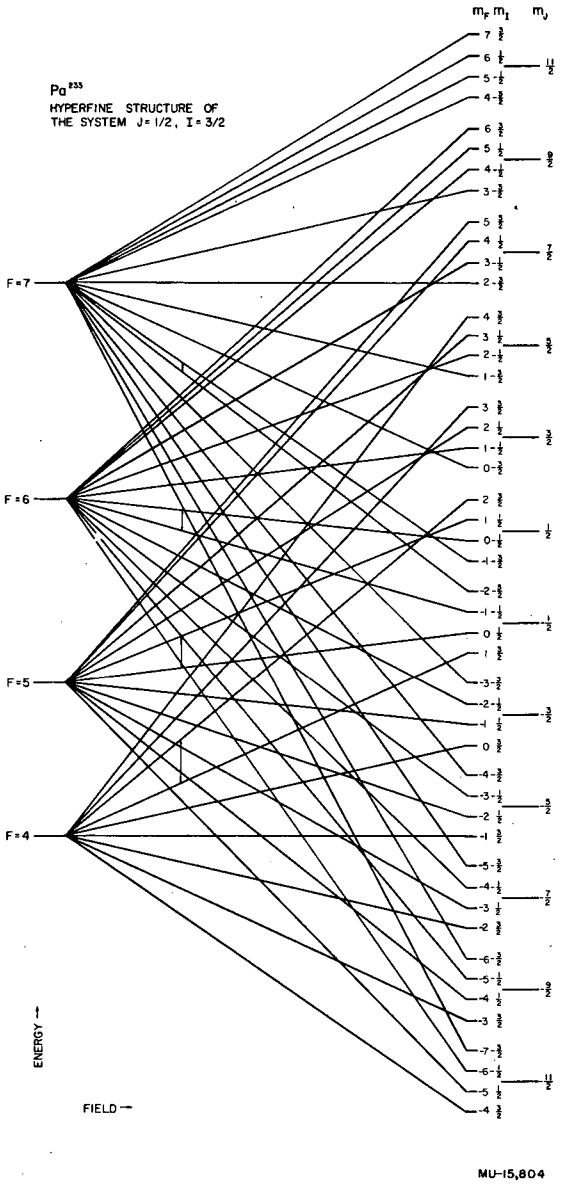

Fig. 8. Schematic diagram of the hyperfine-structure levels of Pa^{233} in a magnetic field.

Table II

Pa^{233} low-field data

J	H (gauss)	$\frac{\nu(Mc)}{g_J}$			
		F=7	F=6	F=5	F=4
11/2	2.819(30)	2.512(35) 0.810(11)			
	5.567(30)		5.582(50) 0.813(7)	6.535(50) 0.812(6)	
	10.865(30)	9.700(50) 0.8117(40)	10.912(35) 0.8144(28)	12.812(35) 0.8152(22)	16.112(50) 0.8150(25)
	20.755(30)	18.590(25) 0.8144(11)	20.812(50) 0.8132(20)	24.450(60) 0.8145(20)	30.800(60) 0.8155(16)
9/2	2.819(30)		2.400(35) 0.811(11)		
	10.865(30)		9.162(50) 0.8033(43)	10.412(35) 0.8055(27)	12.560(60) 0.8058(40)
	20.755(30)		17.575(30) 0.8067(15)	19.912(50) 0.8065(20)	24.000(50) 0.8060(17)
7/2	10.865(30)			8.425(50) 0.7914(48)	
	20.755(30)			16.115(30) 0.7924(15)	

2. Hyperfine-Structure Data

The hfs constants are determined from the field dependence of the observed transitions. The resonant frequency in an intermediate field is a function of a, b, g_J, and g_I. Three transitions associated with different values of the total angular momentum, F, for the electronic state J = 11/2 were observed at successively higher values of the field. The observations are shown in Figs. 9, 10, and 11. The IBM-704 routine described in section II-C was employed to analyze the experimental data. While a, b, and g_J were allowed to vary, g_I was kept fixed. The program was then repeated for another value of g_I. The results of a series of data analyses for different values of g_I are shown in Table III. The variation of g_I as a function of χ^2 is plotted in Fig. 12. The experimental data and the calculated residuals for $g_I = 12.4 \times 10^{-4}$ (referred to the Bohr magnetron) are presented in Table IV.

To interpret χ^2 (see section IIC for the definition), we assume that if a series of measurements of a resonant frequency were made, they would obey a normal distribution. Experimentally, only one measurement of each frequency is made; hence, the standard deviation is undetermined. Instead, an arbitrary fraction of the observed line width is selected to be the measured uncertainty. If this chosen uncertainty is equal to one standard deviation, then the resulting χ^2 will correspond to a probability P equal to approximately 0.3, where P is the probability that χ^2 should exceed its observed value.

For example, in the Pa^{233} analysis, one-fourth of the full width at half maximum was chosen as the experimental uncertainty in the measurement of a resonance. Fourteen sets of data were analyzed with the IBM-704 computer, as a function of a, b, g_J, and g_I. The minimum value of χ^2 was 1.23. For 14 observations adjusted to four independent variables, there are n=14-4=10 degrees of freedom. The value of χ^2 corresponding to n=10, and P=0.3 is 11.8.[28]

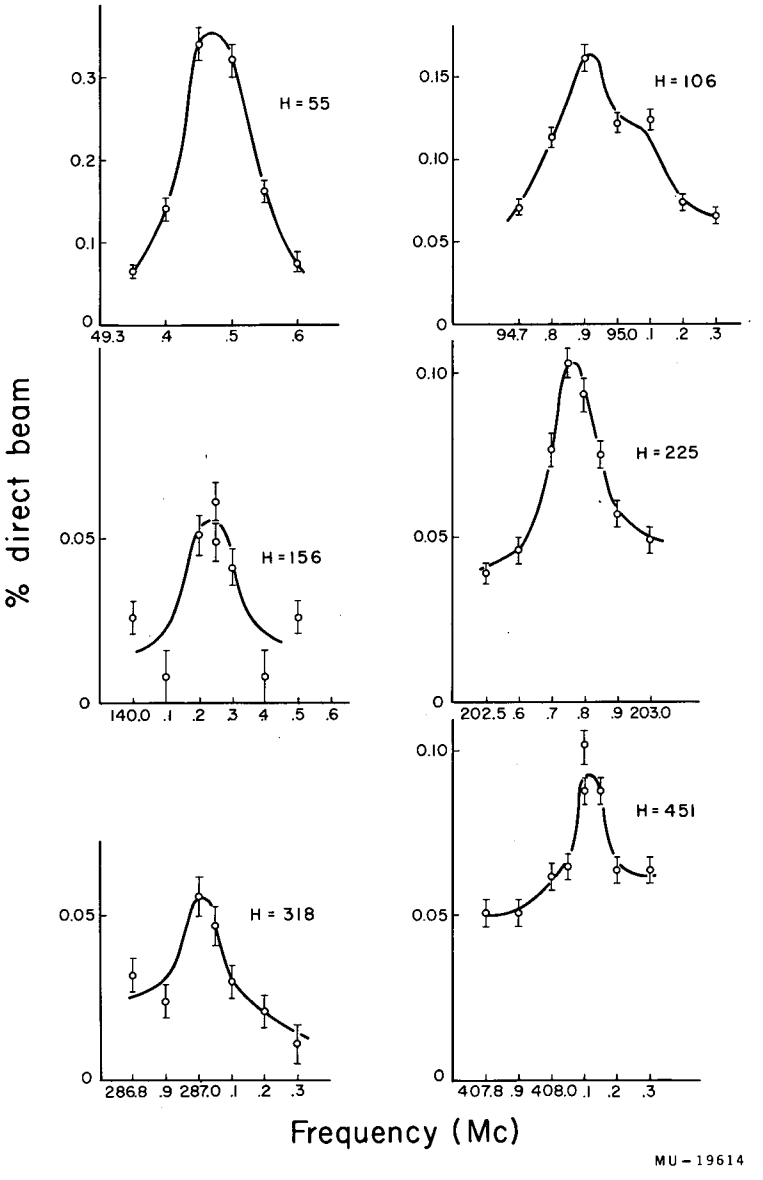

Fig. 9. Observations of the (7, -1 ⟷ 7, -2) transition of Pa^{233} at progressive values of the magnetic field.

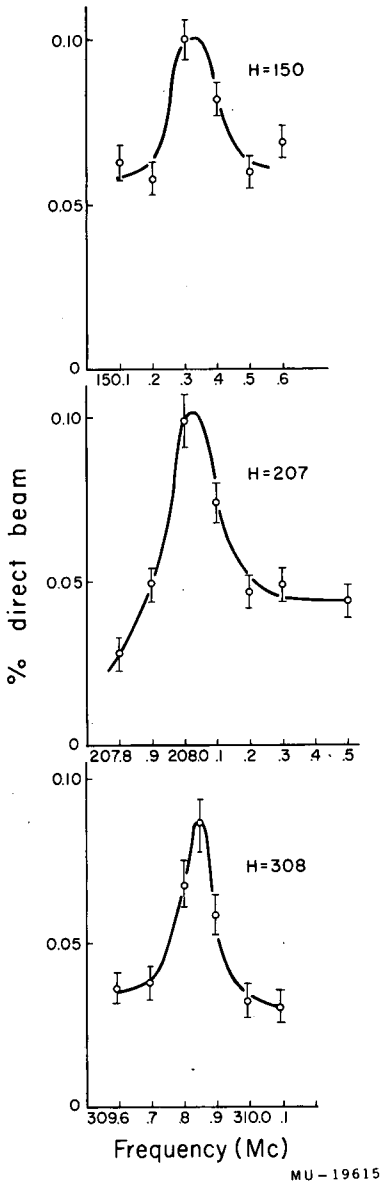

Fig. 10. Observations of the $(6, 0 \longleftrightarrow 6, -1)$ transition of Pa^{233} at progressive values of the magnetic field.

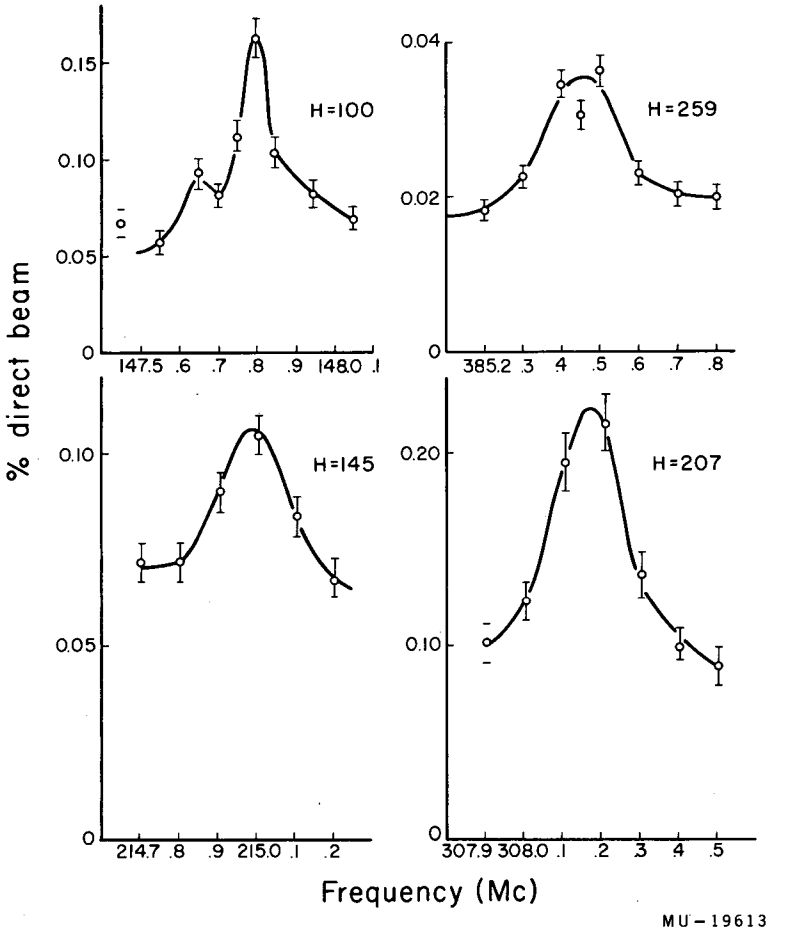

Fig. 11. Observations of the (4, 2 $\longleftrightarrow$ 4, 1) transition of Pa^{233} at progressive values of the magnetic field.

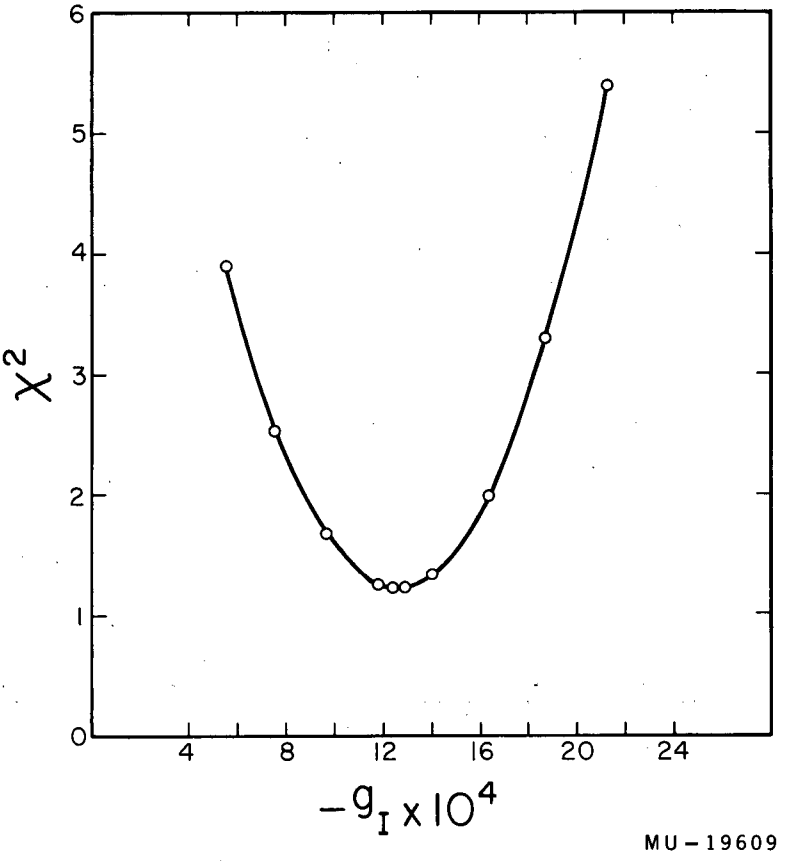

Fig. 12. Plot of χ^2 vs g_I for Pa^{233}.

Table III

Pa^{233} data analysis

$g_I \times 10^4$	g_J	a(Mc)	b(Mc)	χ^2
5.66	-0.81391	566	-2086	3.85
7.65	-0.81396	574	-2172	2.56
9.71	-0.81401	582	-2267	1.68
11.84	-0.81406	592	-2370	1.26
12.39	-0.81408	595	-2396	1.227
12.94	-0.81409	597	-2423	1.231
14.06	-0.81412	603	-2483	1.34
16.38	-0.81418	614	-2608	1.99
18.83	-0.81424	628	-2750	3.31
21.40	-0.81431	643	-2911	5.41

Table IV

Pa^{233} hfs data

Data No.	H (gauss)	$\nu_{obs.}$ (Mc)	$\nu_{obs.}-\nu_{calc.}$	Transition
1	20.754(18)	18.590(12)	+0.008	a
2	55.192(21)	49.470(50)	+0.017	a
3	105.804(24)	94.910(75)	-0.002	a
4	156.142(29)	140.230(40)	-0.010	a
5	225.371(42)	202.770(40)	-0.009	a
6	318.227(58)	287.010(40)	-0.042	a
7	450.668(74)	408.120(30)	+0.031	a
8	149.713(30)	150.330(40)	+0.018	b
9	207.147(39)	208.025(40)	+0.014	b
10	308.464(58)	309.840(30)	-0.010	b
11	99.548(25)	147.800(25)	-0.003	c
12	144.665(30)	214.980(50)	+0.011	c
13	207.147(39)	308.160(50)	-0.006	c
14	258.908(48)	385.460(63)	-0.018	c

[a] $(7, -1 \leftrightarrow 7, -2)$

[b] $(6, 0 \leftrightarrow 6, -1)$

[c] $(4, 2 \leftrightarrow 4, 1)$

This means that the uncertainties were chosen approximately $(11.8/1.23)^{1/2} \simeq 3$ times larger than an rms uncertainty, and therefore the calculated errors in a, b, and g_J are about three times the rms error. The factor of three absorbs any unknown systematic error. The measured value of g_J is more sensitive to systematic errors in the field calibration, and one part in 2000 is chosen as the upper limit of accuracy with which g_J can be measured.

The value of g_I which minimizes χ^2 is $+ 12.5 \times 10^{-4}$. The experimental error in g_I is determined from Fig. 12. The value of Δg_I is chosen such that if g_I gives a χ^2 for which P=0.3, then $g_I + \Delta g_I$ will give a χ^2 for which P = 0.02. The uncertainties in a, b, and g_J must be modified to include the effect of the uncertainty in g_I. The final data is:

$g_I = + 12.5(4.5) \times 10^{-4}$ or $\mu_I = + 3.4(1.2)$ nm

$g_J = - 0.8141(4)$

a = + 595(40) Mc

b = - 2400 (300) Mc.

Figure 13 shows the behavior of the hfs levels as a function of b/a.

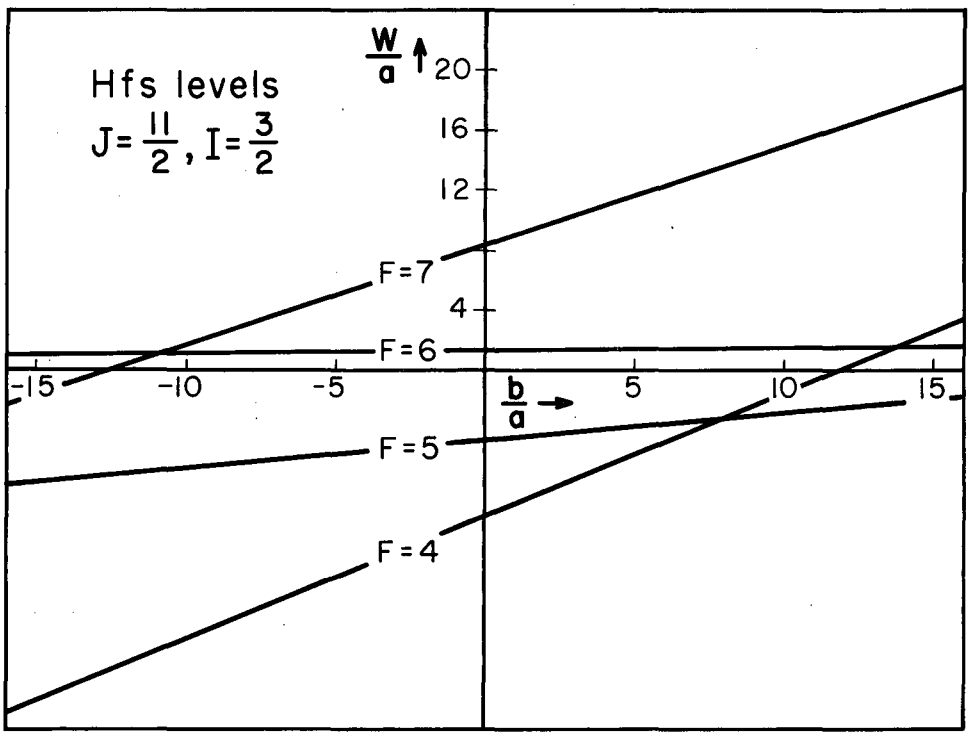

Fig. 13. Hyperfine-structure energy levels of the system I = 3/2, J = 11/2, in the absence of an applied field. W_{hfs}/a vs b/a.

D. Interpretation of Data

1. Electronic structure

Protactinium, with 91 electrons, has an inert core of 86-electrons, and 5 electrons in outer shells. The ground-state configuration of thorium is $(7s)^2(6d)^2$, and that of uranium is $(7s)^2(5f)^3 6d$. Therefore the most reasonable configuration assignments for protactinium are $(6d)^3$, $5f(6d)^2$, $(5f)^2 6d$, or $(5f)^3$. Of these, only the configuration $(5f)^2 6d$ has a ground state $J = 11/2$ as predicted by Hund's rule. This plus the fact that the calculated g_J values agree with the measured ones indicate that the ground-state configuration of protactinium is almost certainly $(5f)^2 6d$.

The best model for interpretation of the data is one in which the electrons in each shell couple independently to the Hund's-rule ground state. The Hund's-rule ground-state of the configuration $(5f)^2$ is $^3H_4$ with $g_J = -0.800$; for 6d it is $^2D_{3/2}$, with $g_J = -0.800$. In the limit of pure J-J coupling between shells, four levels characterized by $J = 11/2$, $9/2$, $7/2$, and $5/2$, with $g_J = -0.800$ for all of them is predicted. In comparison, the calculated g_J values for pure L-S coupling among all electrons is $g_J(^4K_{11/2}) = -0.769$, $g_J(^4I_{9/2}) = -0.727$, and $g_J(^4H_{7/2}) = -0.702$. The values of g_J in J-J coupling are in better agreement with the observed values.

In the J-J scheme, the ground-state multiplet is produced by the weak electrostatic interactions between 5f and 6d electrons. The energy of interaction can be calculated by first expanding the J-J wave function into the sum of determinantal wave functions, and then taking matrix elements of the electrostatic energy operator between these wave functions. This procedure can become very tedious. For example, the $J = 7/2$ wave function contains 42 determinants, and the diagonal element involves several hundred nonvanishing direct and exchange integrals.

It will be more convenient to calculate the electrostatic energy in the L-S scheme, and then transform the energy matrix to the J-J scheme. The energy in L-S coupling can be calculated by means of the diagonal sum rule. However if a term exists that can be formed in more than one way, this method gives the mean energy of the identical terms. The terms are then separated by diagonalizing the matrix connecting them.

Another method of calculation applicable to the L-S scheme is that of tensor algebra.[29, 30] The tensor method eliminates the necessity for calculating electronic wave functions, and displays the functional dependence of the energy matrix in compact form. The tensor method is particularly useful for studying the electronic structure of protactinium and will be employed in the following analysis.

The L-S matrix elements of the electrostatic energy have the form

$$(\ell_1{}^2 L_1 S_1;\ \ell_2;\ LS \left| \frac{e^2}{r_{12}} \right| \ell_1{}^2 L'_1 S'_1;\ \ell_2;\ LS) \qquad \text{(III-2)}$$

The subscripts 1 and 2 refer to the configurations $(5f)^2$ and 6d, respectively. Thus $\ell_1=3$, and $\ell_2=2$. The matrix (III-2) may be written as a sum over the radial integrals $F^k(5f, 6d)$ and $G^k(5f, 6d)$.[31] (The radial integrals are defined in Appendix C.)

$$(LS \left| \frac{e^2}{r_{12}} \right| LS) = \sum_{k=2,4} f^k F^k + \sum_{k=1,3,5} g^k G^k . \qquad \text{(III-3)}$$

The interaction among the $(5f)^2$ electrons is independent of L and S and merely adds a constant term to (III-3). Judd[32] has derived an expression for these coefficients for the general case in which an ℓ_2 electron interacts with an arbitrary number (n) of equivalent ℓ_1 electrons. He expands f^k and g^k into a sum over fractional parentage states. When n=2, this sum reduces to a single term, and the expressions for f^k and g^k become

$$f^k = 2(2\ell_1+1)(2\ell_2+1)\,\delta(S_1, S'_1)\left[(2L_1+1)(2L'_1+1)\right]^{1/2}\begin{pmatrix}\ell_1 & k & \ell_1\\ 0 & 0 & 0\end{pmatrix}\begin{pmatrix}\ell_2 & k & \ell_2\\ 0 & 0 & 0\end{pmatrix}$$

$$(-)^{k+\bar{L}+L_1+L'_1+L}\begin{Bmatrix}k & \ell_1 & \ell_1\\ \bar{L} & L'_1 & L_1\end{Bmatrix}\begin{Bmatrix}L_1 & k & L'_1\\ \ell_2 & L & \ell_2\end{Bmatrix} \qquad \text{(III-4)}$$

and

$$g^k = 2(2\ell_1+1)(2\ell_2+1)\begin{pmatrix}\ell_2 & k & \ell_1\\ 0 & 0 & 0\end{pmatrix}^2 (-)^{S_1+S'_1}\left[(2S_1+1)(2S'_1+1)(2L_1+1)(2L'_1+1)\right]^{1/2}$$

$$\begin{Bmatrix}\frac{1}{2} & \frac{1}{2} & S'_1\\ \frac{1}{2} & S & S_1\end{Bmatrix}\begin{Bmatrix}\bar{L} & \ell_2 & L'_1\\ \ell_1 & k & \ell_2\\ L_1 & \ell_2 & L\end{Bmatrix}, \qquad \text{(III-5)}$$

where $\bar{L}$ is the resultant orbital angular momentum L of the parent term. Any term of f^2 has the parent ^2F; therefore $\bar{L} = 3$. In Appendix B, we derive the form of f^k and g^k for the configuration $\ell_1^2\ell_2$ by an alternate method, and obtain agreement with Judd's result when n = 2.

We shall assume that the electrostatic interaction between the 5f electrons and the 6d electron is small in comparison with the electrostatic interaction among the 5f electrons. This means that matrix elements involving excited terms of the $(5f)^2$ configuration can be neglected. The ground term of f^2 is ^3H. Therefore we have $L_1 = L'_1 = 5$, and $S_1 = S'_1 = 1$, only. Tables of 3-j and 6-j symbols are found in Edmonds.[33]

The 3-j symbols appearing in Eq. (III-4) are

$$\begin{pmatrix} 3 & k & 3 \\ 0 & 0 & 0 \end{pmatrix} = \qquad \underline{k=2} \qquad \underline{k=4}$$

$$(4/105)^{1/2} \quad -(2/77)^{1/2}$$

and

$$\begin{pmatrix} 2 & k & 2 \\ 0 & 0 & 0 \end{pmatrix} = \qquad -(2/35)^{1/2} \quad (2/35)^{1/2}.$$

The 3-j symbol in Eq. (III-5) is

$$\begin{pmatrix} 2 & k & 3 \\ 0 & 0 & 0 \end{pmatrix} = \qquad \underline{k=1} \qquad \underline{k=3} \qquad \underline{k=5}$$

$$-(3/35)^{1/2} \quad (4/105)^{1/2} \quad -(10/231)^{1/2}.$$

The 6-j symbol in Eq. (III-5) is

$$\begin{Bmatrix} \frac{1}{2} & \frac{1}{2} & 1 \\ \frac{1}{2} & S & 1 \end{Bmatrix} = \qquad \underline{S=1/2} \qquad \underline{S=3/2}$$

$$1/6 \qquad -1/3 .$$

The 9-j symbol in Eq. (III-5) is evaluated from its definition as the sum over three 6-j symbols:

$$(-)^{k+L+1} \begin{Bmatrix} 3 & 3 & 5 \\ 3 & k & 3 \\ 5 & 2 & L \end{Bmatrix} = \begin{Bmatrix} 5 & 2 & L \\ 3 & k & 2 \\ 3 & 3 & 5 \end{Bmatrix} = \sum_r (-)^{2r}(2r+1) \begin{Bmatrix} 5 & 3 & 3 \\ 3 & 5 & r \end{Bmatrix} \begin{Bmatrix} 2 & k & 3 \\ 3 & r & 2 \end{Bmatrix} \begin{Bmatrix} L & 2 & 5 \\ r & 5 & 2 \end{Bmatrix}. \quad \text{(III-6)}$$

In Table V are listed all of the 6-j symbols required in order to evaluate the 9-j symbol. The 6-j symbols in Eq. (III-4) are also contained in this table and do not have to be evaluated separately.

Table V

Some 6-j symbols used in calculating f^k and g^k

6-j symbol	k	L	r=0	r=1	r=2	r=3	r=4
$\begin{Bmatrix} 5 & 3 & 3 \\ 3 & 5 & r \end{Bmatrix}$				$(5/616)^{1/2}$	$-(13/154)^{1/2}/6$	0	$(13/7)^{1/2}/33$
$\begin{Bmatrix} 2 & k & 3 \\ 3 & r & 2 \end{Bmatrix}$	1		$(1/35)^{1/2}$	$-(8/35)^{1/2}/3$	$(24)^{1/2}/35$		$(11/5)^{1/2}/21$
	3		$(1/35)^{1/2}$	$-(1/280)^{1/2}$	$-11/70(6)^{1/2}$		$(11/5)^{1/2}/21$
	5		$(1/35)^{1/2}$	$(1/70)^{1/2}$	$1/7(6)^{1/2}$		$(1/42)(55)^{1/2}$
$\begin{Bmatrix} L & 2 & 5 \\ r & 5 & 2 \end{Bmatrix}$		7	$(1/55)^{1/2}$	$1/3(11)^{1/2}$	$(3/1001)^{1/2}$		$1/3(50055)^{1/2}$
		6	$-(1/55)^{1/2}$	$-1/10(11)^{1/2}$	$(33/91)^{1/2}/10$		$(4/5005)^{1/2}$
		5	$(1/55)^{1/2}$	$-1/10(11)^{1/2}$	$-(7/429)^{1/2}/2$		$(4/715)^{1/2}/3$
		4	$-(1/55)^{1/2}$	$-2/5(11)^{1/2}$	0		$(91/55)^{1/2}/18$
		3	$(1/55)^{1/2}$	$-2/5(11)^{1/2}$	$(2/5)(13/231)^{1/2}$		$(13/385)^{1/6}$

Performing the indicated summation in Eq. (III-6) yields

$$\begin{Bmatrix} 5 & 2 & L \\ 2 & k & 2 \\ 3 & 3 & 5 \end{Bmatrix} = \qquad \text{(III-7)}$$

L	k=1	k=3	k=5
7	-2/231	-1/308	-1/8,470
6	1/385	1/210	41/50,820
5	1/385	-19/13,860	-79/30,492
4	1/990	1/315	23/4,356
3	1/5,390	79/48,510	-8321/1,067,220

Having evaluated each of the n-j symbols in (III-4) and (III-5), we can now calculate f^k and g^k. The result is

	f^2	f^4	g^1	g^3	g^5
^4K:	2/21	-4/693	-4/7	-2/21	-10/2541
^4I:	-11/105	8/231	-6/35	-44/315	-205/7,623
^4H:	-1/9	-8/99	6/35	-38/945	-1,975/22,869
^4G:	0	26/297	-1/15	-88/945	-575/3267
^4F:	52/315	-26/693	3/245	316/6,615	-41,605/160,083.

The energies of the doublet terms can be obtained from the above table by leaving f^k unchanged and multiplying g^k by -1/2.

No experimental or theoretical values of the radial integrals F^k and G^k are available for protactinium. However, Racah, in an analysis of the Th(III) spectra has calculated the values of the radial integrals which give the best agreement with the observed spectra.[34] We have evaluated the radial integrals for the Hartree, relativistic, normal-uranium atom wavefunctions Cohen,[35] with the help of an IBM 653 computer. A brief description of this program is given in

Appendix C. The 5f and 6d uranium electron densities are plotted in Fig. 14. The values of the radial integrals of Th(III) and U(I) are compared in Table VI.

Table VI

Values of the radial integrals

k	$F^k(5f, 6d)cm^{-1}$		$G^k(5f, 6d)cm^{-1}$		$F^k(5f)cm^{-1}$	
	Th	U	Th	U	Th	U
2	19,950	34,808			43,425	77,631
4	15,662	20,222			39,531	59,596
6					25,030	51,747
1			14,805	21,413		
3			13,545	16,308		
5			8,995	13,840		

Although the F^k's and G^k's are sensitive to the electronic wave functions, their ratios should not be very sensitive to the wave functions. This statement is approximately verifed by the values in Table VI. At this time, there is no preference for either set of calculated integrals. We will therefore calculate the electrostatic energy from each set and compare the results.

Table VII

Term energies in cm^{-1}		
Term	From Th	From U
^4K	-7976	-10645
^4I	-6219	- 9267
^2H	-4091	- 6412
^4G	-2460	- 3612
^4H	-2266	- 3682
^2I	788	214
^4F	1196	2432
^2G	3287	4461
^2F	3460	6265
^2K	6702	10120

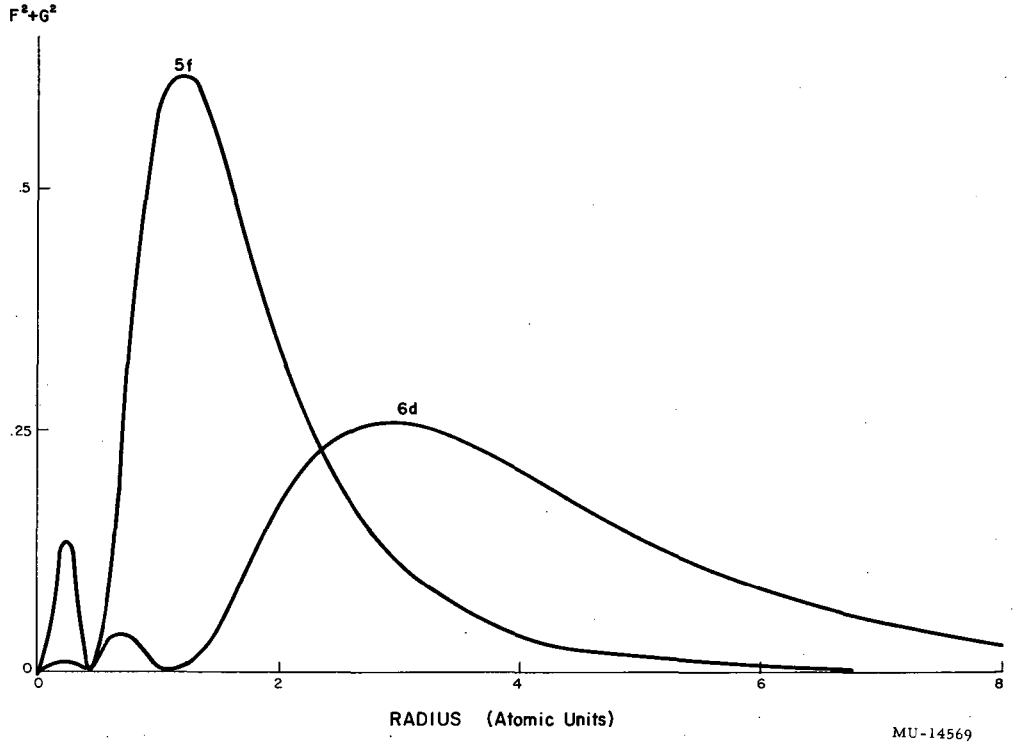

Fig. 14. Uranium 5f and 6d electron densities (after S. Cohen).

The term energies are listed in Table VII. It is encouraging to note the similarity between the level ordering predicted by the radial integrals of Racah and those calculated from Cohen's uranium wave functions.

We now proceed to obtain the electrostatic energy in the J-J coupling scheme. The LS-JJ transformation coefficient is given by

$$\left((L_1 L_2)L, (S_1 S_2)S, J \,\middle|\, (L_1 S_1)\, J_1, (L_2 S_2) J_2, J \right)$$

$$= \left[(2L+1)\,(2S+1)\,(2J_1+1)(2J_2+1) \right]^{1/2} \begin{Bmatrix} L_1 & L_2 & L \\ S_1 & S_2 & S \\ J_1 & J_2 & J \end{Bmatrix}. \quad \text{(III-8)}$$

The smallest argument appearing in the 9-j symbol is $S_2=1/2$. Therefore the formula for the 9-j symbol can be simplified to an expression involving the sum of only two 6-j symbols.

The ground $(5f)^2\ ^3H$ term is split by the fine-structure interaction into the levels $J_1=4$, 5, and 6; the $6d\ ^2D$ term is split into $J_2=3/2$, and 5/2. The electrostatic interaction between these two systems gives rise to the following states in the J_1J_2J coupling scheme: 4(3/2)J, 4(5/2)J, 5(3/2)J, 5(5/2)J, 6(3/2)J, and 6(5/2)J. Neither the electronic g factor nor the hfs-interaction operators couple any of the three last-mentioned J_1J_2J states with the 4(3/2)J ground state. Since they do not produce any first-order effects, these states will be neglected. The LS-JJ transformation coefficients to the states 4(3/2)J, 4(5/2)J, and 5(3/2)J, with J=11/2, 9/2, 7/2, and 5/2, are presented in Table VIII.

Table VIII

LS-JJ transformation coefficients

$((52)\ L\ (1\ \tfrac{1}{2})\ S;\ J \mid (51)4(2\ \tfrac{1}{2})\ \tfrac{3}{2}\ ;J)$

$2S+1$ L	J			
	11/2	9/2	7/2	5/2
^4K	$(9/11)^{1/2}$			
^4I	$-(26)^{1/2}/110$	$(18/55)(91/15)^{1/2}$		
^4H	$-(7/10)(2/165)^{1/2}$	$-(2/5)(13/165)^{1/2}$	$(182/15)^{1/2}/5$	
^4G	$-(6/5)^{1/2}/55$	$-(13/110)(6/5)^{1/2}$	$-(6/5)^{1/2}/5$	$(3/10)^{1/2}$
^4F		$-(14/165)^{1/2}/10$	$-(2/3)^{1/2}/5$	$-(1/6)^{1/2}$
^2I	$(182/11)^{1/2}/10$			
^2H	$(26/33)^{1/2}/10$	$(8/5)(13/110)^{1/2}$		
^2G		$(4/5)(3/110)^{1/2}$	$(3/5)(7/6)^{1/2}$	
^2F			$(1/2)^{1/2}/5$	$(8/15)^{1/2}$
^4K	$-(1/26)^{1/2}$			
^4I	$(71/30)/(11)^{1/2}$	$-(273/55)^{1/2}/10$		
^4H	$-(41/10)/(195)^{1/2}$	$(7/10)\ (13/15)^{1/2}$	$-(13/15)^{1/2}/5$	
^4G	$-(39/55)^{1/2}/5$	$-(19/5)\ (2/165)^{1/2}$	$(4/5)\ (7/15)^{1/2}$	
^4F		$-(14/15)^{1/2}/5$	$-(2/5)\ (7/3)^{1/2}$	

Table VIII(Continued)

$^{2S+1}$L	J			
	11/2	9/2	7/2	5/2
^{2}I	$(2/15)(7)^{1/2}$			
^{2}H	$(4/5)/(3)^{1/2}$	$(13/10)^{1/2}/5$		
^{2}G		$(7/5)(2/15)^{1/2}$	$(1/3)^{1/2}/5$	
^{2}F			$(7)^{1/2}/5$	
^{4}K	$3(2/143)^{1/2}$			
^{4}I	34/55	$(14/55)(39/10)^{1/2}$		
^{4}H	$(58/5)(1/2145)^{1/2}$	$(546/55)^{1/2}/5$	$(546/55)^{1/2}/5$	
^{4}G	$(39/5)^{1/2}/55$	$(7/55)(21/5)^{1/2}$	$(19/10)(6/55)^{1/2}$	$(3/5)^{1/2}$
^{4}F		$(3/55)^{1/2}/5$	$(3/5)(3/22)^{1/2}$	$(1/3)^{1/2}$
^{2}I	$-(4/5)(7/11)^{1/2}$			
^{2}H	$-(4/5)/(33)^{1/2}$	$-(2/5)(91/55)^{1/2}$		
^{2}G		$-(21/55)^{1/2}/5$	$-(42/11)^{1/2}/5$	
^{2}F			$-(2/11)^{1/2}/5$	$-(1/15)^{1/2}$

Transformation of the electrostatic energy in the L-S scheme to the J_1-J_2 scheme yields the following energy matrices:

J=11/2

	$4\frac{3}{2}$	$5\frac{3}{2}$	$4\frac{5}{2}$
$4\frac{3}{2}$	-6455	1507	-2489
$5\frac{3}{2}$	1507	-4513	-1915
$4\frac{5}{2}$	-2489	-1915	-3287

cm^{-1}

	$4\frac{3}{2}$	$5\frac{3}{2}$	$4\frac{5}{2}$
	-8768	1867	-3052
	1867	-6889	-2681
	-3052	-2681	-5159

cm^{-1}

J=9/2

$4\frac{3}{2}$	-5290	865	-1174
$5\frac{3}{2}$	865	-1011	296
$4\frac{5}{2}$	-1174	296	-3669

cm^{-1}

	-7989	1249	-1634
	1249	-1733	369
	-1634	369	-5633

cm^{-1}

J=7/2

$4\frac{3}{2}$	264	1213	-1574
$5\frac{3}{2}$	1213	646	-1044
$4\frac{5}{2}$	-1574	-1044	-1283

cm^{-1}

	104	1955	-2413
	1955	1515	-1620
	-2413	-1620	-2038

cm^{-1}

J=5/2

	$4\frac{3}{2}$	$5\frac{3}{2}$	$4\frac{5}{2}$
$4\frac{3}{2}$	1307		-1978
$5\frac{3}{2}$			
$4\frac{5}{2}$	-1978		- 847

cm^{-1}

	$4\frac{3}{2}$	$5\frac{3}{2}$	$4\frac{5}{2}$
	2663		-3287
	-3287		- 939

cm^{-1}

The matrices in the first column are calculated from Racah's values of the radial integrals; the matrices in the second column are calculated from the uranium radial integrals.

To complete the energy matrix, we must add the spin-orbit energy which splits the J_1J_2 states. This is

	$4\frac{3}{2}$	$5\frac{3}{2}$	$4\frac{5}{2}$
$4\frac{3}{2}$	0		
$5\frac{3}{2}$		$(5/2)a_{5f}$	
$4\frac{5}{2}$			$(5/2)a_{6d}$

The rows and columns of the above matrices are identified by the J_1J_2 states as shown at the left of the rows and above the columns. The matrix of the total energy may be written in the form

$$W = S + \lambda E, \qquad \text{(III-9)}$$

where **W** is the sum of the spin-orbit matrix, S, plus the calculated electrostatic matrix, **E**, multiplied by λ. Here λ is a parameter which is proportional to the strength of the electrostatic interaction; in effect, it is a constant which multiplies each of the radial integrals. The justification for introducing λ rests on the fact that the ratios

of the calculated integrals can be approximately correct, even if the magnitude of each integral is incorrect. The eigenvalues and eigenfunctions of W are a function of λ, which is chosen so as to yield the best agreement between the observed g_J values and those values calculated from the eigenvectors.

Before proceeding to diagonalize W, we shall first calculate the matrix elements of g_J. The electronic g factor, g_J, is defined by

$$g_J m_J = (Jm_J \left| \sum_i (g_\ell \ell_z + g_s s_z)_i \right| Jm_J) . \qquad \text{(III-10)}$$

Here $g_\ell = -1$ is the electron-orbital g factor, $g_s = -2.0023$ is the electron-spin g factor, and ℓ_z and s_z are the z components of the orbital and spin angular momenta. The sum is restricted to unfilled shells, if we assume that the core is not polarized. The g_J matrix in the J_1-J_2 scheme can be obtained by a transformation of the diagonal g_J matrix from the L-S scheme via the coefficients in Table VIII. It can also be calculated with the use of the tensor method, by considering the angular momenta as tensors of rank one. The most general tensor that we will need to evaluate in the J-J coupling scheme is

$$(\ell_1{}^2L_1S_1, \ell_2, J'_1J'_2J'm_J \left| T_{k0} \right| \ell_1{}^2L_1S_1, \ell_2, J_1J_2Jm_J) ,$$

where T_{k0} is an arbitrary tensor of rank k. The spatial dependence is obtained from the Wigner-Eckart theorem:

$$(J'm_J \left| T_{k0} \right| Jm_J) = (-)^{J-m_J} \begin{pmatrix} J & k & J \\ -m_J & 0 & m_J \end{pmatrix} (J' \| T_k \| J) . \qquad \text{(III-11)}$$

Tensor T_k may be written as the sum of a tensor $T_k(1)$ which operates on system (1), and a tensor $T_k(2)$ which operates on system (2). Therefore the reduced matrix element may be written

$$(J'_1 J'_2 J' \| T_k(1) + T_k(2) \| J_1 J_2 J) = (2J+1)(2J'+1)^{1/2}$$

$$\times \delta(J_2, J'_2)\,(-)^{J'_1 + J_2 + J + k} \begin{Bmatrix} J_1 & J' & J_2 \\ J & J_1 & k \end{Bmatrix} (J'_1 \| T_k(1) \| J_1)$$

$$+ \delta(J_1, J'_1)\,(-)^{J_1 + J_2 + J' + k} \begin{Bmatrix} J_2 & J' & J_1 \\ J & J_2 & k \end{Bmatrix} (J'_2 \| T_k(2) \| J_2) . \quad \text{(III-12)}$$

The reduced matrix elements in (III-12) can be further reduced, since $T_k(1)$ and $T_k(2)$ are each the sum of a tensor that acts on ordinary space and a tensor that acts on spin space. Equation (III-12) may be reapplied with $J_1 = L_1$, $J_2 = S_1$, and $J = J_1$. For $T_{k0} = \Sigma(-\ell_z + g_s s_z)_i$, the matrix element of T_{k0} can be ultimately reduced until it involves only the reduced matrix elements

$$(\ell \| \ell \| \ell) = [\ell\,(\ell+1)\,(2\ell+1)]^{1/2} \quad \text{(III-13)}$$

and

$$(s \| s \| s) = (3/2)^{1/2} . \quad \text{(III-14)}$$

Application of Eqs. (III-11), (III-12), (III-13), and (III-14) yields the following expression for g_J with $J_1 = J'_1$ and $J_2 = J'_2$:

$$g_J = g_{J_1} C_1/2J(J+1) + g_{J_2} C_2/2J(J+1). \quad \text{(III-15)}$$

Here g_{J_1} and g_{J_2} are the Lande' g factors of systems (1) and (2) respectively, and we have

$$C_1 = J(J+1) + J_1(J_1+1) - J_2(J_2+1) \quad \text{(III-16a)}$$

and

$$C_2 = J(J+1) + J_2(J_2+1) - J_1(J_1+1) \quad \text{(III-16b)}$$

Calculation of the matrix elements off-diagonal in J_1 or J_2 is straightforward. Consider $(J'_1 J_2 J m_J \| \Sigma\,(-\ell_z + g_s s_z)_i \| J_1 J_2 J m_J)$, where $J_1 = 4$, $J'_1 = 5$, $J_2 = 3/2$, and J is arbitrary. The 3-j symbol in (III-11) is

$$\begin{pmatrix} J & 1 & J \\ -m_J & 0 & m_J \end{pmatrix} = \frac{(-)^{J-m_J}\, m_J}{J(J+1)\,(2J+1)}\ 1/2\ .$$

The 6-j symbol in (III-12) is

$$\begin{Bmatrix} J'_1 & J' & J_2 \\ J & J_1 & 1 \end{Bmatrix} = \begin{Bmatrix} 5 & J & 3/2 \\ J & 4 & 1 \end{Bmatrix} = (-)^{J+1/2}\left[\frac{(J+15/2)(J+7/2)(-J+13/2)(J-5/2)}{990(2J+1)(2J+2)J}\right]^{\frac{1}{2}}.$$

The second part of (III-12) is zero because of the δ function. To evaluate $(J'_1 \| \Sigma\,(-\ell_z+g_s s_z)_i \| J_1)$, we need to know

$$\begin{Bmatrix} 5 & 5 & 1 \\ 4 & 5 & 1 \end{Bmatrix} = -\,1/55, \qquad \begin{Bmatrix} 1 & 5 & 5 \\ 4 & 1 & 1 \end{Bmatrix} = -\,(1/55)^{1/2},$$

$$(\ell_1\,{}^2L_1 \| \ell_1 \| \ell_1\,{}^2L_1) = (165/2)^{1/2}, \text{ and}$$

$$(s_1\,{}^2S_1 \| g_s s_1 \| s_1\,{}^2S_1) = g_s(3/2)^{1/2}.$$

Taking both of the ℓ_1 electrons into account leads finally to

$$({}^3H_5 \| \Sigma\ (-\ell_z+g_s s_z)_i \| {}^3H_4) = -\,3(6/5)^{1/2}(g_s+1) \qquad \text{(III-17)}$$

and

$$(5(3/2)\,Jm_J \mid \Sigma\,(-\ell_z+g_s s_z)_i \mid 4(3/2)Jm_J)/m_J \qquad \text{(III-18)}$$
$$= -\left[6(J+15/2)(J+7/2)(13/2-J)(J-5/2)\right]^{1/2}(g_s+1)/10J(J+1).$$

A similar calculation of the matrix element nondiagonal in J_2 yields

$$({}^2D_{5/2} \| -\ell_{2_z} + g_s s_z \| {}^2D_{3/2}) = -\,2(3/5)^{1/2}\,(g_s+1) \qquad \text{(III-19)}$$

and

$$(4(5/2)Jm_J \mid -\ell_{2_Z} + g_s s_z \mid 4(3/2)Jm_J)/m_J \qquad \text{(III-20)}$$
$$= \left[(J+15/2)(J-3/2)(13/2-J)(J+5/2)\right]^{1/2}(g_s+1)/10J(J+1)\ .$$

The matrix elements of $(g_s s_z - \ell_z)$ vanish between a state with $J_1=6$, and any other state, and between states that differ in both J_1 and J_2.

So far in the discussion, we have assumed that the f^2 configuration couples to a pure ground ^3H term. This assumption must be modified when we calculate g_J, because the spin-orbit interaction admixes excited terms into the $J_1=4$ ground level, which significantly affect the g_J of the $4(3/2)J$ state. We shall treat this effect in first order, and consider the perturbation of the state $4(3/2)J$ only. The possible terms of an f^2 configuration are ^1SDGI and ^3PFH.[31] Of these, the terms ^3H, ^3F, and ^1G can give rise to a $J_1=4$ level. The matrix of the spin-orbit plus electrostatic interaction is[36]

	^3H	^1G	^3F
^3H	$-3a_{5f}$	$-(10/3)^{1/2}a_{5f}$	
^1G	$-(10/3)^{1/2}a_{5f}$	G	$(11/3)^{1/2}a_{5f}$
^3F		$(11/3)^{1/2}a_{5f}$	$F+(3/2)a_{5f}$

(III-21)

Here G and F are the electrostatic energies of the ^1G and ^3F terms with respect to the ^3H term, and are given in reference 31. These energies can be written in terms of $F_2(5f) = F^2(5f)/225$, if some values of F^4/F^2, and F^6/F^2 are assumed. Use of the calculated uranium radial integrals (Table VI) to obtain these ratios yields $G=20.3F_2$, and $F=12.3F_2$. In section (IVD), we find that $F_2=153\ cm^{-1}$ gives the best agreement with the observed g_J values of americium. The radial integral, F_2, is proportional to $(Z-\sigma)$. The value of the screening constant, σ, usually used for the actinide elements is 58.[37] Therefore the extrapolated value of F_2 for protactinium is $(33/37)153=136.5\ cm^{-1}$. Judd has found that the low lying electronic levels in U(I) can be fitted satisfactorily by assuming $a_{5f} = 1300\ cm^{-1}$, and $a_{6d} = 1700\ cm^{-1}$.[32] The eigenvector of the lowest-energy state of the above written matrix, in which $F_2=136.5\ cm^{-1}$ and $a_{5f}=1300\ cm^{-1}$, is

$$\left|J = 4\right) = -0.939\left|{}^3H_4\right) - 0.323\left|{}^1G_4\right) + 0.095\left|{}^3F_4\right) \qquad \text{(III-22)}$$

and the g factor of this state is g_J=0.8226. In pure J-J coupling between the systems f^2(J=4) and $^2D_{3/2}$, the calculated g factors are $g_{J=11/2}$= - 0.8185, $g_{J=9/2}$=-0.8211, and $g_{J=7/2}$=-0.8260. The complete matrices of g_J in the J-J coupling scheme are:

$g_{J=11/2}$:

	$4\frac{3}{2}$	$5\frac{3}{2}$	$4\frac{5}{2}$
$4\frac{3}{2}$	- 0.8185	-0.0388	+0.0572
$5\frac{3}{2}$	-0.0388	-1.0023	
$4\frac{5}{2}$	+0.0572		-0.9369

$g_{J=9/2}$:

	$4\frac{3}{2}$	$5\frac{3}{2}$	$4\frac{5}{2}$
$4\frac{3}{2}$	-0.8211	-0.0586	+0.0909
$5\frac{3}{2}$	-0.0586	-1.0405	
$4\frac{5}{2}$	+0.0909		-0.9089

$g_{J=7/2}$

	$4\frac{3}{2}$	$5\frac{3}{2}$	$4\frac{5}{2}$
$4\frac{3}{2}$	-0.8260	-0.0714	+0.1266
$5\frac{3}{2}$	-0.0714	-1.1114	
$4\frac{5}{2}$	+0.1266		-0.8568

The eigenvalues and eigenvectors of the energy matrices W were calculated with the use of an IBM-704 computer routine described in (IIC). The eigenvalues of the J=11/2, 9/2, and 7/2 matrices are shown in Fig. 15. The g_J matrices were then transformed with the

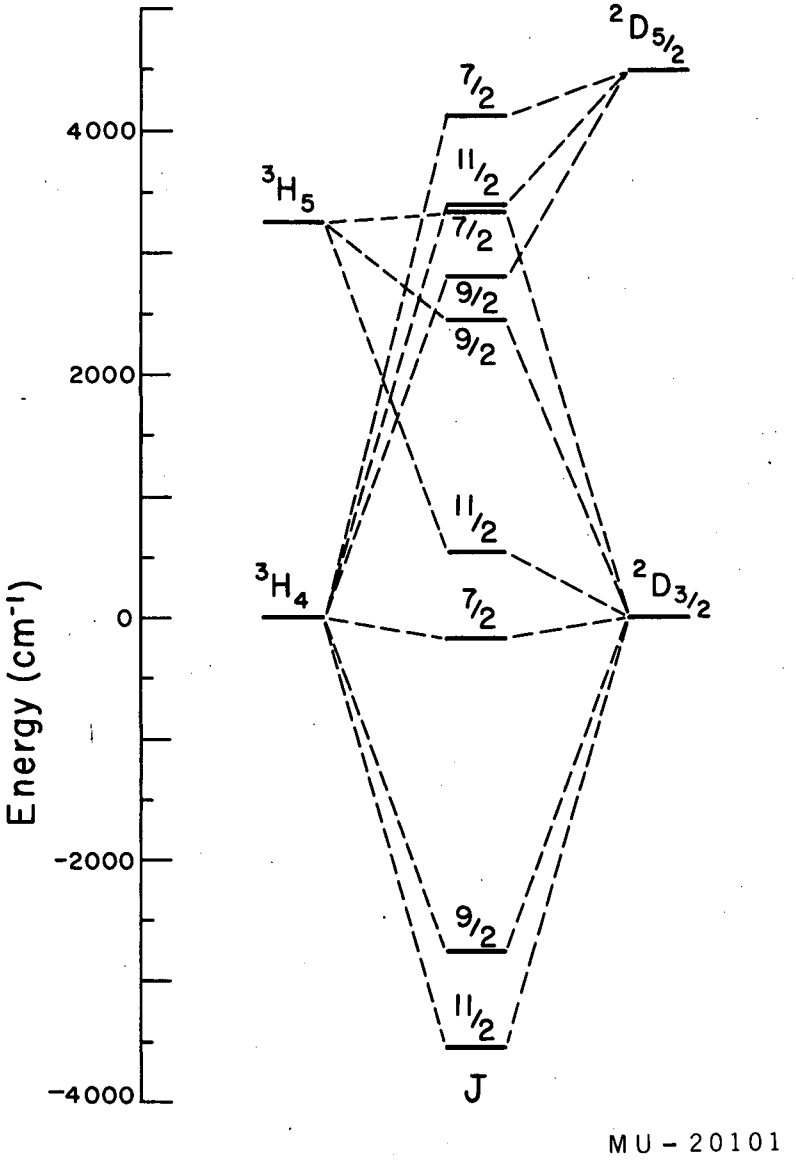

Fig. 15. Calculated electronic energy levels J-11/2, J=9/2, and J=7/2 of protactinium, in J-H coupling.

same unitary matrix which brings the energy matrix into diagonal form. The elements occuring along the diagonal of the g_J matrix are the characteristic g factors.

Figure 16 shows how g_J (calculated from Th(III) radial integrals) varies with λ for the three lowest J states. The observed g_J values are indicated by the arrows. There is no single value of λ for which the observed and calculated g factors are in satisfactory agreement. However, the situation can be improved by taking into account the other electronic states that are admixed by the electrostatic interaction into the ground level. These are the states that were previously neglected because they are not directly coupled by the single-particle operators $(-\ell_z+g_s s_z)$ and N_k. The excited states all have larger g_J values than the ground state and will therefore increase the calculated g factor. The calculation of this correction would require first evaluating (III-4) and (III-5) for each term of the configuration f^2 that can interact with a d electron to form a $|J_1 J_2 J)$ state for which J=11/2, 9/2, or 7/2, and then transforming the L-S energy matrix via Eq. (III-8) to the J_1-J_2 coupled states. An additional complication is the occurence of matrix elements between states that differ in L_1 and S_1. This would be a useful problem to program for a high-speed computer.

2. Hyperfine Structure

The nuclear magnetic-dipole and electric-quadrupole moments can be evaluated from the observed hfs constants. The desired relationship is given by (II-6). This formula may be placed in a more convenient form by using (II-15a, b) plus the Wigner-Eckart theorem to yield

$$A_1 = \mu_I \left[J/(J+1)\ (2J+1)\right]^{1/2} (J \| N_1 \| J) \qquad \text{(III-23)}$$

and

$$A_2 = (eQ/2) \left[J(2J-1)/(2J+3)\ (J+1)(2J+1)\right]^{1/2} (J \| N_2 \| J). \qquad \text{(III-24)}$$

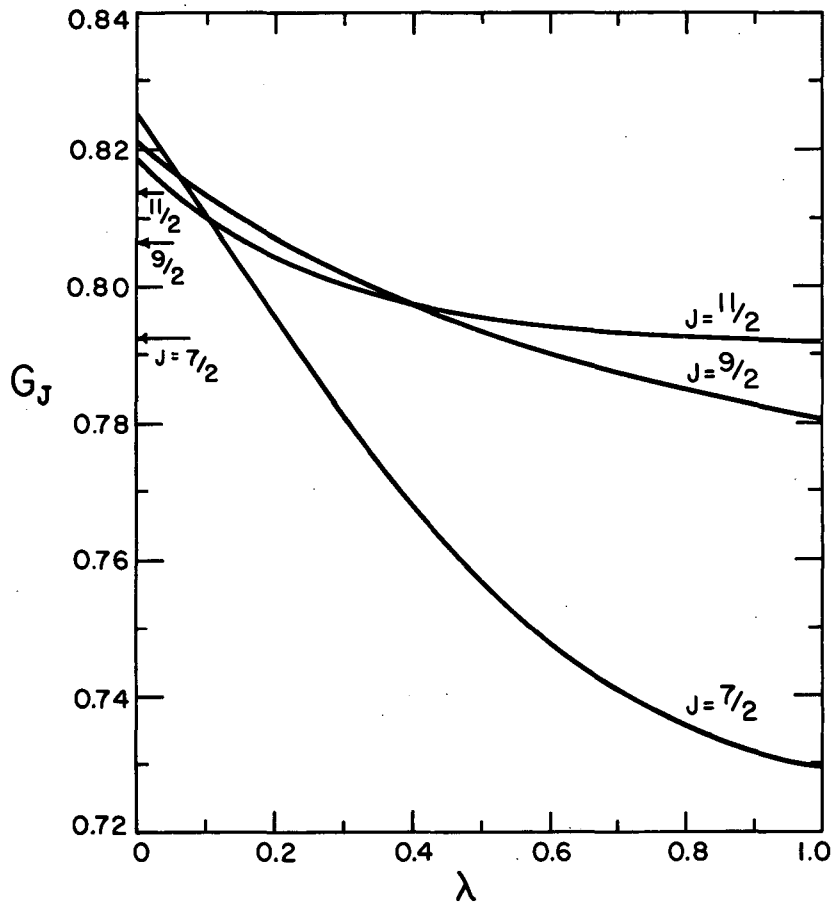

Fig. 16. Calculated g_J-factors of the levels J=11/2, 9/2 and 7/2 of protactinium as a function of the strength of the electrostatic interaction, in J-J coupling.

The problem now is to evaluate the reduced matrix elements $(J'_1 J'_2 J \,||N_k||\, J_1 J_2 J)$ for $k = 1$ and $k = 2$. Since N_k may be expressed as the sum of a part which acts on system (1) and a part which acts on system (2), Eq. (III-12) is applicable. For the special case when $J_1 = J'_1$ and $J_2 = J'_2$, we can derive expressions for A_1 and A_2 in terms of the hfs constants calculated from Eqs. (II-15) and (II-16 a, b) for each configuration. The result is

$$A_1 = \left[C_1 A_1(L_1, S_1, J_1)/J_1 + C_2 A_1(L_2, S_2, J_2)/J_2 \right] /2(J+1)$$

and

$$A_2 = \frac{\left[3C_1(C_1-1) - 4J_1(J_1+1)\ J(J+1)\right] A_2(L_1, S_1, J_1)}{J_1(2J_1-1)(2J+2)(2J+3)}$$

$$+ \frac{\left[3C_2(C_2-1) - 4J_2(J_2+1)\ J(J+1)\right] A_2(L_2, S_2, J_2)}{J_2\ (2J_2-1)(2J+2)\ (2J+3)}$$

Here $A_k(L_1, S_1, J_1)$ and $A_k(L_2, S_2, J_2)$ are the calculated hfs constants of system (1) and system (2), respectively, and C_1 and C_2 are defined by Eq. (III-16 a, b).

To obtain the matrix elements that are nondiagonal in J_1 or J_2, we must expand N_k into a sum of tensors, each of which acts on only a single electron. For the quadrupole interaction, it is easy to show that

$$N_2 = -(e/r^3)C_2 \qquad \text{(III-25)}$$

where $C_{km} \equiv (4\pi/(2k+1))\, Y_{km}$, and Y_{km} is a normalized spherical harmonic.

The dipole tensor, as shown by Trees,[38] may be written

$$N_1 = (2\mu_0/r^3)\ \left[(\underline{\ell} - (10)^{1/2} (\underline{s} \times C_2)_1 \right] \qquad \text{(III-26)}$$

where $\underline{\ell}$ is a first-rank tensor that arises from the orbital motion of the electron, and $(\underline{s} \times C_2)_1$ is a tensor of rank 1 formed from the product of a tensor of rank 1 with a tensor or rank 2, which arises from the interaction of the nucleus with the spin moment of an electron.

The reduced matrix elements of $\underline{\ell}$ have already been calculated in section (III-D1), where we found the reduced matrix elements of the quantity $(-\underline{\ell} + g_s \underline{s})$. The reduced matrix element of the spin tensor is

$$(L_1 S_1 J'_1 \| (\underline{s} \times C_2)^{(1)} \| L_1 S_1 J_1) = \left[3(2J_1+1)(2J'_1+1)\right]^{1/2} (S_1 \| \underline{s} \| S_1)(L_1 \| C_2 \| L_1) \begin{Bmatrix} L_1 & L_1 & 2 \\ S_1 & S_1 & 1 \\ J'_1 & J_1 & 1 \end{Bmatrix}. \quad \text{(III-27)}$$

A similar expression applies to the reduced matrix element of system (2). Here $(\ell\ell L \| C_2 \| \ell\ell L)$ is determined by further application of Eq. (III-12) and the fact that we have

$$(\ell' \| C_k \| \ell) = (-)^{\ell'} \left[(2\ell'+1)(2\ell+1)\right]^{1/2} \begin{pmatrix} \ell' & k & \ell \\ 0 & 0 & 0 \end{pmatrix}. \quad \text{(III-28)}$$

In the previous section, we showed that first-order calculations employing the J-J coupling model were inadequate to explain the observed electronic g factors. Nevertheless, the J-J coupling scheme is more appropriate to protactinium than is the L-S coupling scheme; therefore it will be used as the basis for calculating the hfs constants. Table IX presents a list of dipole and quadrupole matrix elements evaluated for J-J coupling. The value of $\langle 1/r^3 \rangle_{n\ell}$ is estimated from relativistic, uranium wave functions (see Appendix C):

$$\langle 1/r^3 \rangle_{n\ell} = \frac{5f}{3.99} \quad \frac{6d}{2.39} \quad a_0^{-3}$$

$$\text{"}\langle 1/r^3 \rangle\text{"}_{n\ell} = 3.89 \quad 1.99 \quad a_0^{-3}.$$

We use $\langle 1/r^3 \rangle$, and "$\langle 1/r^3 \rangle$" as the expectation value of $1/r^3$ for the quadrupole and dipole matrix elements, respectively. This yields

Table IX

Hfs matrix elements

1. Dipole

$$({}^3H_4 \| N_1 \| {}^3H_4) = \frac{1184}{15\sqrt{5}}\,\mu_0 \left\langle 1/r^3 \right\rangle_{5f}$$

$$({}^1G_4 \| N_1 \| {}^1G_4) = 12\sqrt{5}\,\mu_0 \left\langle 1/r^3 \right\rangle_{5f}$$

$$({}^3H_5 \| N_1 \| {}^3H_4) = +\,(77/75)\sqrt{30}\,\mu_0 \left\langle 1/r^3 \right\rangle_{5f}$$

$$({}^2D_{\frac{5}{2}} \| N_1 \| {}^2D_{\frac{3}{2}}) = +\,2(3/5)^{1/2}\,\mu_0 \left\langle 1/r^3 \right\rangle_{6d}$$

$$({}^2D_{\frac{3}{2}} \| N_1 \| {}^2D_{\frac{3}{2}}) = 48/\sqrt{15}\,\mu_0 \left\langle 1/r^3 \right\rangle_{6d}$$

$$({}^3H_4\,{}^2D_{\frac{3}{2}}\ \tfrac{11}{2} \| N_1 \| {}^3H_4\,{}^2D_{\frac{3}{2}}\ \tfrac{11}{2}) = 48\sqrt{\frac{13}{33}}\left[\frac{296}{225}\left\langle 1/r^3 \right\rangle_{5f} + \frac{3}{5}\left\langle 1/r^3 \right\rangle_{6d}\right]\mu_0$$

$$({}^1G_4\,{}^2D_{\frac{3}{2}}\ \tfrac{11}{2} \| N_1 \| {}^1G_4\,{}^2D_{\frac{3}{2}}\ \tfrac{11}{2}) = 48\sqrt{\frac{13}{33}}\left[\left\langle 1/r^3 \right\rangle_{5f} + \frac{3}{5}\left\langle 1/r^3 \right\rangle_{6d}\right]\mu_0$$

$$({}^3H_5\,{}^2D_{\frac{3}{2}}\ \tfrac{11}{2} \| N_1 \| {}^3H_5\,{}^2D_{\frac{3}{2}}\ \tfrac{11}{2}) = \frac{16}{5}\sqrt{\frac{3}{143}}\left[\frac{3472}{45}\left\langle 1/r^3 \right\rangle_{5f} + 19\left\langle 1/r^3 \right\rangle_{6d}\right]\mu_0$$

$$({}^3H_4\,{}^2D_{\frac{5}{2}}\ \tfrac{11}{2} \| N_1 \| {}^3H_4\,{}^2D_{\frac{5}{2}}\ \tfrac{11}{2}) = -\,\frac{16}{5}\sqrt{\frac{3}{143}}\left[\frac{3478}{45}\left\langle 1/r^3 \right\rangle_{5f} + 21\left\langle 1/r^3 \right\rangle_{6d}\right]\mu_0$$

$$({}^3H_4\,{}^2D_{\frac{5}{2}}\ \tfrac{11}{2} \| N_1 \| {}^3H_4\,{}^2D_{\frac{3}{2}}\ \tfrac{11}{2}) = +\,(8/5)\,(6/11)^{1/2}\,\mu_0 \left\langle 1/r^3 \right\rangle_{6d}$$

$$({}^3H_5\,{}^2D_{\frac{3}{2}}\ \tfrac{11}{2} \| N_1 \| {}^3H_4\,{}^2D_{\frac{3}{2}}\ \tfrac{11}{2}) = -\,(14/25)\sqrt{6}\,\mu_0 \left\langle 1/r^3 \right\rangle_{5f}$$

Table IX (continued)

2. Quadrupole

$$(^3H_4 \| N_2 \| {}^3H_4) = (52/165)\,(77/5)^{1/2}\, e \left\langle 1/r^3 \right\rangle_{5f}$$

$$(^1G_4 \| N_2 \| {}^1G_4) = 12(1/385)^{1/2}\, e \left\langle 1/r^3 \right\rangle_{5f}$$

$$(^3H_5 \| N_2 \| {}^3H_4) = (26/15)\,(1/15)^{1/2}\, e \left\langle 1/r^3 \right\rangle_{5f}$$

$$(^2D_{\frac{5}{2}} \| N_2 \| {}^2D_{\frac{3}{2}}) = 2(3/35)^{1/2}\, e \left\langle 1/r^3 \right\rangle_{6d}$$

$$(^2D_{\frac{3}{2}} \| N_2 \| {}^2D_{\frac{3}{2}}) = (4/5)^{1/2}\, e \left\langle 1/r^3 \right\rangle_{6d}$$

$$(^3H_4\, ^2D_{\frac{3}{2}}\ \tfrac{11}{2} \| N_2 \| {}^3H_4\, ^2D_{\frac{3}{2}}\ \tfrac{11}{2}) = 4\sqrt{\frac{273}{55}}\, e \left[\frac{364}{2475}\left\langle 1/r^3 \right\rangle_{5f} + \frac{1}{10}\left\langle 1/r^3 \right\rangle_{6d}\right]$$

$$(^1G_4\, ^2D_{\frac{3}{2}}\ \tfrac{11}{2} \| N_2 \| {}^1G_4\, ^2D_{\frac{3}{2}}\ \tfrac{11}{2}) = 4\sqrt{\frac{273}{55}}\, e \left[\frac{4}{55}\left\langle 1/r^3 \right\rangle_{5f} + \frac{1}{10}\left\langle 1/r^3 \right\rangle_{6d}\right]$$

$$(^3H_5\, ^2D_{\frac{3}{2}}\ \tfrac{11}{2} \| N_2 \| {}^3H_5\, ^2D_{\frac{3}{2}}\ \tfrac{11}{2}) = \frac{28}{65}\sqrt{\frac{273}{55}}\, e \left[\frac{6}{5}\left\langle 1/r^3 \right\rangle_{5f} - 1/2\left\langle 1/r^3 \right\rangle_{6d}\right]$$

$$(^3H_4\, ^2D_{\frac{5}{2}}\ \tfrac{11}{2} \| N_2 \| {}^3H_4\, ^2D_{\frac{5}{2}}\ \tfrac{11}{2}) = 4\sqrt{\frac{273}{55}}\, e \left[\frac{259}{2475}\left\langle 1/r^3 \right\rangle_{5f} + \frac{17}{455}\left\langle 1/r^3 \right\rangle_{6d}\right]$$

$$(^3H_4\, ^2D_{\frac{5}{2}}\ \tfrac{11}{2} \| N_2 \| {}^3H_4\, ^2D_{\frac{3}{2}}\ \tfrac{11}{2}) = (24/5)\,(6/385)^{1/2}\, e \left\langle 1/r^3 \right\rangle_{6d}$$

$$(^3H_5\, ^2D_{\frac{3}{2}}\ \tfrac{11}{2} \| N_2 \| {}^3H_4\, ^2D_{\frac{3}{2}}\ \tfrac{11}{2}) = -(52/275)\,(14/15)^{1/2}\, e \left\langle 1/r^3 \right\rangle_{5f}$$

$$a = \begin{array}{c|ccc} & 4\frac{3}{2} & 5\frac{3}{2} & 4\frac{5}{2} \\ \hline 4\frac{3}{2} & 285.8 & -8.2 & 3.6 \\ 5\frac{3}{2} & -8.2 & 240.5 & \\ 4\frac{5}{2} & 3.6 & & 243.7 \end{array} \quad \mu_I(\text{nm})\ \text{Mc}$$

and

$$b = \begin{array}{c|ccc} & 4\frac{3}{2} & 5\frac{3}{2} & 4\frac{5}{2} \\ \hline 4\frac{3}{2} & 745.6 & -76.9 & 151.1 \\ 5\frac{3}{2} & -76.9 & 363.7 & \\ 4\frac{5}{2} & 151.1 & & 476.4 \end{array} \quad Q\ (\text{barns})\ \text{Mc}\ .$$

Here $(4\frac{3}{2}\ \frac{11}{2} \left\| N_k \right\| 4\frac{3}{2}\ \frac{11}{2})$ has been evaluated for the wave function (III-22), omitting the $\left\| {}^3F_4 \right)$ state.

The ground-state electronic wave function is the eigenvector of the W matrix for an appropriate value of λ. We shall use $\lambda = \frac{1}{2}$, because this is the value which Judd estimates that the radial integrals calculated by Racah should be multiplied by in order to obtain agreement with the observed U(I) spectrum.[32] For $\lambda = \frac{1}{2}$, the ground-state wave function is

$$\left| J = \frac{11}{2} \right) = -0.976 \left| 4\frac{3}{2}\ \frac{11}{2} \right) + 0.124 \left| 5\frac{3}{2}\ \frac{11}{2} \right) - 0.178 \left| 4\frac{5}{2}\ \frac{11}{2} \right). \qquad \text{(III-29)}$$

The hfs constants in this electronic state are calculated on the IBM-704 computer by transforming the hfs matrices with the same matrix that diagonalizes W. The results are:

$$a = 287\ \mu_I(\text{nm})\ \text{Mc}$$
$$b = 802\ Q\ (\text{barns})\ \text{Mc}.$$

The measured hfs constants are a = 595(40) Mc, and b = - 2400(300) Mc. Therefore the nuclear moments are inferred to be:

$$\mu_I = 595/287 = +\ 2.1 \text{ nm}$$
$$Q = -2400/802 = -\ 3.0 \text{ barns.}$$

3. Second-Order Perturbation

So far, we have assumed that J is a good quantum number. This assumption is valid as long as the second-order contribution to the energy,

$$W_F = \sum_{F'} (J\text{-}1\ IF'm \left| \mathcal{H}_{hfs} + \mathcal{H}_{mag.} \right| JIFm)^2/(E_J - E_{J-1}), \tag{III-30}$$

is negligible in comparison with the first-order energy. If it is not, then the second-order field-dependent energy terms, which cannot be distinguished experimentally from those of first order, will affect the computed value of g_I and, to a smaller extent, a, b, and g_J.

An approximate upper limit to the second-order energy is

$$W_F \cong \frac{2 W_{hfs} W_{mag.}}{E_J - E_{J-1}} \cong \frac{2.4000.700}{1.5 \times 10^7} = 0.2 \text{ Mc.}$$

This amount is larger than a line width. However, we will show by means of more exact calculations that the second-order effect is really quite negligible.

The second-order dipole and quadrupole interactions, calculated in J-J coupling by means of the tensor methods previously described, are

$$(J\text{-}1\ \ IFm \left| N_1 \cdot M_1 \right| JIFm) = \frac{32\, \mu_0 \mu_I}{165\sqrt{15}} \left[(F+8)(7-F)(F+4)(F-3) \right]^{1/2} \left[-(37/15) \left\langle 1/r^3 \right\rangle_{5f} + 3 \left\langle 1/r^3 \right\rangle_{6d} \right]$$

and

$$(J\text{-}1\ \ IFm\ \Big|N_2 \cdot M_2\Big|\ JIFm) = \frac{2e^2Q}{495\sqrt{15}}\left[F(F+1)-33\right]\left[(F+8)(7-F)(F+4)(F-3)\right]^{1/2}$$
$$\left[-(91/165)\left\langle 1/r^3\right\rangle_{5f}+\left\langle 1/r^3\right\rangle_{6d}\right]. \qquad \text{(III-31)}$$

The matrix element of the magnetic-field interaction, $\mathcal{H}_{mag.} = \sum_i (-\ell_z+g_s s_z)_i\ \mu_0 H_z$, may be written

$$(J\text{-}1\ \ IFm\Big|\mathcal{H}_{mag.}\Big|\ JIFm) = f(F,m)(J\text{-}1\Big\|\sum_i (-\ell_z+g_s s_z)_i\Big\|J)\ \mu_0 H_z\ ,$$

where

$$f(F,m) = (-)^{1-m}(2F+1)\begin{pmatrix} F & 1 & F \\ -m & 0 & m\end{pmatrix}\begin{Bmatrix} 3/2 & F & 11/2 \\ 1 & 9/2 & F\end{Bmatrix}. \qquad \text{(III-32)}$$

Matrix elements of $\mathcal{H}_{mag.}$ between states that differ in the total angular momentum, F, are neglected, because no hfs matrix elements occur between these states.

It is not sufficient to calculate the reduced electronic matrix element in pure J-J coupling, because it vanishes in lowest order:

$$(4\ \tfrac{3}{2}\ \tfrac{9}{2}\Big\|\sum_i (-\ell_z+g_s s_z)_i\Big\|4\ \tfrac{3}{2}\ \tfrac{11}{2}) = -\frac{12}{\sqrt{11}}\ (g_{J_2}-g_{J_1}) \overset{\checkmark}{\neq} 0\ . \qquad \text{(III-34)}$$

We must therefore evaluate matrix elements between the ground state and states which are admixed by the electrostatic interaction. These are

$$(^3H_4\ ^2D_{3/2}\ \tfrac{9}{2}\Big\|\sum_i (-\ell_z+g_s s_z)_i\Big\|\ ^3H_5\ ^2D_{3/2}\ \tfrac{11}{2}) = 36(26)^{1/2}(g_s+1)/55, \qquad \text{(III-35a)}$$

$$(^3H_4\ ^2D_{3/2}\ \tfrac{9}{2}\Big\|\sum_i (-\ell_z+g_s s_z)_i\Big\|^3H_4\ ^2D_{5/2}\ \tfrac{11}{2}) = -(6/5)(26/11)^{1/2}(g_s+1), \qquad \text{(III-35b)}$$

$$(^3H_5\ ^2D_{3/2}\ \tfrac{9}{2}\Big\|\sum_i (-\ell_z+g_s s_z)_i\Big\|^3H_4\ ^2D_{3/2}\ \tfrac{11}{2}) = -(6/55)(g_s+1), \qquad \text{(III-35c)}$$

and

$$({}^3H_4\ {}^2D_{5/2}\ \frac{9}{2}\ \Big\|\ \sum_i (-\ell_z + g_s s_z)_i\ \Big\|\ {}^3H_4\ {}^2D_{3/2}\ \frac{11}{2}) = -(2/5)(14/11)^{1/2}(g_s+1). \quad \text{(III-35d)}$$

The electronic wave function of the J=11/2 state is given by Eq. (III-29). For the J=9/2 state, it is (for $\lambda = \frac{1}{2}$)

$$\Big|J = \frac{9}{2}\Big) = 0.990\Big|4\ \frac{3}{2}\ \frac{9}{2}\Big) - 0.081\Big|5\ \frac{3}{2}\ \frac{9}{2}\Big) + 0.115\Big|4\ \frac{5}{2}\ \frac{9}{2}\Big). \quad \text{(III-36)}$$

The coefficients f(F, m) for the observed transitions are

$$f(7, m) = 0,$$
$$f(6, 0) - f(6, -1) = (1/12)\ (1/77)^{1/2},$$

and

$$f(4, 2) - f(4, 1) = (1/20)\ (6/55)^{1/2}. \quad \text{(III-37)}$$

The electrostatic energy calculations indicate that the J=9/2 state is approximately 800 cm^{-1} above the ground state. It is difficult to estimate the uncertainty, but ± 600 cm^{-1} would be reasonable.

On the basis of the previous assumptions, we find that the second-order perturbation at a magnetic field of 500 gauss is less than 1 kc for any state, F, and hence may be entirely neglected.

4. Nuclear Structure

Protactinium-233 falls in the region of nuclides that are best interpreted in terms of the Bohr-Mottelson-Nilsson spheroidal-core model.[39-43] This model pictures the nucleons as moving in an axially symmetric but nonspherical nuclear potential. Assuming a two-dimensional harmonic oscillator-type potential, Nilsson has calculated the eigenvalues and eigenvectors of the individual nucleons as a function of the axial deformation. The single-particle levels are shown in Figs. 17 and 18.

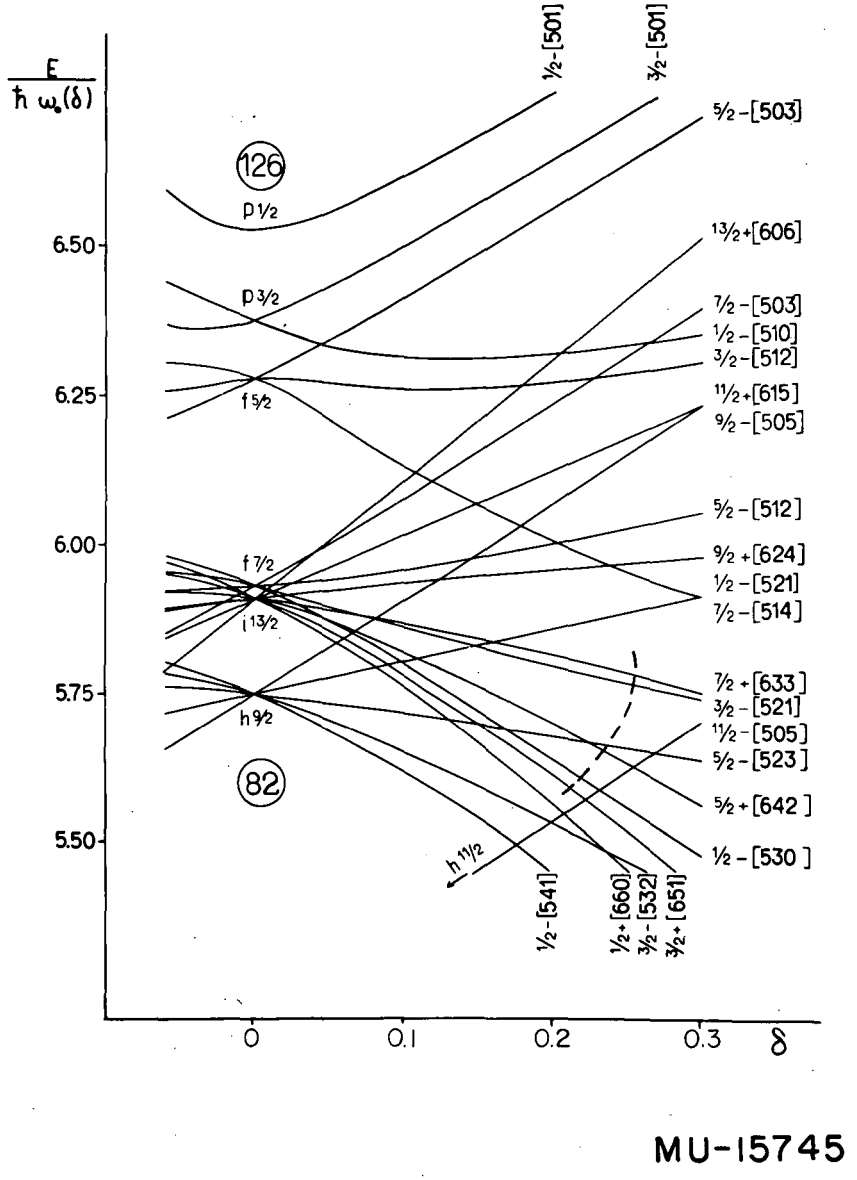

Fig. 17. Nilsson diagram for protons in the region $82 \leq X \leq 126$. The dashed line indicates very roughly the deformations thought to be appropriate to actinide isotopes.

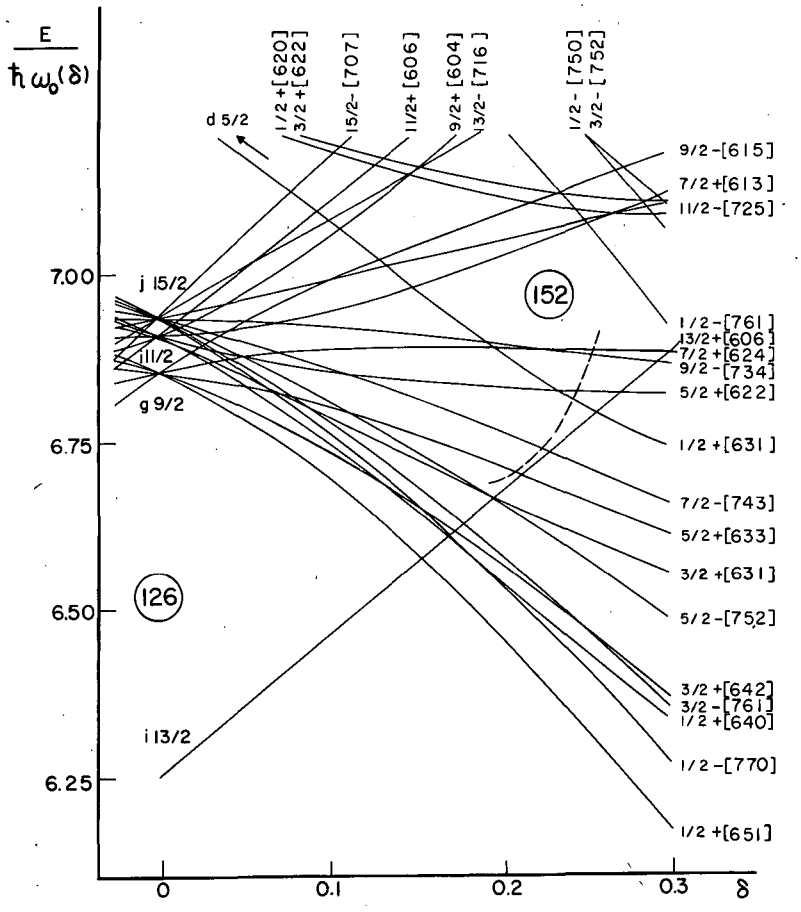

MU-15744

Fig. 18. Nilsson diagram for neutrons in the region $126 \leq N \leq 160$. The dashed line indicates very roughly the deformations thought to be appropriate to actinide isotopes.

In addition to the quantum numbers I and m_I, he introduces several other quantum numbers to distinguish the different single-particle states in a nonspherical field. These are K, the component of I along the nuclear symmetry axis; the parity, $\pi = \pm$; N, the total number of nodes perpendicular to the symmetry axis; Λ, the component of the particle's orbital angular momentum along the symmetry axis; Σ, the spin component along the symmetry axis, and $\Omega = \Lambda + \Sigma$. The state of a nucleon is written in this notation as $K\pi\left[Nn_z\,\Lambda\right]$. Figure 19 shows the relationships among these quantum numbers.

A rotational band is associated with each intrinsic configuration. The energy of the rotational levels is approximately given by

$$E_{rot.} = \frac{\hbar^2}{2\mathcal{I}}\left[I(I+1) + d(-)^{I+1}(I+1/2)\,\delta\,(K, 1/2)\right]. \qquad \text{(III-38)}$$

Here $\mathcal{I}$ is the effective moment of inertia of the nucleus, and d is the decoupling constant. If $K = 1/2$, this formula shows that the level $I = K = 1/2$ may not necessarily lie lowest.

The irregularity in the observed energy levels of Pa^{233} suggest that they belong to a $K = 1/2$ band. Mottelson finds that the levels are fitted quite well by assuming $\hbar^2/2\mathcal{I} = 6$ kev and $d = -1.3$.[43] Figure 20 shows the observed vs the theoretical levels of the $K = 1/2$ band. Thus the observed spin $I = 3/2$ is in agreement with this interpretation. The 91st proton in Pa^{233} is assigned the orbital $1/2-\left[530\right]$ (see Fig. 17).

An expression for the nuclear-dipole moment μ_I, in terms of the eigenvectors $a_{\ell\Lambda}$ of the last odd nucleon has been given by Nilsson.[41] For $K = 1/2$, it is

$$\mu_I = \frac{1}{I+1}\left\{(g_S - g_L)\left[\frac{1}{4}\sum_{\ell}\left(a_{10}^{\,2} - a_{\ell 1}^{\,2}\right) + (-)^{I-\frac{1}{2}+\ell}\frac{1}{2}\left(I+\frac{1}{2}\right)\Sigma_{\ell}\,a_{10}^{\,2}\right]\right.$$
$$\left. + (g_L - g_R)\left[\frac{1}{4} + (-)^{I-\frac{1}{2}}\frac{1}{2}\left(I+\frac{1}{2}\right)d\right] + g_R I(I+1)\right\}. \qquad \text{(III-39)}$$

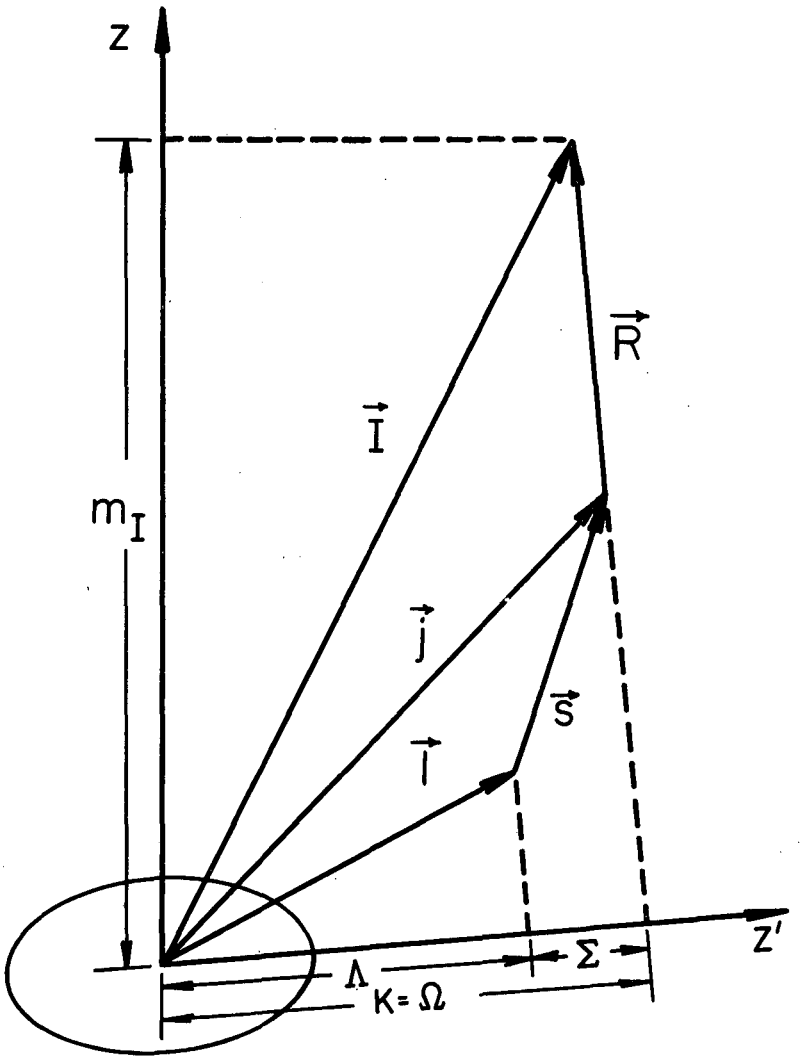

Fig. 19. Angular-momentum relationships for deformed nuclei in the ground state.

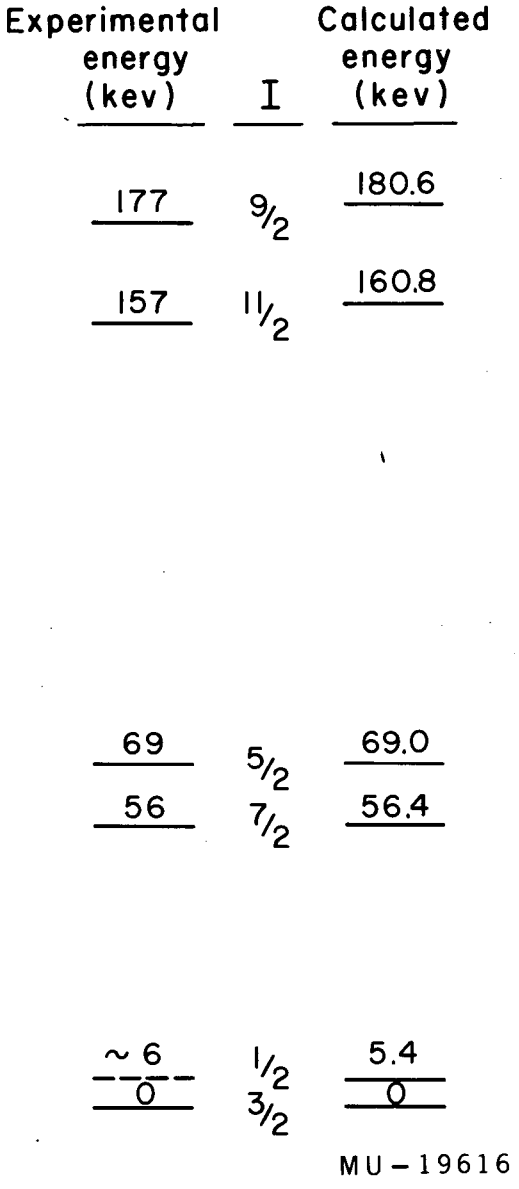

Fig. 20. The K=1/2 nuclear rotational band of Pa^{233}.

Here we have $g_S = \begin{pmatrix} 5.585 \\ -3.826 \end{pmatrix}$ and $g_L = \begin{pmatrix} 1 \\ 0 \end{pmatrix}$ for protons and neutrons, respectively. The g factor of the core, g_R, is equal to $Z/A \cong 0.4$ for a uniformly charged nucleus. The nuclear moment μ_I, was calculated from the revised wave functions of Mottelson-Nilsson.[42] The results for $d = -1.3\varepsilon$ are:

δ	$\cong$	0	0.1	0.2	0.3
μ_I(nm)	=	2.09	2.32	2.63	2.77

where δ is a parameter that characterizes the eccentricity of the nuclear potential. Nuclear systematics indicate that $\delta \cong 0.23$,[44] although this value of δ predicts that $d = -2.5$. The value of δ may be estimated from the measured nuclear Q. The intrinsic quadrupole moment, Q_o, is approximately

$$Q_0 = (4/5)ZR_0^2\,\delta\,(1+\frac{1}{2}\,\delta)\,, \qquad \text{(III-40)}$$

$R_0 \cong 1.2\times10^{-13}\,A^{1/3}$ cm is the mean charge radius of the nucleus. The relation between Q and Q_0 is

$$Q = \frac{3K^2-I(I+1)}{(I+1)\,(2I+3)}\,Q_0 \qquad \text{(III-41)}$$

For $K = \frac{1}{2}$ and $I = 3/2$, we have $Q_0 = -5Q$. The measured Q is -3.0 barns; therefore Q_0 is +15 barns, and δ is 0.3. The predicted value of the nuclear moment corresponding to $\delta = 0.3$ is $\mu_I = 2.77$ nm. This value is intermediate between the inferred moment of 2.1 nm and the measured moment of 3.4 (1.2) nm. For a nuclear spin, $I = 3/2$, the measured Q can be negative only if $K = \frac{1}{2}$. Thus the observed sign and magnitude of Q are in agreement with the configuration assignment $\frac{1}{2}\,-\,[530]$ for the odd proton.

E. Summary

The electronic angular momenta and associated g factors of the three lowest-lying energy levels of protactinium have been measured. The results are:

$J=11/2 \quad g_J = -0.8141(4)$

$J=9/2 \quad g_J = -0.8062(15)$

$J=7/2 \quad g_J = -0.7923(15)$.

The L-S coupling model is unsatisfactory because it predicts that the lowest-lying levels should be the J=11/2, 13/2, 15/2, and 17/2 multiplet of the term ^4K. The J-J coupling model, on the other hand, correctly predicts the observed level sequence, as arising from the interaction of the system $(5f)^2\ ^3H_4$ with (6d) $^2D_{3/2}$ to yield J=11/2, 9/2, 7/2, and 5/2. The calculated energy separations are in agreement with very crude estimates that can be made from observed resonance intensities. The g_J values calculated by means of the J-J model in the first order of perturbation are (for $\lambda = \frac{1}{2}$)

$J=11/2 \quad g_J = -0.796,$

$J=9/2 \quad g_J = -0.794,$

and

$J=7/2 \quad g_J = -0.757$.

Thus we see that although the J-J coupling model provides the most accurate basis for interpretation of the electronic coupling, the real situation is significantly more complicated. The reason as shown by the previous calculations, is that the electrostatic interaction between shells is comparable with the fine-structure interaction. The J-J coupling approximation should improve for the heavier actinides, because the fine-structure interaction which increases with the fourth power of $Z_{effective}$ will predominate over the electrostatic interaction.

The nuclear spin is measured to be I = 3/2. From the measured dipole-interaction constant, a = 595 (40) Mc, and the quadrupole interaction constant, b = - 2400(300) Mc, we have inferred that μ_I=2.1 nm

and $Q = -3.0$ barns. The nuclear moments are subject to errors arising from incomplete knowledge of the electronic wave functions and uncertainty in the value of $\left\langle 1/r^3 \right\rangle$. The dipole moment μ_I has been measured directly from its interaction with the applied magnetic field. The result is $\mu_I = 3.4\ (1.2)$ nm. We have shown that the second-order perturbation from the $J=9/2$ level does not effect the data sufficiently to alter the measured μ_I. The value of μ_I calculated on the basis of the spheroidal-core model of the nucleus is 2.77 nm. The sign of the measured quadrupole moment is negative, in agreement with the orbital assignment $\frac{1}{2}\,-\left[530\right]$ of the 91st proton in Pa^{233}.

IV. AMERICIUM-241

A. Introduction

Americium was first sythesized and identified by Seaborg, James, Morgan, and Ghiorso, in 1944.[26] Fred and Tomkins[43] photographed the spectrum of Am(I) with a 30-ft. spectrograph, and observed many lines with wide hfs, all with 6 components. They concluded that I=5/2. Later, Thorne[46] observed the spark spectra of Am^{241} and confirmed that I=5/2. Manning, Fred, and Tomkins[47] determined the dipole moment $\mu_I = 1.4$ nm from spark lines in the ground $(5f)^7(7s)\ ^9S_4$ and $^7S_3$ terms, using the Goudsmit Fermi-Segrè formula. They determined the quadrupole moment $Q = 4.9$ barns from arc lines due to transitions from $(5f)^7 7s7p\ ^{10}P_{9/2}$ and $^{10}P_{7/2}$ to $(5f)^7(7s)^2\ ^8S_{7/2}$. Fred and Tomkins[48,49] have measured over 3000 americium lines. To date, they have classified 112 Am(I) lines and 173 Am(II) lines, but have made only a few term assignments in the excited spectra. They have measured the ionization potential of Am(I) to be 6.0 ev.

The objective of this research was to measure the electronic g factor, g_J, and the hfs interaction constants a and b. They can be interpreted to yield information concerning the coupling of electrons in the electronic ground state. Furthermore, the values of a and b together with the optically measured nuclear moments can serve as a basis for determining the moments of other americium isotopes(see section V).

The results of the g_J measurement of americium, taken together with the curium data,[9] are very significant. The ground-state configuration of curium is $(5f)^7 6d(7s)^2$, giving rise to four low-lying levels. The observed g_J values of these levels are in good agreement with values calculated on the assumption that the 5f electrons couple to a pure Hund's-rule ground state, $^8S_{7/2}$, which then interacts with a slightly perturbed $^2D_{3/2}$ state of the 6d electron.

However, the results of the present investigation definitely show that the g_J value of americium, which has a $(5f)^7(7s)^2$ ground-state configuration, is less than the pure L-S coupled g_J by several percent. Since the $(5f)^7$ configuration of curium should have approximately the same g_J value as americium, this indicates that the previous agreement in curium was most likely accidental. More recent calculations of the curium g_J factors in intermediate coupling show that they can be fitted on the assumption of an impure $(5f)^7$ ground state.[32]

B. Beam Production

Americium-241 was obtained from the A. E. C. stockpile in a weak HCl solution. The isotope was identified by a pulse-height analysis of its γ spectrum with a RCL 256-channel analyser.

We experimented with several chemical procedures before finding one that would produce a satisfactory beam of atoms. The carbon-reduction method described in section IIIB yielded a weak beam constituted mainly of molecules. Next a barium reduction technique in which barium metal is added to $AmFl_3$ was unsuccessfully tried. The success of this method depends upon holding the mixture in equilibrium at a critical temperature until the reduction process is completed. In the atomic-beam apparatus, there is no fine control over the reaction rate, and the barium would boil out of the oven before the reduction could take place.

An atomic beam was eventually made by using lanthanum metal to reduce americium oxide. The procedure is, first, to separate approximately 10 mg of americium from the stock solution, and then to add concentrated NH_4OH dropwise until a white $Am(OH)_3$ precipitate forms. Next the precipitate is transferred to a platinum crucible and is heated in an induction heater until it becomes oxidized. The americium oxide is then transferred to the inner liner of the atomic-beam oven. An excess of lanthanum metal is added. The oven (Fig. 21)

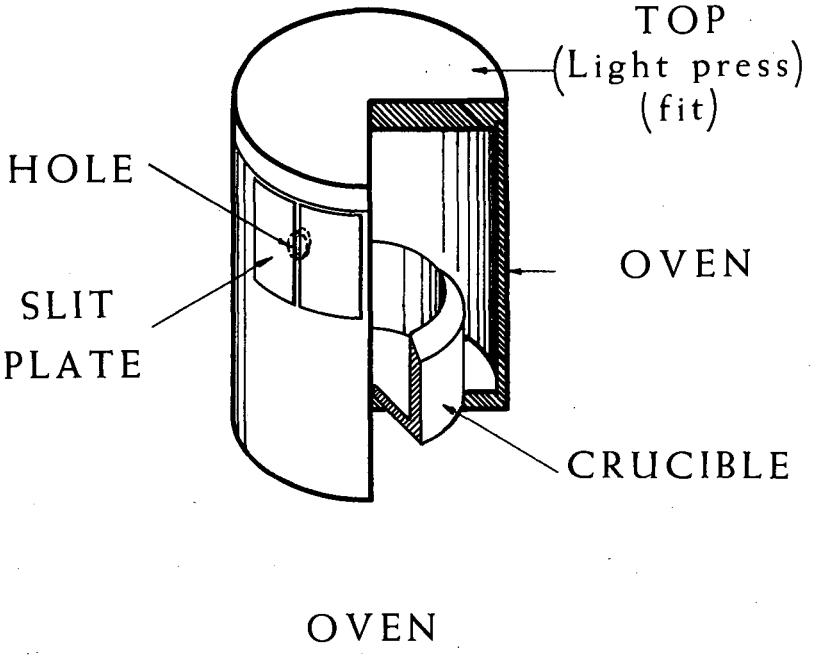

Fig. 21. Cutaway view of molybdenum oven used for production of the americium beam.

is made from molybdenum and has a sharp edged inner liner to prevent the lanthanum from creeping up the wall of the oven and clogging the slit. After the oven is inserted and heated to a temperature of about 1000°C, a beam of atoms with a throwout ratio of 20/1 is formed. The reduction process takes place very rapidly, and one must be careful to lower the temperature before too much of the material escapes.

After the initial success of the method, it was used exclusively for the remainder of the investigation, and no subsequent failures occurred. We found, on the average, that 1 mg of americium-241 would yield a full beam of 100 counts per minute (c/m) at the detector for approximately 1 hr. Typical resonance intensities were about 2 c/m. The counting of the platinum discs exposed during the runs was done in 2π alpha counters with backgrounds of 0.1 c/m.

C. Experimental Observations

A search to find transitions between the Zeeman components of the hfs of Am^{241} was performed at a field of 2.1 gauss. Four resonances were observed (Fig. 22), each of which approximately fit the low-field formula

$$\nu = \frac{F(F+1) + J(J+1) - I(I+1)}{2F(F+1)} g_J \mu_0 H_z / h, \qquad \text{(IV-1)}$$

with I=5/2 and J=7/2, but with g_J significantly smaller than the L-S coupled value of 2.002. Figure 23 is a schematic of the hfs splitting of a system with I=5/2 and J=7/2. In order to improve the precision of the g_J measurement, and to measure the hfs interaction constants, we decided to follow the resonance associated with the state F=6 to higher values of the magnetic field. Resonances were observed at 8.2, 12.1, and 20.8 gauss.

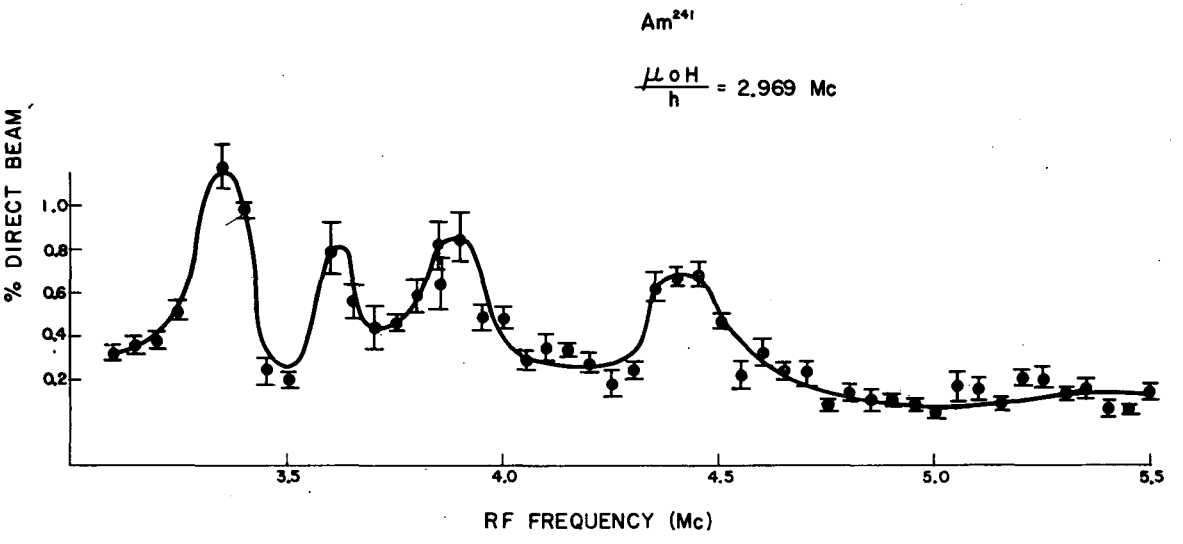

MU-19817

Fig. 22. Results of Am^{241} low-field search at 2.1 gauss.

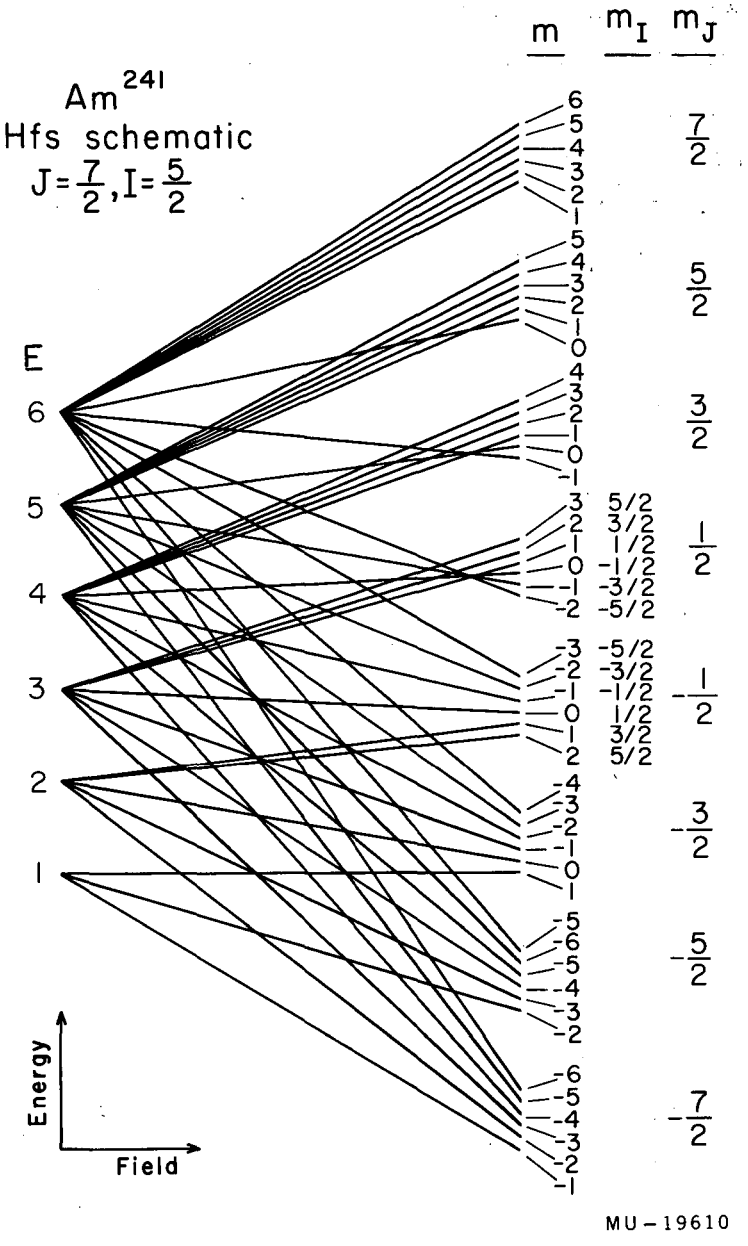

Fig. 23. Schematic diagram of the hyperfine-structure levels of Am^{241} in a magnetic field.

With the aid of the IBM-653 computer routines discussed in section IIC, the data was fitted to the transition $(6, -2 \leftrightarrow 6, -3)$. Fairly satisfactory agreement between experiment and theory was obtained from the values $a = 7$ Mc, $b/a = 0$, and $g_J = -1.9$. These values were then used to predict transition frequencies at higher values of the field. Resonances were found successively at 26.5, and 36.2 gauss, but in each case the resonant frequency differed from the predicted frequency by much more than the uncertainties in a, b, and g_J could account for.

Because the hfs constants are small, the high-field solution to the Hamiltonian is a good approximation to use at the last value of the magnetic field. The eigenvalue of the Hamiltonian in a high-field or $m_I m_J$ representation is given by Eqs. (II7) plus (II21). Omitting higher-order interactions than k = 2 gives

$$W = g_J \mu_0 H_z m_J + g_I \mu_0 H_z m_I + a m_J m_I + b \frac{\left[3m_J^2 - J(J+1)\right]\left[3m_I^2 - I(I+1)\right]}{4I(2I-1)\,J\,(2J-1)} . \quad \text{(IV2)}$$

The frequency of a $\Delta F=0$ transition at high fields becomes

$$\nu = g_J \mu_0 H_z / h + \text{constant}. \quad \text{(IV3)}$$

Instead of using the approximate values of a, b, and g_J to predict the frequencies at higher values of the field, we used an extrapolation method based on Eq. (IV-3). In this way, resonances were successively observed at 46.1, 71.6, 93.0, 121.7, 250.4, and 540.9 gauss. From the last few resonances, we could obtain the value of g_J, because we have

$$g_J = h\,(\nu_2 - \nu_1)/\mu_0(H_2 - H_1), \quad \text{(IV-4)}$$

where the subscripts 1 and 2 refer to a particular high-field measurement. Using this measured value of g_J, we attempted to determine a and b from the observed data; but no values of a and b could be found that would fit the data to the transition $(6, -2 \longleftrightarrow 6, -3)$.

We decided to make a search at the highest field reached, namely 540.9 gauss, in order to find the other flop-in transitions. Their measurement would yield a direct determination of a, which is independent of the value of g_J. The theoretical frequencies of these transitions are

$$\nu_6(-5/2, 1/2 \longleftrightarrow -5/2, -1/2) = (g_J\mu_0 H_z - 5a/2)/h$$

$$\nu_5(-3/2, 1/2 \longleftrightarrow -3/2, -1/2) = (g_J\mu_0 H_z - 3a/2)/h$$

$$\nu_4(-1/2, 1/2 \longleftrightarrow -1/2, -1/2) = (g_J\mu_0 H_z - a/2)/h$$

and

$$\nu_3(+1/2, 1/2 \longleftrightarrow +1/2, -1/2) = (g_J\mu_0 H_z + a/2)/h \qquad \text{(IV-5)}$$

The $m_I m_J$ quantum numbers are written in the parentheses. The subscript is the value of F that this transition is associated with at low field. Since the quadrupole interaction depends quadratically on m_I and m_J, b does not enter into the high-field expression for ν.

The frequency separation between any two adjacent resonances is exactly equal to a/h Mc. One resonance, presumably due to the transition ν_6, had been observed at 540.9 gauss. The other three $\Delta F=0$ transitions must occur at the frequencies ν_6+a/h, ν_6+2a/h, and ν_6+3a/h. Starting from the observed resonance frequency, exposures were taken at 1-Mc intervals. The line width at this field was also 1 Mc, thus permitting the use of such large frequency increments.

Four resonances were observed, two at higher frequencies than the first observed resonance, and two at lower frequencies. The five resonances were spaced at regular intervals of approximately 17 Mc each (Fig. 24). These results were very significant, because they enabled us to correctly interpret the previous data. At 20.8 gauss, we had observed the transition ν_4 rather than ν_6, without

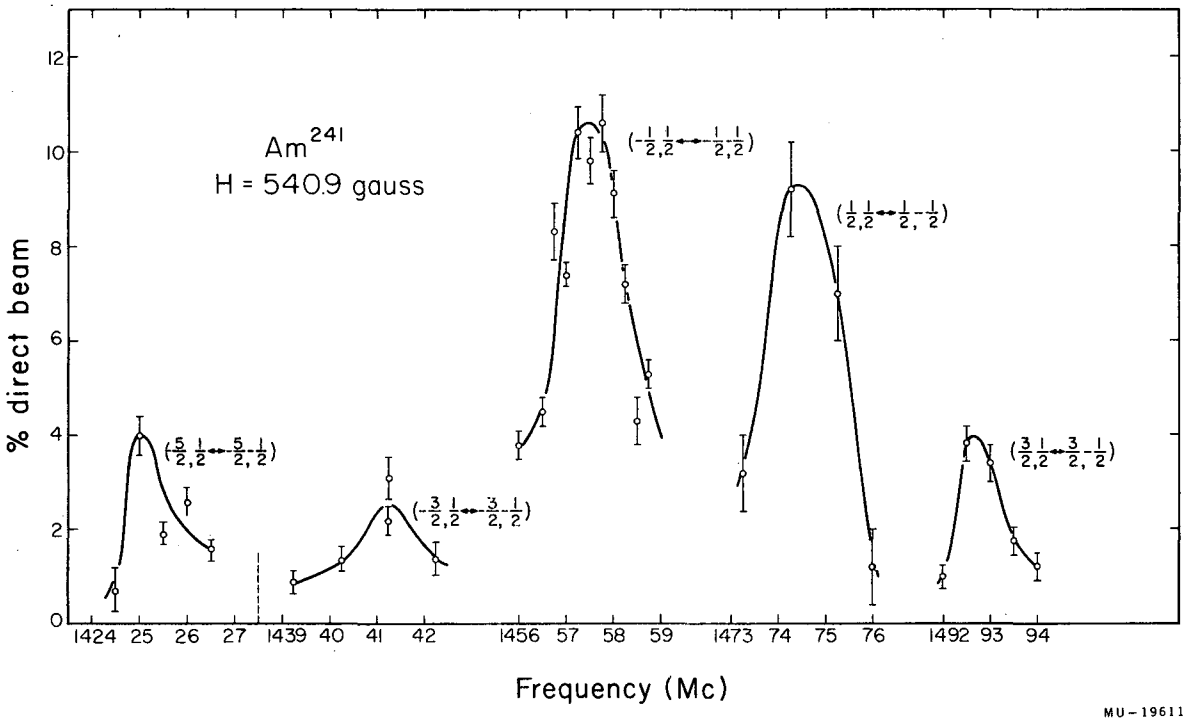

Fig. 24. Observed Am^{241} resonances at 540.9 gauss.

realizing it. All subsequently observed high-field resonances were due to this same transition, ν_4. The resonance at 8.2 gauss was also incorrectly identified. It is the transition ν_5. The fifth resonance at 540.9 gauss is the first of the two $\Delta F=1$, $\Delta m=1$ transitions:

$$\nu(3/2, 1/2 \longleftrightarrow 3/2, -1/2) = (g_J \mu_0 H_z + 3a/2)/h$$

and (IV-6)

$$\nu(5/2, 1/2 \longleftrightarrow 5/2, -1/2) = (g_J \mu_0 H_z + 5a/2)/h .$$

Having correctly identified the resonances, we obtained close agreement between experimental frequencies, and theoretical frequencies calculated from $g_J = -1.937$, $a = 17$ Mc, and $b/a = -7$. These values of a and b imply that the frequencies associated with the F=6 and F=5 flop-in transitions cross at a field of about 5 gauss. This fact helps to explain why we inadvertently jumped from one transition to another when the field was increased.

The zero-field separations between the hfs levels were calculated from the values of a and b that fitted the data best. A search was then made at 1.4 gauss to find the direct transitions allowed by the selection rules $\Delta F=\pm 1$, $\Delta m=0, \pm 1$. Four different $\Delta m=0$ or sigma transitions were induced (see Fig. 25).

All observed data is presented in Table X. Values of a, b, and g_J were determined with the IBM-704 routine previously described. The results for $g_I > 0$ are:

$$a = \pm 17.144(8) \text{ Mc}$$
$$b = \mp 123.82(10) \text{ Mc}$$
$$g_J = -1.9369(3)$$
$$\chi^2 = 2.9.$$

Figure 26 shows the behavior of the hfs levels as a function of b/a. The results of negative g_I were identical for this number of significant digits.

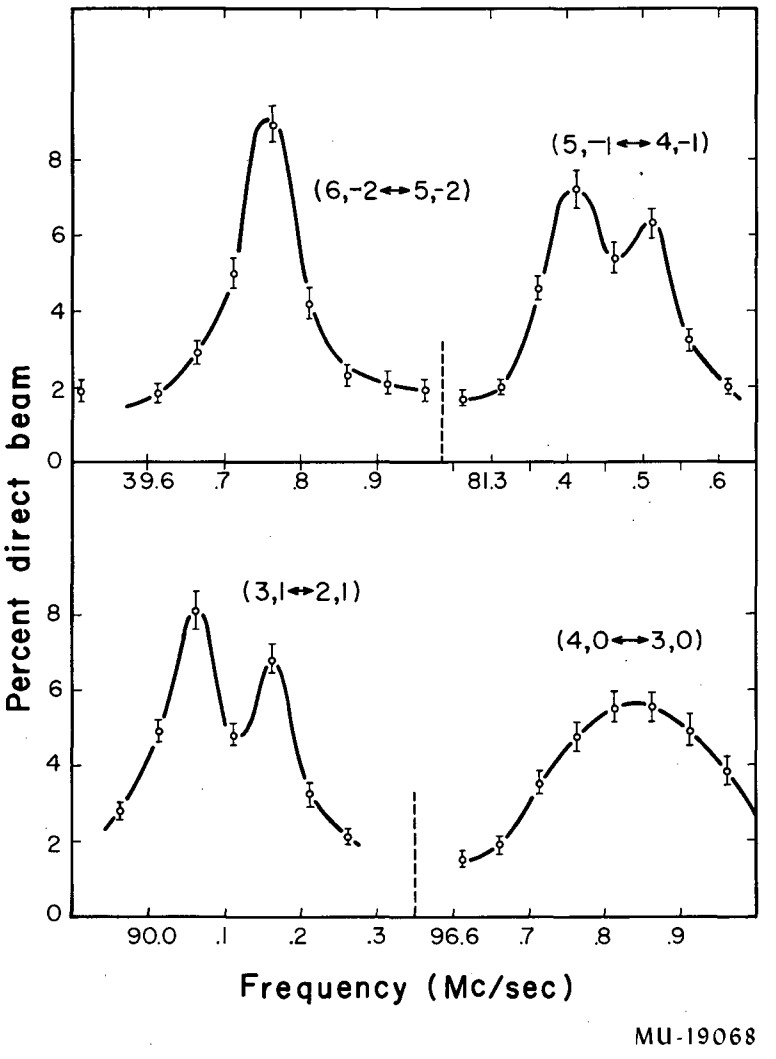

Fig. 25. Observed $\Delta F=1$ transitions of Am^{241} at 1.4 gauss.

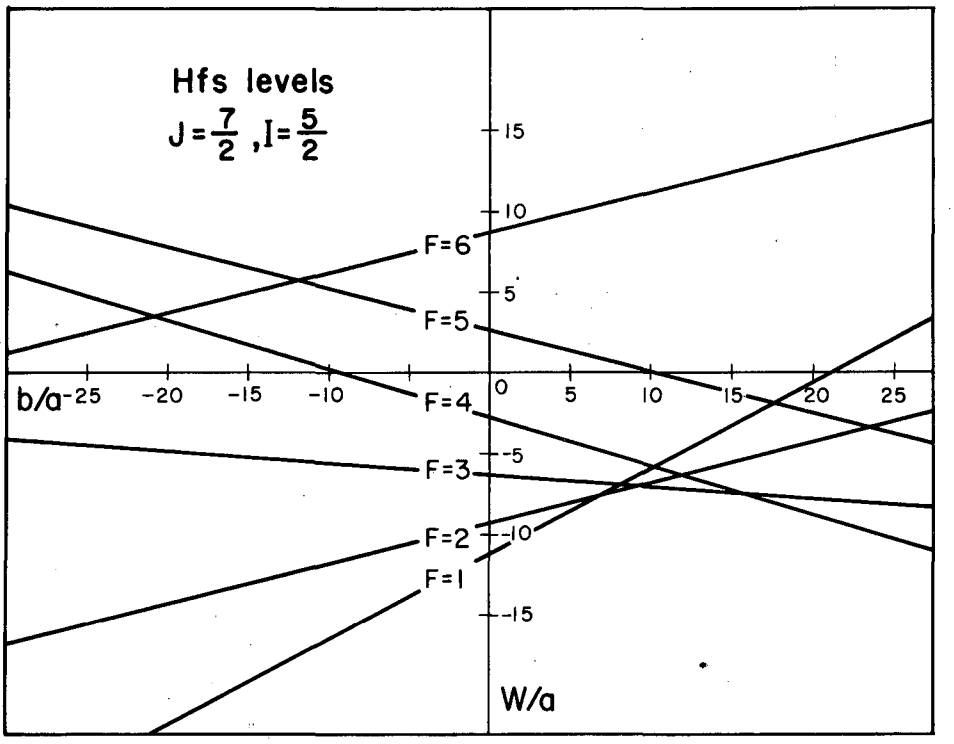

MU-19258

Fig. 26. Hyperfine-structure energy levels of the system I=5/2, J=7/2 in the absence of an applied field. W_{hfs}/a vs b/a.

Table X

Am^{241} Data

Data No.	H (gauss)	$\nu_{obs.}$ (Mc)	$\nu_{obs.} - \nu_{calc.}$ (Mc)	Transition
1	8.248(40)	14.08(07)	-0.02	b
2	12.150(38)	21.95(10)	-0.01	c
3	20.754(35)	42.35(25)	0.15	a
4	20.754(35)	39.86(10)	0.03	c
5	26.517(44)	56.30(20)	-0.18	a
6	36.198(41)	82.40(20)	-0.04	a
7	46.077(47)	110.45(25)	0.05	a
8	71.628(39)	181.85(30)	-0.02	a
9	93.043(40)	240.80(40)	-0.13	a
10	121.670(42)	319.10(50)	-0.19	a
11	169.074(59)	448.50(60)	0.06	a
12	250.442(81)	669.60(60)	0.09	a
13	540.90(15)	1425.0 (8)	0.20	c
14	540.90(15)	1441.2 (1.0)	0.41	b
15	540.90(15)	1457.5 (1.0)	0.06	a
16	540.90(15)	1474.5 (6)	-0.14	$(3,1 \longleftrightarrow 3,0)$
17	540.90(15)	1492.7 (6)	0.35	$(3,2 \longleftrightarrow 2,1)$

Table X (continued)

Am^{241} Data				
Data No.				
18	1.418(28)	90.10(10)	-0.01	(3, 1⟷2,1)
19	1.418(28)	96.84(12)	0.00	(4, 0⟷3,0)
20	1.418(28)	81.45(10)	0.01	(5, -1⟷4, -1)
21	1.418(28)	39.75(05)	0.00	(6, -2⟷4, -2)

[a](4, 0⟷4, -1)

[b](5, 1⟷5, -2)

[c](6, -2⟷6, -3)

The uncertainties in the individual frequency measurements which in turn determine χ^2 as well as the uncertainties in a, b, and g_J, are chosen arbitrarily as one-half of the full width at half-maximum. There are 22 sets of data fitted to three parameters, to give 19 degrees of freedom. The value of χ^2 which corresponds to P=0.3 is 21.7.[28] Thus the calculated uncertainties are probably about $(21.7/2.9)^{1/2} = 2.7$ times as small as the rms uncertainties. This factor allows for unknown systematic errors. To account for field-dependent systematic errors affecting g_J, we take one part per 2000 as the uncertainty. In the next section, an independent measurement of the g_J of Am^{242} is made. The weighted mean is

$$g_J = -1.9371(10) .$$

In principle, there can be higher-order interaction constants than dipole and quadrupole. The limitation is that the highest-order pole must be equal to 2I or 2J, whichever is smaller. To within the accuracy of the experiment, no higher-order multipoles were observed.

D. Electronic Structure

1. Electronic Coupling

The observed value of $g_J = -1.9371(10)$ is significantly different from the L-S coupled value of -2.002. The major contribution to this deviation comes from the breakdown of L-S coupling. The possible terms of an f^7 configuration have been given by Condon and Shortley:[31]

^8S ^6PDFGHI $^4SPDFGHIKLMN$ $^2SPDFGHIKLMNOQ$

226575533 257 $\sqrt{}$ 997542

10

The number beneath the term designation shows the number of times this term occurs in the configuration. The fine-structure interaction couples states, that differ by $\Delta L=0\pm1$, $\Delta S=0\pm1$, and $\Delta J=0$. Thus only the ^6P term is mixed into the ground state by the second-order perturbation. However, a ground state that is a linear combination of ^8S and ^6P has no matrix element of the quadrupole interaction. Thus it is necessary to include the ^6D term, which is admixed in the next higher order of the perturbation. The ground-state wave function in this approximation is written

$$\left|Jm_J\right) = (1-\alpha^2-\beta^2)^{1/2}\left|{}^8S_{7/2}m_J\right) + \alpha\left|{}^6P_{7/2}m_J\right) + \beta\left|{}^6D_{7/2}m_J\right), \tag{IV-7}$$

where

$$\alpha = -\left({}^8S_{7/2}\left|\sum_i a_{5f}\vec{l}_i\cdot\vec{s}_i\right|{}^6P_{7/2}\right)/E({}^6P) \tag{IV-8a}$$

and

$$\beta = -\left({}^6P_{7/2}\left|\sum_i a_{5f}\vec{l}_i\cdot\vec{s}_i\right|{}^6D_{7/2}\right)/E({}^6D)\,. \tag{IV-8b}$$

Here $E(^6P)$ and $E(^6D)$ are the energies of the ^6P and ^6D terms with respect to the ^8S ground term and a_{5f} is the find structure of a 5f electron. The magnetic quantum numbers in Eq. (IV-8) are omitted since the matrix elements are independent of them. Using the results derived in the next section, α and β may be written

$$\alpha = (14)^{1/2}a_{5f}/E(^6P), \text{ and } \qquad \beta = (9/10)\,(5/14)^{1/2}\,\alpha^2/1.1\,.$$

The value of α which yields the measured g_J value is

$$\left|\alpha_{obs.}\right| = 0.46(1)\,.$$

An approximate value of a_{5f} deduced from optical data in Am(III) is 2700 cm^{-1}.[50] The separation of the ^6P and ^8S terms of Cm^{+3} in a crystalline field of $LaCl_3$ was found to be 25,000 cm^{-1}.[51] Using these values gives

$$\left|\alpha_{calc.}\right| = 0.40\,.$$

The agreement between the observed and calculated values of a is close enough to show that the observed g_J can be interpreted on the basis of the breakdown of L-S coupling. Because a is so large, the perturbation treatment is probably inaccurate. Therefore the eigenvectors were calculated more accurately with the aid of the IBM-704 eigenvalue routine described in section IIC. We will discuss the results of this calculation in the next section, after first deriving the appropriate matrix elements of the electrostatic and spin-orbit energy.

2. Electrostatic and Spin-Orbit Energy

The electrostatic energy is calculated by means of the diagonal sum rule. This says that the sum of the roots of the secular equation is equal to the sum of the diagonal matrix elements occurring in it. Following the method of Condon and Shortley,[31] we classify the zero-order states of f^7 according to m_S and m_L. Only $m_S=5/2$ needs to be listed, because we are interested only in the sextet terms:

m_S	m_L			
5/2	6	A	$(3^+2^+1^+0^+ - 1^+ -2^+3^-)$	$[^6I]$
5/2	5	B	$(3^+2^+1^+0^+ - 1^+ -2^+2^-)$	$[^6I$
		C	$(3^+2^+1^+0^+ - 1^+ -3^+3^-)$	$^6H]$
5/2	4	D	$(3^+2^+1^+0^+ - 1^+ -2^+0^-)$	$[^6I$
		E	$(3^+2^+1^+0^+ - 1^+ -3^+2^-)$	^6H
		F	$(3^+2^+1^+0^+ - 2^+ -3^+3^-)$	$^6G]$
5/2	3	G	$(3^+2^+1^+0^+ - 1^+ -2^+0^-)$	$[^6I$
		H	$(3^+2^+1^+0^+ - 1^+ -3^+1^-)$	^6H
		I	$(3^+2^+1^+0^+ - 2^+ -3^+2^-)$	^6G
		J	$(3^+2^+1^+ -1^+ -2^+ -3^+3^-)$	$^6F]$
5/2	2	K	$(3^+2^+1^+0^+ -1^+ -2^+ -1^-)$	$[^6I$
		L	$(3^+2^+1^+0^+ -1^+ -3^+ 0^-)$	^6H
		M	$(3^+2^+1^+0^+ -2^+ -3^+ 1^-)$	^6G
		N	$(3^+2^+1^+ -1^+ -2^+ -3^+2^-)$	^6F
		O	$(3^+2^+0^+ -1^+ -2^+ -3^+3^-)$	$^6D]$

m_S	m_L			
5/2	1	P	$(3^+2^+1^+0^+ -1^+ -2^+ -2^-)$	^6I
		Q	$(3^+2^+1^+0^+ -1^+ -3^+ -1^-)$	^6H
		R	$(3^+2^+1^+0^+ -2^+ -3^+ 0^-)$	^6G
		S	$(3^+2^+1^+ -1^+ -2^+ -2^+3^-)$	^6F
		T	$(3^+2^+0^+ -1^+ -2^+ -3^+2^-)$	^6D
		U	$(3^+1^+0^+ -1^+ -2^+ -3^+3^-)$	^6P .

The terms that have components in each partition are placed in the brackets. Writing ^6I for the first-order energy of the term ^6I, and **A** for the diagonal matrix element of **A**, etc., (it will be clear from the context whether **A** is a wave function or a matrix element) we obtain:

$$^6I = A$$

$$^6I + {}^6H = B + C$$

$$^6H = B + C - A$$

etc.

The diagonal matrix elements A, B, ... U can be written as a sum over Slater intergrals, by using $7^6(7)$ and Table 2^6 of Condon and Shortley.[31] The term energies become:

$$^8S = 0$$

$$^6P = 15F_2 + 165F_4 + 3003F_6$$

$$^6D = 41F_2 + 297F_4 + 1001F_6$$

$$^6F = 70F_2 + 231F_4 + 2002F_6$$

$$^6G = 90F_2 + 101F_4 + 1638F_6$$

$$^6H = 85F_2 + 249F_4 + 1729F_6$$

$$^6I = 35F_2 + 189F_4 + 1715F_6 , \qquad \text{(IV-9)}$$

where $F_2 = F^2/225$, $F_4 = F^4/1089$, $F_6 = F^6/7361.64$, and $F_k = F_k(5f, 5f)$. The ratio of the F_k's is fairly insensitive to the form of the potential. Using hydrogenic wave functions, Elliott et al. calculated $F_4/F_2 = 0.142$ and $F_6/F_2 = 0.0161$.[52] We have also calculated these ratios from the uranium wave functions of Cohen (see Table VI), and find $F_4/F_2 = 0.1586$ and $F_6/F_2 = 0.02037$. These ratios predict the following energies for the terms of interest:

	(1)	(2)	
$^8S =$	0	0	
$^6P =$	86.8	102.3	
$^6D =$	99.3	108.5 ,	(IV-10)

where columns (1) and (2) give the electrostatic energy in units of F_2, for the two F_k ratios determined from hydrogenic and uranium wave functions, respectively.

To find the spin-orbit-energy matrix elements, we first expand the $SLJm_J$ wave function into the sum of antisymmetric zero-order states. The $^8S_{7/2}$ wave function is obviously

$$^8S_{7/2}\ 7/2) = (3^+2^+1^+0^+ - 1^+-2^+ -3^+) . \qquad \text{(IV-11)}$$

The wave functions of the other two terms are obtained by the procedure described in Condon and Shortley.[31] The lowering operator $L_- = L_x - iL_y$ is applied to $A = |^6I\ m_L=6)$. This yields $^6I\ m_L=5)$. Then $|^6H\ m_L=5)$ is determined from the fact that it is orthogonal to $|^6I\ m_L=5)$. This process is continued until all of the $|SLm_Sm_L)$ wave functions of $S=5/2$, $m_S=5/2$ have been obtained. The $SLJm_J$ states are then determined either by application of the operator $J_- = J_x - iJ_y$ to the state of maximum m_J, or else by use of Wigner coefficients to vector-add the SLm_Sm_L wave functions. In this way, the $^6P_{7/2}$ and $^6D_{7/2}$ wave functions were found to be

$$\left|{}^6P_{7/2}\ 7/2\right) = (3/28)^{1/2}\Big[P-(5/3)^{1/2}Q + (2)^{1/2}R - (2)^{1/2} S + (5/3)^{1/2}\,T - U\Big] \qquad \text{(IV-12)}$$

and

$$\left|{}^6D_{7/2}\ 7/2\right) = (5/6)(1/21)^{1/2}\Big[(5)^{1/2}\,P-(3)^{1/2}Q+(2/5)^{1/2}R-(3)^{1/2}T+(5)^{1/2}U\Big] \quad \downarrow +(2/5)^{1/2}S$$

$$-(1/3)(2/21)^{1/2}\ (K_3+K_2+K_1+K_0+K_{-2})$$

$$-(2)^{1/2}(L_3+L_2+L_1+L_{-1}+L_{-3})$$

$$+2(3/5)^{1/2}(M_3+M_2+M_0+M_{-2}+M_{-3})$$

$$-(2)^{1/2}(N_3+N_1+N_1+N_{-1}+N_{-2}+N_{-3})$$

$$+(0_2+0_0+0_{-1}+0_{-2}+0_{-3}) \ , \qquad \text{(IV-13)}$$

where K_3 is that wave function which results when $m_\ell=3^+$ in K is replaced by $m_\ell=3^-$. The other wave functions written with a subscript are defined similarly.

The matrix elements of the spin-orbit operator in the $s\ell m_s m_\ell$ scheme are

$$(s\ell m_s m_\ell \left|\vec{l}\cdot\vec{s}\right| s\ell' m_s' m_\ell') = \delta(\ell m;\ell' m')m_\ell m_s + 1/2\ \delta(m_s', m_s\pm1) \times\Big[(\ell-m+1/2)(\ell+m+1/2)\Big]^{1/2} \qquad \text{(IV-14)}$$

where $m = m_s + m_\ell$, and $m'=m_s' + m_\ell'$. The spin-orbit matrix elements in the $SLJm_J$ scheme are found by repeated application of formula (IV12) to the products occuring in the expansion of $(SLJm_J \left|\Delta\right| S'L'Jm_J)$, where Δ is $\sum_i a_{5f}\,\vec{l}_i\cdot\vec{s}_i$. The results are:

$$\left({}^8S_{7/2}\left|\mathbb{A}\right|{}^6P_{7/2}\right) = (14)^{1/2}\, a_{5f}$$

$$\left({}^6P_{7/2}\left|\mathbb{A}\right|{}^6D_{7/2}\right) = (9/10)\,(5)^{1/2}\, a_{5f}$$

$$\left({}^6P_{7/2}\left|\mathbb{A}\right|{}^6D_{7/2}\right) = 0$$

$$\left({}^6D_{7/2}\left|\mathbb{A}\right|{}^6D_{7/2}\right) = 0\,. \qquad \text{(IV-15)}$$

Adding the electrostatic energies in column (2) of (IV-10) to the spin-orbit energy yields the following matrix for the total energy W;

$$W = \begin{array}{c} \\ {}^8S \\ {}^6P \\ {}^6D \end{array} \begin{array}{c} \begin{array}{ccc} {}^8S & {}^6P & {}^6D \end{array} \\ \begin{bmatrix} 0 & (14)^{1/2}x & \\ (14)^{1/2}x & 102.3 & (9/10)(5)^{1/2}x \\ & (9/10)(5)^{1/2}x & 108.5 \end{bmatrix} \end{array}, \qquad \text{(IV-16)}$$

where $x = a_{5f}/F_2$. The eigenvalues of this matrix were computed by the IBM-704 computer for a range of values of x. The matrix that transformed W into diagonal form was then applied to the g matrix,

$$g_J = \begin{array}{c} \\ {}^8S \\ {}^6P \\ {}^6D \end{array} \begin{array}{c} \begin{array}{ccc} {}^8S & {}^6P & {}^6D \end{array} \\ \begin{bmatrix} 2.0023 & & \\ & 1.7159 & \\ & & 1.5886 \end{bmatrix} \end{array}, \qquad \text{(IV-17)}$$

to yield g_J as a function of x. The value of x corresponding to $g_J = -1.9371(10)$ is $x = 17.7(2)$. The eigenvalues are ${}^8S=0$, ${}^6P=123F_2$, and ${}^6D=203F_2$. The eigenvector of the ground state is

$$\left|\frac{7}{2}\ \frac{7}{2}\right) = 0.882\left|S_{\frac{7}{2}}\ \frac{7}{2}\right) - 0.457\left|P_{\frac{7}{2}}\ \frac{7}{2}\right) + 0.114\left|D_{\frac{7}{2}}\ \frac{7}{2}\right)\,. \qquad \text{(IV-18)}$$

Taking the optically observed $a_{5f}=2700\ cm^{-1}$ together with the measured $x=17.7$ yields $F_2=153\ cm^{-1}$ and $W(^6P) = 1880\ cm^{-1}$. This is in reasonable agreement with the 25,000 cm^{-1} separation between the ^8S and ^6P terms of Cm^{+3} in a crystalline field of $LaCl_3$,[51] because the crystalline field increases the interaction energy.

3. Hyperfine Structure

A pure ^8S ground term cannot give rise to any hfs interaction. Therefore we look first to the breakdown of L-S coupling as an explanation of the observed hfs. The hfs interaction constants will be calculated for the electronic ground state [Eq. (IV-18)]. Since μ_I and Q have been measured, this will give information relating to the electronic system.

The dipole constant, a, is equal to

$$a = -\mu_I(JJ \left| H_z \right| JJ)/IJ, \qquad \text{(IV-19)}$$

where H_z is the z component of the magnetic field at the nucleus due to all of the electrons and is given classically by

$$H_z = -2\mu_0 \sum_i (1/r_i^3) \left[\ell_z - \left[\frac{s_z \vec{r}^2 + 3(\vec{r}\cdot\vec{s})\, z}{r^2} \right]_i \right]. \qquad \text{(IV-20)}$$

The diagonal matrix elements in the zero-order scheme are[11]

$$(\ell s m_\ell m_s \left| H_z \right| \ell s m_\ell m_s) = -2\mu_0 \left\langle 1/r^3 \right\rangle_{n\ell} \sum_i \left[m_\ell - \frac{2m_s\left[3m_\ell^2 - \ell(\ell+1)\right]}{(2\ell-1)(2\ell+3)} \right]_i . \qquad \text{(IV-21)}$$

We will also need to evaluate matrix elements that are not diagonal in m_ℓ and m_s. By the Wigner-Eckart theorem, the matrix elements of $\vec{r}$ are proportional to those of $\vec{\ell}$. Therefore we have

$$(\ell s m_\ell m_s \left| H_s \right| \ell s m_\ell' m_s') = (\ell s m_\ell m_s \left| \sum_i \left\{ c_1 \ell_z + c_2 \left[\frac{3}{2}(\ell_z(\vec{\ell}\cdot\vec{s}) + (\vec{\ell}\cdot\vec{s})\ell_z) - s_z \ell^2 \right] \right\}_i \right| \ell s m_\ell' m_s'). \qquad \text{(IV-22)}$$

The constants c_1 and c_2 can be determined by setting the diagonal matrix element in (IV-22) equal to (IV-21). This yields

$$c_1 = -2\mu_0(1/r^3)$$

and

$$c_2 = 4\mu_0(1/r^3)/(2\ell - 1)(2\ell+3). \qquad \text{(IV-23)}$$

When these values of c_1 and c_2 are substituted into Eq. (IV-22), the matrix elements of the magnetic field can be calculated in the $\ell s m_\ell m_s$ scheme. Application of the field operator to the wave functions (IV-12) and (IV-13) yields the following nonvanishing matrix elements:

$$\left(\frac{7}{2}\ {}^6P_{7/2}\ \middle|H_z\middle|\ {}^6P_{7/2}\ \frac{7}{2}\right) = -(8/5)\mu_0\left\langle 1/r^3\right\rangle_{5f} \qquad \text{(IV-24)}$$

$$\left(\frac{7}{2}\ {}^8S_{7/2}\middle|\ H_z\middle|\ {}^6D_{7/2}\ \frac{7}{2}\right) = -(2/3)(14/15)^{1/2}\mu_0\left\langle 1/r^3\right\rangle_{5f} \qquad \text{(IV-25)}$$

The quadrupole interaction constant, b, can be written

$$b = -e^2Q(JJ\ \Big|\ \sum_i (3\cos^2\theta - 1)_i/r_i^3\ \Big|\ JJ). \qquad \text{(IV-26)}$$

The matrix element of $3\cos^2\theta - 1$ in the zero-order scheme is

$$(\ell s m_\ell m_s\ \Big|\ 3\cos^2\theta - 1\ \Big|\ \ell s m_\ell' m_s') = -2\delta(m_\ell m_s, m_\ell' m_s')\frac{3m_\ell^2 - \ell(\ell+1)}{(2\ell-1)(2\ell+3)}. \qquad \text{(IV-27)}$$

The only nonvanishing matrix element of this operator in the $|JJ)$ ground state is

$$\left(\frac{7}{2}\ {}^6P_{7/2}\middle|\ 3\cos^2\theta - 1\ \middle|\ {}^6D_{7/2}\ \frac{7}{2}\right) = 2(5)^{1/2}/15. \qquad \text{(IV-28)}$$

For the ground-state wave function (IV18), the hfs constants defined by Eq. (IV19) and (IV26) become

$$a=-(\mu_I\mu_0/IJ)\left\langle 1/r^3\right\rangle_{5f}\left[(-0.457)^2\left(\frac{7}{2}\ {}^6P_{7/2}\left|H_z\right|{}^6P_{7/2}\ \frac{7}{2}\right)\right.$$

$$\left.+2(0.882)(0.114)\left(\frac{7}{2}\ {}^8S_{7/2}\left|H_z\right|{}^6D_{7/2}\ \frac{7}{2}\right)\right] \quad \text{(IV-29)}$$

and

$$b=-e^2Q2(-0.457)\ (0.114)\left(\frac{7}{2}\ {}^6P_{7/2}\left|3\cos^2\theta-1\right|{}^6D_{7/2}\ \frac{7}{2}\right). \quad \text{(IV-30)}$$

Evaluation of these expressions, using the optically measured nuclear moments $\mu_I=1.4$ nm and $Q=4.9$ barns, and the values of $\left\langle 1/r^3\right\rangle_{5f}$ $\left\langle 1/r^3\right\rangle_{5f}=3.99\ a_0^{-3}$ and " $\left\langle 1/r^3\right\rangle$ " $_{5f}=3.89\ a_0^{-3}$, yields

$$a=+16.6 \text{ Mc}$$

and

$$b=+137 \text{ Mc}.$$

These numbers agree in magnitude very well with the measured values

$$a=\mp 17.144(8) \text{ Mc}$$

and

$$b=\pm 123.82(10) \text{ Mc},$$

but there is a disagreement in the sign of one of the hfs constants. This is similar to the situation in other atoms with half-filled shells, namely $Mn\ (3d)^5$ and $Eu\ (4f)^7$. Heine has calculated the effect of the exchange interaction between the half-filled shell and the core "s" electrons in Mn^{++} and was able to obtain agreement with the observed hfs.[53] In Eu, the sign and magnitude of the measured a and b disagree with the calculated values.[54] However, the measured quadrupole constant in Eu is only of the order of 1 Mc. This could be due to the relativistic breakdown of L-S coupling, since only a small perturbation is needed to effect a sign change. In Am, it is unlikely that relativistic effects can produce the observed magnitude of b. Therefore, we believe that the sign of b in Am^{241} is positive. On the other hand, the dipole interaction, which is very sensitive to a small admixture of an excited s state (because of the hfs of an s electron is usually quite large) is probably negative.

V. AMERICIUM-242

A. Introduction

Previous to our investigation of 16-hr Am^{242}, it was believed that this isotope was the metastable state of the two isomers of Am^{242} (half lives of 16 hr and 152 yr). We measured the nuclear spin and obtained a value I=1, which was not in agreement with the interpretation of the nuclear energy-level scheme. This result led members of the nuclear spectroscopy group at the Lawrence Radiation Laboratory to renew investigations of the isomeric pair.[55] They were able to perform an isomeric separation of 16-hr Am^{242} from an old sample containing 152-yr Am^{242} by collecting recoils from the internal conversion of the isomeric transition, thus proving that the 16-hr activity is the ground state. Study of the conversion-electron intensities in Am^{242m} showed that this isomer decays by an E4 transition.[56] This result, coupled with the spin measurement, leads to a spin assignment of 5 for Am^{242m}. They also conclude from β^--transition probabilities that the 16-hr Am^{242} (henceforth called Am^{242}) belongs to a K=0 rotational band. Our measurements of the nuclear magnetic-dipole and electric-quadrupole moments are in agreement with this supposition.

B. Beam Production

Americium-242 was produced by the reaction

$$Am^{241}(n, \gamma)Am^{242}.$$

The isotope is identified by observing its decay rate (Fig. 27), and its γ-pulse-height spectrum (Fig. 28).

The problem of producing a beam of atoms had already been solved by the previous work on Am^{241}. It was necessary, however, to devise a safe means of packaging the americium, for the americium powder which is to be irradiated has a dangerous level of α activity. Figure 29 is a picture of the container used to hold the americium. Approximately 5 mg of americium oxide is poured into an aluminum capsule with a screw-on cap. The capsule is sealed in a quartz tube, which is placed in a larger aluminum capsule. The package is sent to the General Electric nuclear reactor at Vallecitos and placed in the core position, where it receives a flux of 9.5×10^{13} neutrons/sec-cm^2 for a duration of 16 hr.

The beam is detected by counting the emitted beta particles in flow-proportional beta counters. Contamination of the sample due to the presence of Am^{241} decay is not a problem. A typical neutron bombardment yields approximately 1000 times more americium-242 activity than americium-241 activity, as calculated from the thermal-neutron reaction-cross-section value of 620 barns for Am^{241}.[57]

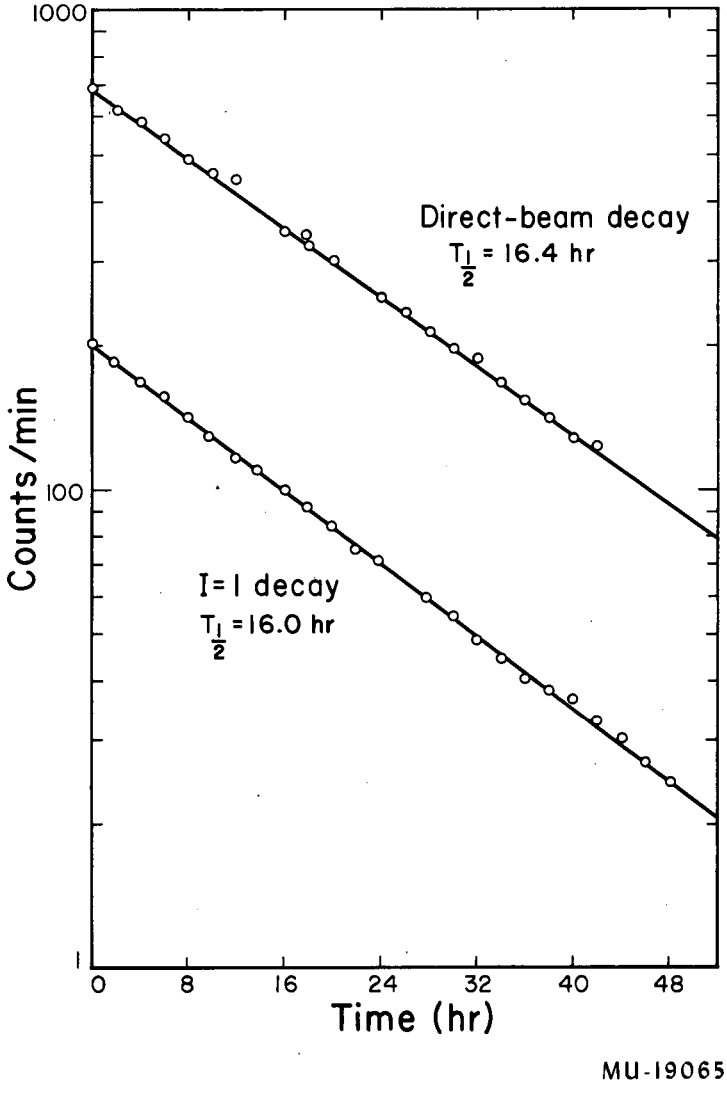

Fig. 27. Decay of full-beam and spin I=1-resonance exposures in Am^{242}.

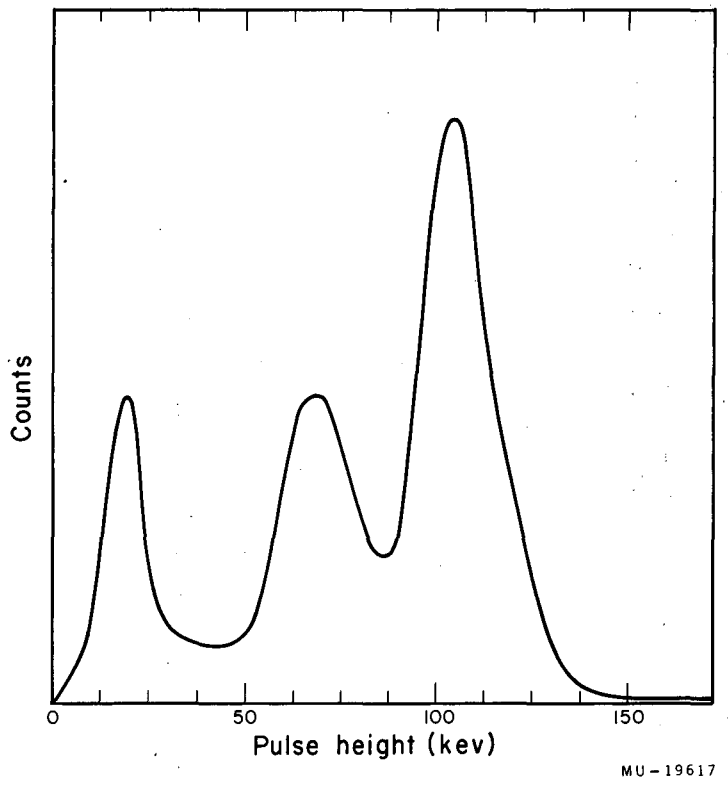

Fig. 28. Gamma pulse-height spectrum of 16-hr Am^{242}.

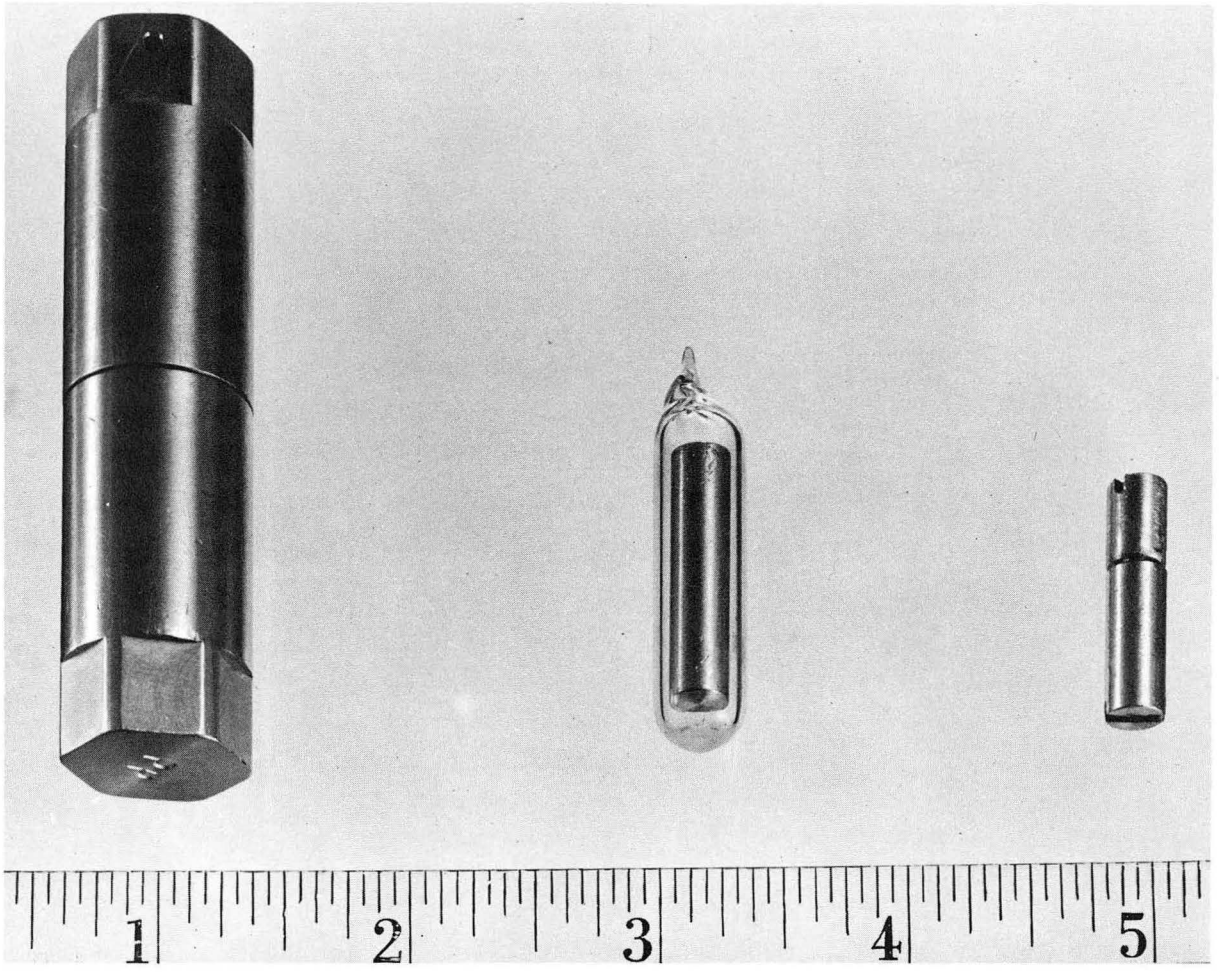

ZN-2452

Fig. 29. Neutron-bombardment container for production of Am^{242}. Left to right: aluminum target capsule, quartz tube, and aluminum container for the americium powder.

C. Experimental Observations

Magnetic transitions between states of the same total angular momentum, F were first induced in a magnetic field of 0.7 gauss. Exposures to the beam were taken at discrete frequencies corresponding to values of the nuclear spin I from 0 to 5. The frequency is calculated from Eq. (IV-1) for the state of maximum F, employing the value of g_J=-1.9371(10) previously measured in Am^{241}. Only the value of the radio frequency that corresponds to a spin of 1 produced an increase in signal at the detector. To confirm the spin assignment and at the same time undertake to measure the hyperfine structure, we observed the same transition at a field of 2.8 gauss. This is the transition associated with the state $F_{max.}$=I+J=1+7/2 = 9/2. Transitions between magnetic sublevels in states F=7/2, and F=5/2 were also found at the last value of the magnetic field. Figure 30 shows these three observed resonances. Even at this low value of the magnetic field, there is considerable quadratic shift, indicating a small hyperfine structure. The arrow labeled ν_{∞} is the frequency calculated from formula (IV-1). Frequency $\nu_{a,b}$ is calculated from the hfs constants that were determined at a later time and is included for comparison. Each of the three transitions were observed again at successively higher values of the field. The ratio of b to a that gave a best fit to the data was approximately 7. From the hfs level diagram in Fig. 31, we see that this value of b/a causes an inversion in the hfs level ordering. Figure 32 is a schematic of the hfs energy levels of Am^{242} in a magnetic field when the level ordering is 9/2, 5/2, and 7/2. The values of m associated with the flop-in transitions are different from what they would be if the level ordering were normal.

There are 12 different flop-in transitions between the states F = 9/2 and F = 7/2. A search was made for the line (9/2, -1/2$\longleftrightarrow$ 7/2, 1/2) at a field of 0.7 gauss. The resonance was observed and identified from its field dependence, by reobserving the same

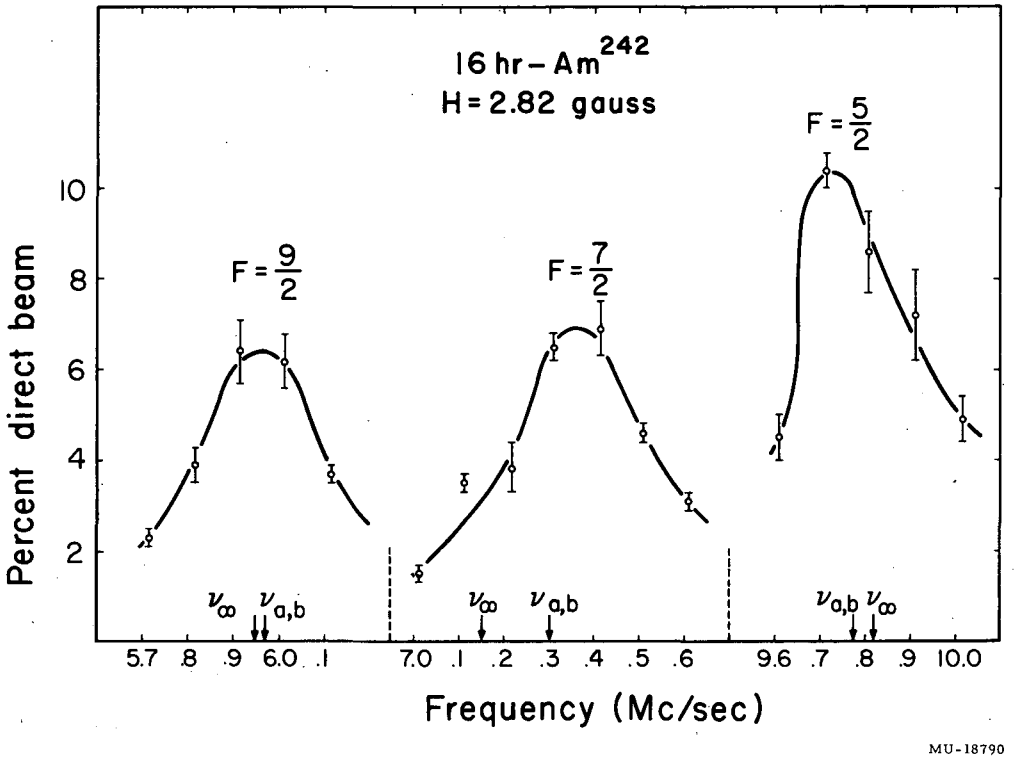

Fig. 30. Observed Am^{242} transitions at 2.8 gauss.

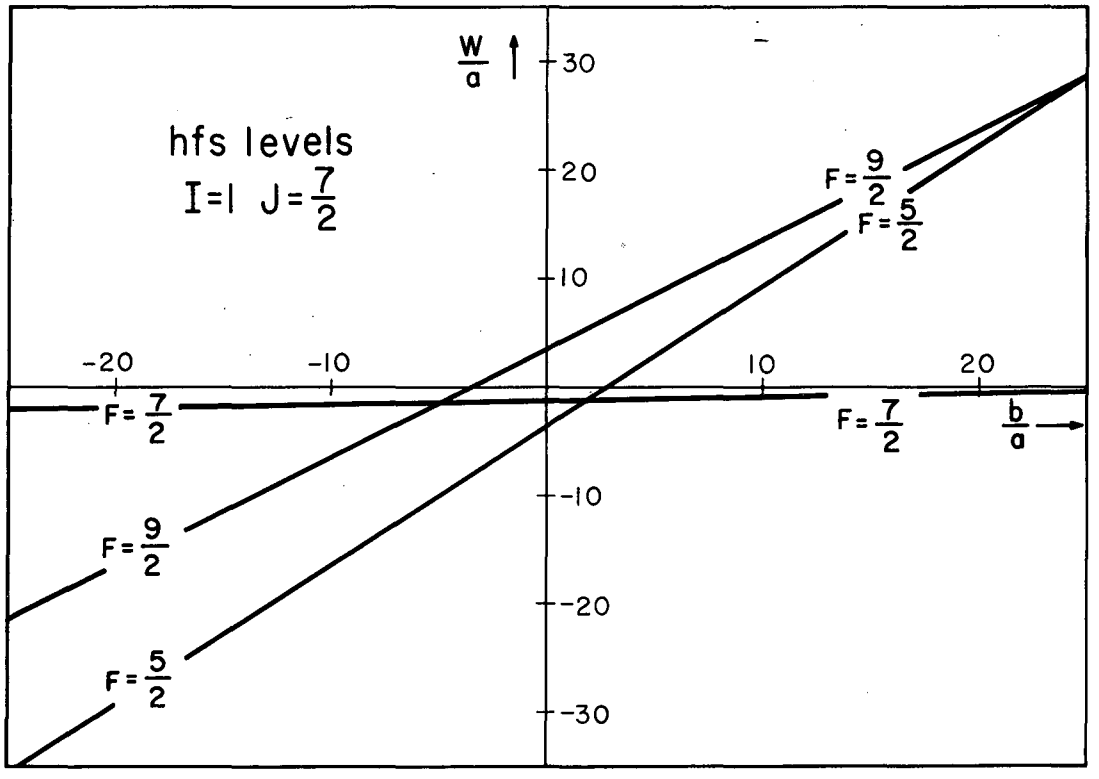

Fig. 31. Hyperfine-structure energy levels of the system I = 1, J = 7/2, in the absence of an applied field. W_{hfs}/a vs b/a.

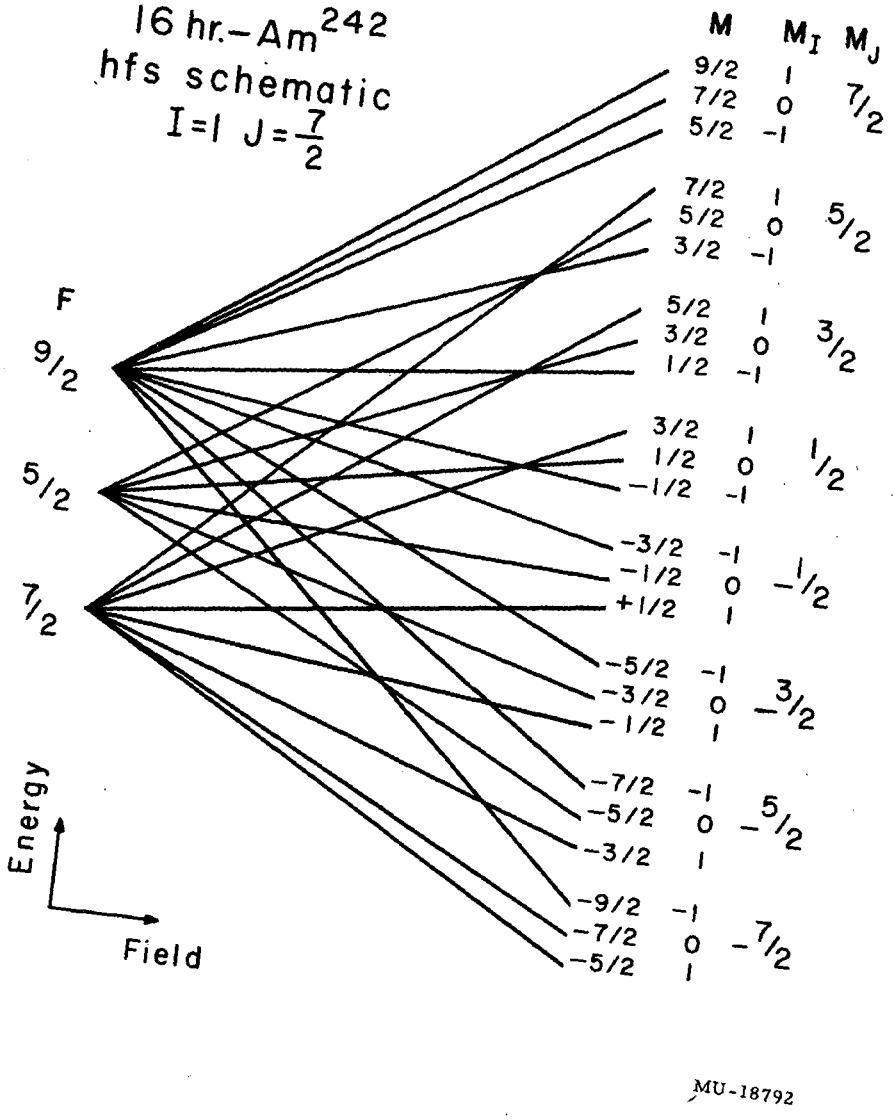

Fig. 32. Schematic diagram of the hyperfine-structure levels of Am^{242} in a magnetic field.

transition between the levels F - 5/2, and F = 7/2. This fact serves to identify the observed resonance, since the transition is induced by a sigma hairpin. Figure 33 shows the observed direct transitions.

The data was analyzed by means of the IBM-704 hyperfine routine previously described. The results of analyzing the 22 observed resonances for g_I positive are:

$$a = \pm 10.124(10)\ \text{Mc}$$
$$b = \pm 69.639\ (40)\ \text{Mc}$$
$$g_J = -1.9385(8)$$
$$\chi^2 = 4.2.$$

The results for g_I taken negative were the same. One half of the full line width at half maximum was selected as the uncertainty in each resonance. The value of χ^2 indicates that these uncertainties are about one-half of the rms uncertainties. The above value of g_J, when appropriately weighted and averaged with the value from the Am^{241} measurements, yields $g_J = -1.9371(10)$. The data was analysed again for a fixed value of g_J equal to the weighted mean (Table XI). The calculated hfs constants did not change. This is reasonable since a and b are determined primarily from the low-field $\Delta F=1$ transitions.

For two isotopes of the same element, the electronic matrix element $(JJ\|N_k\|JJ)$ is the same. Therefore by Eq. (II-6) and (II-14a, b) it is possible to relate the hfs constants of two such isotopes by

$$A_1/\mu_I = A_1'/\mu_I' \quad \text{or} \quad aI/\mu_I = a'I'/\mu_I' \qquad \text{(V-1)}$$

and

$$A_2/Q = A_2'/Q' \quad \text{or} \quad b/Q = b'/Q'. \qquad \text{(V-2)}$$

Application of these formulas to Am^{242} yields

$$\mu_I(Am^{242}) = \pm \frac{10.124}{17.144} \quad \frac{1}{(5/2)}\ (1.4) = \pm 0.33\ \text{nm}$$

and

$$Q(Am^{242}) = \mp \frac{69.639}{123.817}\ (4.9) = \mp 2.76\ \text{barns}.$$

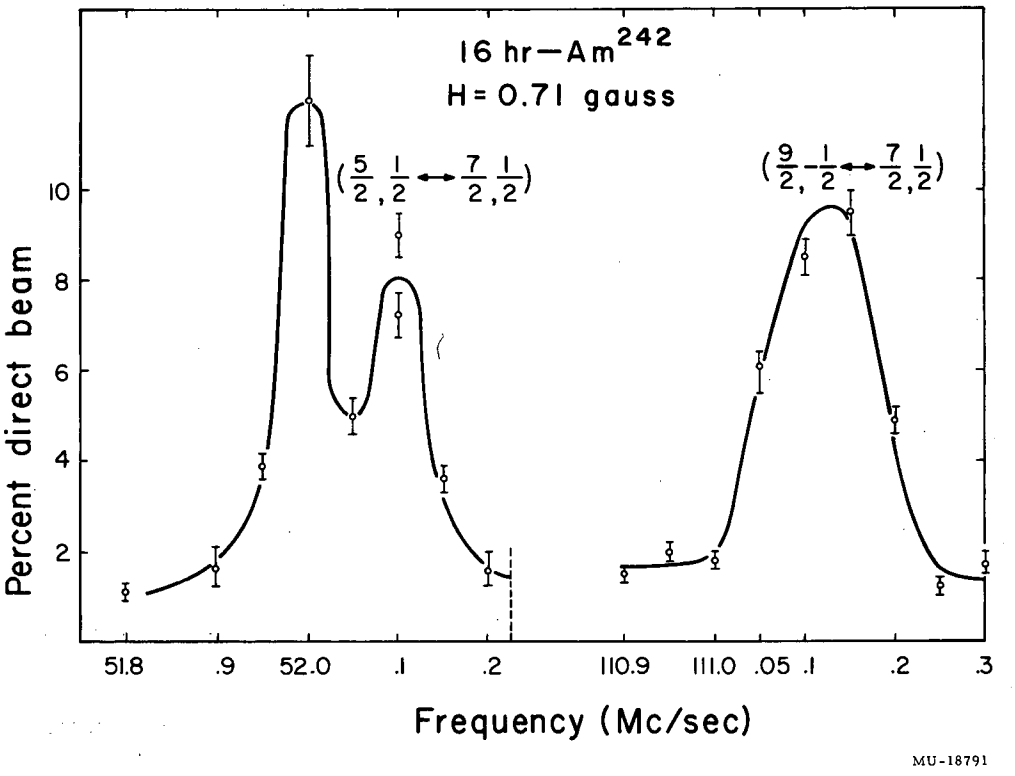

Fig. 33. Observed $\Delta F=1$ transitions of Am^{242} at 0.7 gauss.

D. Nuclear Structure

Americium-242, which has an odd-odd nucleus, can be interpreted in terms of the spheroidal-core model. The odd-proton orbital is most likely $5/2-\,[523]$, which is the ground state of Am^{241} and Am^{243}.[44] The odd-neutron orbital is probably the $5/2+\,[622]$ ground state of the isotones Pu^{241} and Cm^{243} (see Fig. 18). According to Nordheim's coupling rules as modified by Gallagher and Moszkowski,[58] we have

$$K = \Omega_p + \Omega_n$$

for

$$\Omega_p = \Lambda_p \pm 1/2 \quad \text{and} \quad \Omega_n = \Lambda_n \pm 1/2,$$

and

$$K = \left| \Omega_p - \Omega_n \right|$$

for

$$\Omega_p = \Lambda_p \pm 1/2$$

and

$$\Omega_n = \Lambda_n \mp 1/2 \,. \qquad \text{(V-3)}$$

Application of these rules to Am^{242} predicts that K=0 is the ground state. This situation is similar to the one in Pa^{233}, where we have $K=\Omega=1/2$, but $I=3/2$.

The observed signs and magnitudes of the nuclear moments lend support to the assignment K=0. For a K=0 rotational band, the nuclear angular momentum, I, must be perpendicular to the symmetry axis; hence there can be no contribution to the nuclear dipole moment from the odd nucleons. The nuclear core has a magnetic moment $\mu_I = g_R I$, where g_R is the g factor of the collective motion of the core. For a uniformly charged nucleus, $g_R = Z/A$. These relations yield $\mu_I(\text{calc.}) = +0.39$, in good agreement with the magnitude and sign of the observed value, if we assume $\mu_I > 0$ and $Q < 0$.

Table XI

Americium-242 Data

Data No.	H (gauss)	$\nu_{obs.}$ (Mc)	$\nu_{obs.} - \nu_{calc.}$ (Mc)	Transition
1	2.818(27)	5.95(15)	-0.018	a
2	2.818(27)	7.35(15)	0.051	b
3	2.818(27)	9.73(15)	-0.064	c
4	5.566(27)	11.95(10)	0.105	a
5	5.566(27)	14.70(10)	-0.003	b
6	5.566(27)	19.25(8)	0.060	c
7	9.564(26)	20.60(12)	0.067	a
8	9.564(26)	25.90(10)	0.023	b
9	9.564(26)	32.60(12)	0.143	c
10	14.678(31)	31.96(12)	-0.028	a
11	14.678(31)	40.55(10)	0.024	b
12	14.678(31)	48.91(12)	0.191	c
13	21.931(35)	49.20(20)	0.109	a
14	21.931(35)	61.50(20)	0.065	b
15	21.931(35)	70.35(20)	0.069	c
16	46.077(47)	112.20(30)	0.346	a
17	46.077(47)	130.00(40)	0.113	b

Table XI

Americium-242 Data

Data No.				
18	46.077(47)	133.95(30)	0.147	c
19	540.903(220)	1467.80(80)	0.471	c
20	0.711(028)	52.04(10)	-0.004	d
21	0.711(28)	111.125(75)	0.001	e
22	1.418(28)	109.680(75)	0.000	e

[a](9/2, -1/2 $\longleftrightarrow$ 9/2, -3/2) .

[b](7/2, 3/2 $\longleftrightarrow$ 7/2, 1/2) .

[c](5/2, 1/2 $\longleftrightarrow$ 5/2, -1/2) .

[d](5/2, 1/2 $\longleftrightarrow$ 7/2, 1/2) .

[e](9/2, -1/2 $\longleftrightarrow$ 7/2, 1/2) .

The quadrupole measurement can also be analyzed in terms of the Bohr-Mottelson-Nilsson nuclear model. Nuclear systematics indicate that the intrinsic quadrupole moment, Q_0, of nuclides in the transuranic region of the nuclear chart are positive.[44] The relation between the measured quadrupole moment, Q, and Q_0 is

$$Q = \frac{3K^2 - I(I+1)}{(I+1)(2I+3)} \cdot Q_0 \quad . \qquad (V-4)$$

For I=1, K=0, this gives $Q = -Q_0/5$, or $Q_0 = 13.8$ nm. Thus Q_0 has the correct sign if it is assumed that μ_I is greater than zero. The observed magnitude of Q is even more striking when we compare the measured and theoretical values of $Q(Am^{241})/Q(Am^{242})$. By Eq. (V-4), this ratio should be $-25/14 = -1.786$. The measured value is $-123.817/69,639 = -1.778$.

APPENDICES

A. The Quadrupole Interaction Constant

The quadrupole interaction constant, b, is defined by

$$b = -e^2Q(JJ \left| \sum_i (3\cos^2\theta - 1)_i \right| JJ) . \qquad (A-1)$$

In pure L-S coupling among n equivalent electrons, the wave function is

$$|JJ) = |\ell^n LSJJ). \qquad (A-2)$$

In Eq. (A-1) $(3\cos^2\theta - 1)$ behaves like a second-rank tensor. Therefor we can write:

$$(JJ \left| \sum_i (3\cos^2\theta - 1)_i \right| JJ) =$$

$$= (-)^{L+S+J}(2J+1)\begin{pmatrix} J & 2 & J \\ -J & 0 & J \end{pmatrix}\begin{Bmatrix} S & L & J \\ 2 & J & L \end{Bmatrix}(L \left\| \sum_i (3\cos^2\theta - 1)_i \right\| L)$$

$$= b_0(n,\ell,L)\left[3K(K+1) - 4L(L+1)J(J+1)\right]/(J+1)(2J+3) \qquad (A-3)$$

Here b_0 is a constant that depends on the Hund's-rule ground term of the configuration ℓ^n, but does not depend on J, and K is defined in (II-16e). To evaluate b_0, we first evaluate the matrix element (A-3) for the state J = L+S. This gives

$$(L+S, L+S \left| \sum_i (3\cos^2\theta - 1)_i \right| L+S, L+S) = 2b_0L(2L-1). \qquad (A-4)$$

By expanding the electronic wave function into the zero-order scheme, Hubbs et al.[6] have shown for the Hund's-rule term that

$$(L+S, L+S \left| \sum_i (3\cos^2\theta - 1)_i \right| L+S, L+S) = -\frac{n(2\ell-n+1)(2\ell-2n+1)}{(2\ell-1)(2\ell+3)} . \qquad (A-5)$$

Solving (A-4) and (A-5) for b_0, combining (A-3) with (A-1), and then summing over all unfilled shells yields Eq. (II-16b).

B. The Electrostatic Energy

The form of the coefficients f^k and g^k have been derived by Racah[29] for the interaction of two electrons. He finds

$$f^k = (\ell_1 \ell_2 L m_L \left| C_k(1) \cdot C_k(2) \right| \ell_1 \ell_2 L m_L)$$
$$= (-)^{\ell_1+\ell_2+L} (\ell_1 \| C_k(1) \| \ell_1)(\ell_2 \| C_k(2) \| \ell_2) \begin{Bmatrix} L & \ell_2 \ell_1 \\ k & \ell_1 \ell_2 \end{Bmatrix} \quad \text{(B-1)}$$

and

$$g^k = -\left(\left| 1/2 + 2s(1)\cdot s(2) \right| \right) b^k , \quad \text{(B-2)}$$

where

$$b^k = (-)^{\ell_1+\ell_2-L} (\ell_1 \ell_2 L m_L \left| C_k(1)\cdot C_k(2) \right| \ell_2 \ell_1 L m_L)$$
$$= (\ell_1 \| C_k \| \ell_2)^2 \begin{Bmatrix} L & \ell_1 & \ell_2 \\ k & \ell_1 & \ell_2 \end{Bmatrix} . \quad \text{(B-3)}$$

The extension of these results to the configuration $\ell_1^2 \ell_2$ is straightforward for the direct interaction. We use the fact that

$$W(\ell_1^2 \ell_2) = 2W(\ell_1 \ell_2) , \quad \text{(B-4)}$$

and replace

$$(-)^{\ell_1} (\ell_1 \| C_k(1) \| \ell_1)$$

in Eq. (B-1) with

$$(-)^{L_1} (\ell_1^2 L_1 \| C_k(1) \| \ell_1^2 L_1') = (-)^{\ell_1+\ell_2+L_1+L_1'+k} \left[(2L_1+1)(2L_1'+1)\right]^{1/2}$$
$$\begin{Bmatrix} \ell_1 & \ell_2 & L_1 \\ k & L_1 & \ell_2 \end{Bmatrix} (\ell_1 \| C_k \| \ell_1) \quad \text{(B-5)} ,$$

To obtain the exchange interaction, we follow the approach of Racah, and expand the exchange interaction into the sum of "direct" interactions by means of the formula

$$\begin{Bmatrix} L & \ell_1 & \ell_2 \\ k & \ell_1 & \ell_2 \end{Bmatrix} = (-)^{k+L} \sum_r (-)^r (2r+1) \begin{Bmatrix} k & \ell_2 & \ell_1 \\ r & \ell_1 & \ell_2 \end{Bmatrix} \begin{Bmatrix} L & \ell_2 & \ell_1 \\ r & \ell_1 & \ell_2 \end{Bmatrix}. \tag{B-6}$$

Thus b^k may be written

$$b^k = (-)^{k+\ell_1+\ell_2} (\ell_1 \| C_k \| \ell_2)^2 \sum_r (-)^r (2r+1) \begin{Bmatrix} k & \ell_2 & \ell_1 \\ r & \ell_1 & \ell_2 \end{Bmatrix} \left(\left| u_r(1) \cdot u_r(2) \right| \right), \tag{B-7}$$

where u_r is a tensor of rank r defined by its reduced matrix,

$$(n\ell \| u_r \| n'\ell') = \delta(n, n') \, \delta(\ell, \ell') . \tag{B-8}$$

The matrix element of $u_r(1) \cdot u_r(2)$ for the configuration $\ell_1^2 \ell_2$ is

$$(\ell_1^2 L_1, \ell_2, L \left| u_r(1) \cdot u_r(2) \right| \ell_1^2 L_1', \ell_2, L')$$
$$= (-)^{\ell_2+L_1+L_1'+L+r} \left[(2L_1+1)(2L_1'+1) \right]^{1/2} \begin{Bmatrix} L & \ell_2 & L_1' \\ r & L_1 & \ell_2 \end{Bmatrix} \begin{Bmatrix} \ell_1 & \ell_1 & L_1 \\ r & L_1' & \ell_1 \end{Bmatrix}. \tag{B-9}$$

Therefore b^k becomes

$$b^k = (-)^{k+L+\ell_1+L_1+L_1'} (\ell_1 \| C_k \| \ell_2)^2 \sum_r (-)^{2r} (2r+1)$$
$$\begin{Bmatrix} \ell_1 & \ell_2 & k \\ \ell_2 & \ell_1 & r \end{Bmatrix} \begin{Bmatrix} L_1 & L & \ell_2 \\ \ell_2 & r & L_1' \end{Bmatrix} \begin{Bmatrix} \ell_1 & L_1' & \ell_1 \\ r & \ell_1 & L_1 \end{Bmatrix}. \tag{B-10}$$

The sum on the right side of Eq. (B-10) is equal to

$$(-)^{\ell_1+L_1+L_1'+L+k} \begin{Bmatrix} \ell_1 & \ell_1 & L_1' \\ \ell_1 & k & \ell_2 \\ L_1 & \ell_2 & L \end{Bmatrix} . \qquad \text{(B-11)}$$

The spin contribution to g^k is

$$-(s_1^2, S_1, s_2 S \left| 1/2+2s(1) \cdot s(2) \right| s_1^2, S_1, s_2 S)$$

$$= (-)^{S_1+S_1'+S+3/2} \; 3 \left[(2S_1+1)(2S_1'+1)\right]^{1/2} \begin{Bmatrix} S & 1/2 & S_1' \\ 1 & S_1 & 1/2 \end{Bmatrix} \begin{Bmatrix} 1/2 & 1/2 & S_1' \\ 1 & S_1 & 1/2 \end{Bmatrix}$$

$$- 1/2 \; \delta(S_1, S_1'). \qquad \text{(B-12)}$$

This expression has a different form from the spin-dependent part of Eq. (III-5), but they are the same numerically.

Equation (III-4) follows from Eqs. (B-4), (B-4), (B-5), and (III-28). Equation (III-5) follows from (B-2), (B-4), (B-10), (B-11), (B-12), and (III-28).

C. Calculation of Radial Integrals

The Slater integral R^k is defined by

$$R^k(ab, cd) = 2e^2 \int_0^\infty dr_2 \int_0^\infty \frac{r_1^k}{r_2^{k+1}} R_1(a)R_1(c)R_2(b)R_2(d)dr_1, \tag{C-1}$$

where $a \equiv n^a \ell^a$, and the subscripts refer to electrons 1 and 2.

Cohen has calculated the relativistic Hartree wave functions F and G of uranium and has tabulated them as a function of $\rho = \ell n(1000r/a_0)$ in increments $\Delta\rho = 1/4$. In terms of these variables, the numerically calculated integral is

$$27.434 \sum_j \sum_{i=1}^{j} \frac{e^{(k+1)\rho_i}}{e^{k\rho_j}} \left[F_i(a)F_i(c)+G_i(a)G_i(c)\right] \times \left[F_j(b)F_j(d)+G_j(b)G_j(d)\right] \text{ cm}^{-1} \tag{C-2}$$

The radial integrals F^k and G^k are defined in terms of R^k by

$$F^k(a, b) = R^k(ab, ab)$$

and (C-3)

$$G^k(a, b) = R^k(ab, ba).$$

Comparison of Eqs. (II-12a) and (II-17) shows that for the dipole interaction, we have

$$'' \left\langle 1/r^3 \right\rangle '' = \frac{2}{\alpha a_0(\ell+1)} \int r^{-2} FG \, dr. \tag{C-4}$$

Comparison of Eqs. (II-12b) and (II-18) shows that for the quadrupole interaction, we have

$$\left\langle 1/r^3 \right\rangle = \int r^{-3}(F^2+G^2)dr . \tag{C-5}$$

The integrals are evaluated numerically, as follows:

$$\int r^{-2} FG \, dr = (10^3/4) \sum_i F_i G_i e^{-\rho_i} a_0^{-3} \tag{C-6}$$

$$\int r^{-3}(F^2+G^2) \, dr = (10^6/4) \sum_i (F_i^2+G_i^2)e^{-2\rho_i} a_0^{-3} \tag{C-7}$$

ACKNOWLEDGMENTS

Many people have contributed to the completion of this thesis. I am most grateful:

To Professor William A. Nierenberg, who has directed my graduate research and provided the inspiration and approval which have made its culmination possible. His enthusiasm and dedication have been a beacon to me.

To Drs. John C. Hubbs and Richard Marrus, who have shared with me their knowledge of atomic-beam principles and have helped to give direction to my research.

To Professors Howard A. Shugart and Kenneth Smith, and Drs. Edgar Lipworth and Ingvar Lindgren, for many informative discussions regarding atomic-beam techniques.

To Dr. Brian Judd, for guiding me through the calculations of the electronic structure of protactinium.

To members of the chemistry department, in particular Drs. James Wallman, and T. Darrah Thomas, for their help in the development of the chemical procedures.

To the other graduate students of the group, especially Amado Cabezas, who has been of great assistance on many of the runs.

To my parents, for their continual support and encouragement of my education.

And most of all, to my wife, Lee, who has been my greatest source of assistance and understanding.

This work was performed under the auspices of the U. S. Atomic Energy Commission.

REFERENCES

1. J. C. Hubbs and J. Winocur, Bull. Am. Phys. Soc. 3, 319 (1958).
2. J. Winocur, R. Marrus, and W. A. Nierenberg, Bull. Am. Phys. Soc. 4, 451 (1959).
3. R. Marrus, W. A. Nierenberg, and J. Winocur, Phys. Rev. (to be published).
4. R. Marrus, W. A. Nierenberg, and J. Winocur, Phys. Rev. (to be published).
5. Richard Marrus, Hyperfine-Structure Measurements on Some Transuranic Elements (Thesis), UCRL-8547, Nov. 23, 1958.
6. J. C. Hubbs, W. A. Nierenberg, R. Marrus, and J. L. Worcestor, Phys. Rev. 109, 390 (1958).
7. J. C. Hubbs and R. Marrus, Phys. Rev. 110, 287 (1958).
8. R. Albridge, J. C. Hubbs, and R. Marrus, Phys. Rev. 111, 1137 (1958).
9. J. C. Hubbs, R. Marrus, and J. Winocur, Phys. Rev. 114, 586 (1959).
10. H. B. G. Casimir, On the Interaction Between Atomic Nuclei and Electrons (Teyler's Tweede Genootschap, Haarlem, 1936).
11. S. Goudsmit, Phys. Rev. 37, 663 (1931).
12. G. Breit and L. Wills, Phys. Rev. 44, 470 (1933).
13. C. Schwartz, Phys. Rev. 97, 380 (1955).
14. William A. Nierenberg, University of California, private communication.
15. G. Breit and I. I. Rabi, Phys. Rev. 38, 2082 (1931).
16. I. I. Rabi, J. R. Zacharias, S. Millman, and P. Kusch, Phys. Rev. 53, 318 (1938).
17. J. R. Zacharias, Phys. Rev. 61, 270 (1942).
18. Gilbert O. Brink, Nuclear Spins of Thallium-197, Thallium-198m, Thallium-199, and Thallium-204 (thesis), UCRL-3642 June , 1957.
19. N. F. Ramsey, Molecular Beams (Oxford University Press, London, 1956).

20. K. F. Smith, Molecular Beams (Methuen and Co., Ltd., London, 1955).
21. K. F. Smith, Progr. Nuclear Phys. 6, 52 (1957).
22. W. A. Nierenberg, Ann. Rev. Nuclear Sci. 7, 349 (1957).
23. W. A. Nierenberg, Recent Research in Molecular Beams Academic Press New York, N. Y., 1959) Chap. 2.
24. Donald Zurlinden, Lawrence Radiation Laboratory, private communication.
25. Seymour Singer, Lawrence Radiation Laboratory, private communication.
26. J. J. Katz and G. T. Seaborg, The Chemistry of the Actinide elements (Methuen and Co., Ltd., London, 1957).
27. H. Schuler and H. Gollnow, Naturwiss. 22, 511 (1934).
28. R. A. Fisher, Statistical Methods for Research Workers (Oliver and Boyd, Edinburg, 1958).
29. G. Racah, Phys. Rev. 62, 438 (1942).
30. G. Racah, Phys. Rev. 63, 367 (1953).
31. E. U. Condon and G. H. Shortley, The Theory of Atomic Spectra (Cambridge University Press, Cambridge, 1957).
32. Brian Judd, Lawrence Radiation Laboratory, private communication.
33. A. R. Edmonds, Angular Momentum in Quantum Mechanics (Princeton University Press, Princeton, N. J., 1957).
34. G. Racah, Physica 16, 651 (1950).
35. Stanley Cohen, Relativistic Self-Consistent Calculation for the Normal Uranium Atom, UCRL-8633 Feb. 10, 1959.
36. F. H. Spedding, Phys. Rev. 58, 255 (1940).
37. J. K. Dawson, C. J. Mandleberg, and D. Davies, J. Chem. Soc., (London) 2047 (1951).
38. R. E. Trees, Phys. Rev. 92, 308 (1953).
39. A. Bohr, Phys. Rev. 81, 134 (1951).
40. A. Bohr, Dan. Mat. Fys. Medd. 26, No. 14 (1952).
41. A Bohr and B. R. Mottelson, Dan. Mat. Fys. Medd. 27, No. 16(1953).

42. S. G. Nilsson, Dan. Mat. Fys. Medd. 29, No. 16 (1955).

43. B. R. Mottelson and S. G. Nilsson, Mat. Fys. Skr. Dan. Vid. Selsk. 1, No. 8 (1958).

44. F. S. Stephens, F. Asaro, and I. Perlman, Phys. Rev. 113, 212 (1959).

45. M. Fred and F. S. Tomkins, Phys. Rev. 89, 318 (1953).

46. R. P. Thorne, Nature 178, 484 (1956).

47. T. E. Manning, M. Fred, and F. S. Tomkins, Phys. Rev. 102, 1108 (1956).

48. M. Fred and F. S. Tomkins, J. Opt. Soc. Am. 44, 824 (1954).

49. M. Fred and F. S. Tomkins, J. Opt. Soc. Am. 47, 1076 (1957).

50. John G. Conway, Lawrence Radiation Laboratory, private communication.

51. J. G. Conway, J. C. Wallmann, B. B. Cunningham, and G. V. Shalimoff, J. Chem. Phys. 27, 1416 (1957).

52. J. P. Elliott, B. R. Judd, and W. A. Runciman, Proc. Roy. Soc. (London) A240, 509 (1957).

53. V. Heine, Phys. Rev. 107, 1002 (1957).

54. P. G. H. Sandars, Investigation of Hyperfine Structure by the Method Magnetic Resonance in Atomic Beams, Ph. D. Thesis, Oxford, October 1959 (unpublished).

55. F. Asaro, I. Perlman, J. O. Rasmussen, and S. G. Thompson, Bull. Am. Phys. Soc. 4, 461 (1959).

56. I. Perlman, F. Asaro, J. O. Rasmussen, and S. G. Thompson, The Isomers of Am^{242} UCRL-9047(to be published).

57. Neutron Cross Sections, compiled by D. J. Hughes and J. A. Harvey, BNL-325 July 1, 1955.

58. C. J. Gallagher, Jr., and S. A. Moszkowski, Phys. Rev. 111, 1282 (1958).